Åbo Akademi University

Tina Gulin-Sarfraz

Design of Multifunctional Nanoparticles for Cellular Labeling and Tracking, Delivery and Scavenging of Active Substances *in vivo*

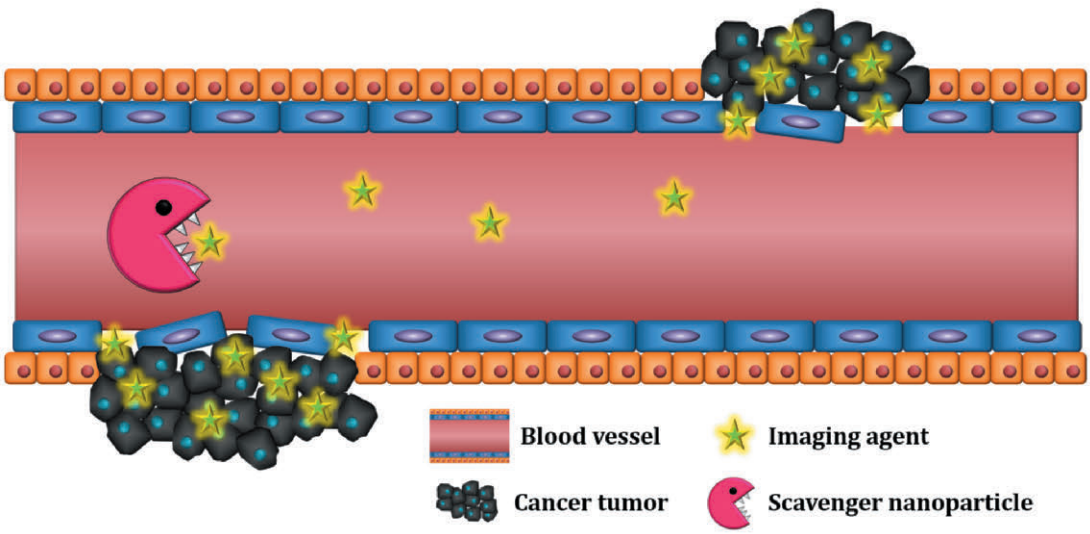

Design of Multifunctional Nanoparticles for Cellular Labeling and Tracking, Delivery and Scavenging of Active Substances *in vivo*

Tina Gulin-Sarfraz

Pharmaceutical Sciences Laboratory
Faculty of Science and Engineering
Åbo Akademi University
Åbo, Finland, 2019

Supervisor

Professor Jessica Rosenholm
Pharmaceutical Sciences Laboratory
Faculty of Science and Engineering
Åbo Akademi University, Turku, Finland

Co-supervisor

Assistant Professor Jixi Zhang
College of Bioengineering
Chongqing University, Chongqing, China

Reviewers

Professor Catharina de Lange Davies
Biophysics and Medical Technology
Department of Physics
Norwegian University of Science and Technology, Trondheim, Norway

and

Associate Professor Anu Airaksinen
Radiopharmaceutical Chemistry
Department of Chemistry
University of Helsinki, Helsinki, Finland

Opponent

Professor Catharina de Lange Davies
Biophysics and Medical Technology
Department of Physics
Norwegian University of Science and Technology, Trondheim, Norway

ISBN 978-952-12-3818-5 (printed)
ISBN 978-952-12-3819-2 (digital)
Painosalama Oy – Turku, Finland 2019

ABSTRACT

Nanomedicine, the application of nanotechnology in the biomedical field, has gained tremendous interest for improving diagnostic and therapeutic interventions with potential in personalized medicine. The aim of personalized medicine is to guarantee that the most suitable medicine is given to each patient, and is further efficiently and safely delivered to the right place of treatment in the body. The research within the diverse field of nanomedicine is steering towards this goal; with high expectations of novel delivery systems for commercially available drugs, tailored for individual patients pre-selected by sophisticated diagnostic tools, and in addition, targeted to a specific site of action with subsequent controlled drug release. To potentially reach this goal, the preparation and modification steps of the nanomedicines have to step-wise be carefully considered, and further studied and evaluated for their specific applications *in vivo*.

In this thesis, the main emphasis was to design and construct multifunctional silica-based nanoparticles and evaluate them for specific diagnostic and therapeutic applications. The influence of different surface coatings was thoroughly investigated for the effect of stabilizing and dispersing the nanoparticles, and subsequently for maximizing cellular internalization. This effect was further explored by developing magnetite-silica core-shell particles and evaluating the synergistic effect of surface coating and an external magnetic field on the cellular uptake, in addition to the performance of the particles as contrast agents for magnetic resonance imaging (MRI).

Diagnostic imaging techniques, such as MRI, are becoming increasingly important for early diagnosis of various pathologies. To improve the quality of generated images, as well as to visualize and track cells (e.g. stem cells after implantation), novel imaging probes are required. Here, porous silica nanoparticles were evaluated to serve as "nano-containers" for carrying a high amount of commercially available fluorescent imaging agents, for long-term cellular tracking. A tumor of pre-labeled breast cancer cells was monitored *in vivo* for a period of one month, and real-time detection of circulating metastatic cells was demonstrated. The same properties that render porous silica nanoparticles good candidates to serve as carriers for imaging agents, are also applicable for drugs. This approach was utilized by loading a large amount of anti-inflammatory drug into the particles, and the therapeutic treatment effect on airway inflammation in mice was studied after pulmonary administration of the particles.

Molecular imaging probes intended for diagnostic imaging, are normally administered through intravenous injection and thus rapidly distributed all over

the body. These contrast agents are typically small molecules capable of crossing the blood-tissue barriers and accumulating in tissues, especially when the barrier is disrupted as in the case of different pathological conditions. When imaging a pathological site, such as a tumor or inflammation, a problem is to accurately differentiate between the signals originating from the contrast agent in the blood circulation and the signals originating from surrounding tissue. Based on this, a nanoparticle-based scavenger-system for catching and quenching the signal of a circulating contrast agent (tracer) is demonstrated. The interaction between tracer and scavenger was investigated by photonic measurements, based on Förster/fluorescence resonance energy transfer (FRET). FRET is a useful tool to visualize short-distance molecular interactions. Thus, this approach is further utilized to develop a nanoparticle-based reporter system to study intracellular redox-induced delivery of an active model compound. Intracellular release can be particularly challenging to study, however highly desired, since many active compounds are non-toxic and can not be validated based on their cytotoxic action. A reporter-system may then serve as a tool for real-time monitoring of intracellular compound cleavage. The results presented in this thesis contribute in the process of developing tailored multifunctional nanoparticles for similar diagnostic and therapeutic applications as presented here.

LIST OF ORIGINAL PUBLICATIONS

I. **Gulin-Sarfraz, T.**; Zhang, J.; Desai, D.; Teuho, J.; Sarfraz, J.; Jiang, H.; Zhang, C.; Sahlgren, C.; Lindén, M.; Gu, H.; Rosenholm, J. M., Combination of magnetic field and surface functionalization for reaching synergistic effects in cellular labeling by magnetic core–shell nanospheres. *Biomaterials Science* **2014,** *2* (12), 1750.

II. Karaman, D. Ş.; **Gulin-Sarfraz, T.**; Hedström, G.; Duchanoy, A.; Eklund, P.; Rosenholm, J. M., Rational evaluation of the utilization of PEG-PEI copolymers for the facilitation of silica nanoparticulate systems in biomedical applications. *Journal of colloid and interface science* **2014,** *418*, 300.

III. **Gulin-Sarfraz, T.**; Pryazhnikov, E.; Zhang, J.; Rosenholm, J. M.; Khiroug, L., Chemical and photonic interactions *in vitro* and *in vivo* between fluorescent tracer and nanoparticle-based scavenger for enhanced molecular imaging. *Submitted manuscript*.

IV. **Gulin-Sarfraz, T.**; Sarfraz, J.; Karaman, D. Ş.; Zhang, J.; Oetken-Lindholm, C.; Duchanoy, A.; Rosenholm, J. M.; Abankwa, D., FRET-reporter nanoparticles to monitor redox-induced intracellular delivery of active compounds. *RSC Advances* **2014,** *4* (32), 16429.

V. Rosenholm, J. M.; **Gulin-Sarfraz, T.**; Mamaeva, V.; Niemi, R.; Özliseli, E.; Desai, D.; Antfolk, D.; von Haartman, E.; Lindberg, D.; Prabhakar, N.; Näreoja, T.; Sahlgren, C., Prolonged dye release from mesoporous silica-based imaging probes facilitates long-term optical tracking of cell populations *in vivo*. *Small* **2016,** *12* (12), 1578.

VI. **Gulin-Sarfraz, T.**; Jonasson, S.; Wigenstam, E.; von Haartman, E; Bucht, A.; Rosenholm, J. M., Feasibility study of mesoporous silica particles for pulmonary drug delivery: therapeutic treatment with dexamethasone in a mouse model of airway inflammation. *Pharmaceutics* **2019**, *11* (4), 149.

CONTRIBUTION OF THE AUTHOR

I. The author was responsible for most of the work in this publication, including synthesis of nonporous and porous silica shells, surface modifications, physicochemical characterizations of the samples, and cellular experiments (flow cytometry and confocal microscopy imaging). The author analyzed most of the results and wrote the first manuscript draft. J. Zhang contributed to manuscript writing and analysis of results. D. Desai performed cell viability measurement, H. Jiang TEM imaging, J. Sarfraz SEM imaging, and J. Teuho MR imaging. The magnetite cores were obtained from Shanghai Allrun Nano Science & Technology Co., Ltd.

II. The author performed the confocal microscopy imaging and analyzed the cellular uptake of nanoparticles. The author contributed to part of the particle characterization and manuscript writing. D. Sen Karaman was responsible for the main part of the experimental work and writing of the manuscript.

III. The author was responsible for the experimental work in this publication, including synthesis, development and characterization of the nanoparticles, except for the TEM images taken by J. Zhang. E. Pryazhnikov conducted the *in vivo* experiments. The author wrote the manuscript with contributions from the other authors in the publication.

IV. The author was responsible for most of the experimental work, including design, development and characterization of the nanoparticles. The author conducted the cellular uptake study by flow cytometry and wrote the first manuscript draft. C. Oetken-Lindholm contributed with cell samples for the experiments. J. Sarfraz, D. Sen Karaman, and J. Zhang carried out the SEM and TEM imaging. FRET confocal imaging was performed together with D. Abankwa.

V. The author was responsible for most of the intracellular evaluation, including nanoparticle uptake studies by flow cytometry and confocal microscopy, and analysis of the results. The author contributed to part of the particle characterization, and to shaping and writing the first manuscript draft. J. Rosenholm was responsible for the main part of the work and writing of the manuscript.

VI. The author was responsible for all the design, development, and characterization of the particles, except for TEM images taken by E. von Haartman. S. Jonasson and E. Wigenstam performed the *in vivo* study.

LIST OF SUPPORTING PUBLICATIONS

i. Karaman, D. Ş.; **Gulin-Sarfraz, T.**; Zhang, J.; Rosenholm, J. M., One-pot synthesis of pore-expanded hollow mesoporous silica particles. *Materials Letters* **2015,** *143*, 140-143.

ii. Prabhakar, N.; Zhang, J.; Desai, D.; Casals, E.; **Gulin-Sarfraz, T.**; Näreoja, T.; Westermarck, J.; Rosenholm, J. M., Stimuli-responsive hybrid nanocarriers developed by controllable integration of hyperbranched PEI with mesoporous silica nanoparticles for sustained intracellular siRNA delivery. *International Journal of Nanomedicine* **2016,** *11*, 6591.

iii. Krishnamoorthy, M.; Li, D.; Sharili, A. S.; **Gulin-Sarfraz, T.**; Rosenholm, J. M.; Gautrot, J. E., Solution conformation of polymer brushes determines their interactions with DNA and transfection efficiency. *Biomacromolecules* **2017,** *18* (12), 4121-4132.

ABBREVIATIONS

APTES	3-Aminopropyltriethoxysilane
BSA	Bovine Serum Albumin
CAM	Chorioallantoic membrane
CT	Computed tomography
Da	Dalton
DAPI	4',6-Diamidino-2-phenylindole (fluorescent nucleic acid stain)
DiI	1,1'-Dioctadecyl-3,3,3',3'-tetramethylindocarbocyanine perchlorate
DiO	3,3'-Dioctadecyloxacarbocyanine perchlorate
DLS	Dynamic light scattering
EPR	Enhanced permeation and retention
ETP	European technology platform
ex vivo	from Latin: "out of the living"
FDA	US Food and drug administration
FITC	Fluorescein isothiocyanate
FRET	Förster/fluorescence resonance energy transfer
HeLa	Human cervical cancer cell line
HEPES	2-(4-(2-Hydroxyethyl)piperazin-1-yl)ethanesulfonic acid
in vitro	from Latin: "in glass", i.e. under simulated physiological conditions
in vivo	from Latin: "in living", i.e. under physiological conditions
IVIS	*in vivo* imaging system
Mag	Magnetite core
MDA-MB-231	Human breast cancer cell line
MFI	Mean fluorescence intensity
MRI	Magnetic resonance imaging
MSN	Mesoporous silica nanoparticles
NIR	Near-infrared
NIRF	Near-infrared fluorescence
PdI	Polydispersity index
PEG	Polyethylene glycol
PEI	Polyethyleneimine
PET	Positron emission tomography
PhTES	Phenyltriethoxysilane
QD	Quantum dot
RES	Reticuloendothelial system

SDA	Structure directing agent
SEM	Scanning electron microscopy
SiO_2	Silica
SPECT	Single photon emission computed tomography
SPION	Superparamagnetic iron oxide nanoparticle
TEM	Transmission electron microscopy
TEOS	Tetraethoxysilane
TGA	Thermogravimetric analysis
TRITC	Tetramethylrhodamine isothiocyanate
US	Ultrasound
UV-Vis	Ultraviolet-visible

CONTENTS

1 INTRODUCTION

Personalized nanomedicine aims to individualize the field of diagnostic and therapeutic interventions, by making use of the expanding area of nanotechnology.[1-4] The development of nanomaterials for the diagnosis, prevention, and treatment of diseases have been extensively studied and raised significant expectations. "Nano-diagnostics" and "nano-pharmaceutics" are thus currently two out of three research areas identified by the European Technology Platform (ETP) for Nanomedicine.[5] ETPs play a key role in defining European research priorities, by fostering a broad collaboration between EU countries, industry, and scientists, in order to develop innovation agendas and roadmaps in the relevant sectors.

Nanoparticles offer many unique advantages as diagnostic and therapeutic tools due to their small sizes and large surface-to-volume ratios. Due to their design flexibility, nanoparticle platforms can be optimized for carrying optical labels for imaging, drug cargoes for therapeutic intervention, and biomolecular ligands for targeted delivery. The nanosize considerably changes the physicochemical properties of a material, such as optical and magnetic properties, as well as reactivity.[6]

There are a broad range of diagnostic imaging techniques, which are becoming increasingly important for early diagnosis of various pathologies. In the field of nanodiagnostics, nanomaterials are developed to be used as contrast agents. Contrast agents, or imaging probes, are materials that interact with the incident radiation and thus providing for better contrast on the resulting image. Consequently, they can greatly increase the sensitivity of an imaging technique. An example of an inherently detectable imaging probe for magnetic resonance imaging (MRI) is iron oxide nanoparticles, out of which SPIONs (superparamagnetic iron oxide nanoparticles) are the main class studied for MRI contrast enhancement. The majority of FDA (US Food and Drug Administration) approved iron oxide nanomaterials are indicated for the treatment of anemia.[7] However, one of them, ferumoxytol (Feraheme®), is under investigation as an imaging agent.[8] Several other SPION formulations have also received FDA approval, but later been withdrawn from the market,[9] due to among others aesthetical reasons.

Fluorescence imaging is a widely utilized imaging technique, especially in pre-clinical studies. Small-molecular organic dyes have traditionally been used for contrast enhancement. These are relatively unstable, and suffer from photobleaching, weak contrast, poor targeting, and limited aqueous solubility. Here, nanoparticles can serve as carriers for already commercially available dyes. Silica nanoparticles are ideal candidates as carriers, both for fluorescent dyes and drugs. They

have attracted much attention as biocompatible, bioerodible, and flexible carrier platforms.[10] In 2011, silica nanoparticles "Cornell dots" received FDA safety approval for the first-in-human clinical trial for targeted imaging of cancer,[11] and the first results of the study in 2014 suggested that the particles are safe to be further studied for human cancer diagnostics.[12] While the non-porous silica shell in the C-dots effectively protect the encapsulated dye molecules, nanoparticle-based drug carrier systems protect the drug from degradation and increase the bioavailability of the drug by controlled and targeted release, thus optimizing the efficacy and decreasing the side effects.[13,14]

One of the main advantages of silica nanoparticles is the rather easy surface-functionalization, which enables tailoring of the surface charge and chemistry, allowing the nanoparticles to be customized for specific applications. Surface functionalization is a critical parameter for optimal biocompatibility and biodistribution, as well as for further attachment of targeting ligands or other active moieties. Due to the flexibility and biocompatibility of the silica material, it can also be utilized as coating material for other core materials,[15] such as for SPIONs, to enable them for biomedical use. Except for the relatively straightforward further functionalization of silica surfaces, a silica coating can also increase the hydrophilicity of inorganic nanoparticles, and thus enhance the dispersibility of the nanoparticles in aqueous media, which is essential for biomedical applications.

Nanoparticle platforms enables highly sophisticated diagnostic and therapeutic tools, and are an emerging field of research both in the academics and in the clinics. However, there is still a wide range of biological questions that need to be tackled, in addition to the necessity of continually improving the nanoparticle-tools and the experimental approaches. In this thesis, the researched work focused on the design of various silica-based nanocomposites, and the evaluation of surface functionalizations for controlling the nanoparticles' bio-behavior. Further the applicability of these nanomaterials was verified for delivery of active compounds (imaging agents/drugs) by different means, as well as the opposite; to scavenge tracer compounds *in vivo*.

2 LITERATURE REVIEW

2.1 Nanoparticles as imaging agents

Recent developments in the field of biomedical imaging have shown a great potential of nanoparticles as imaging agents, as they can be specifically designed to meet a wide range of application criteria.[16] There are several demands on good imaging probes: the transit to the target site and consequent binding should be highly specific with none or low non-specific accumulation, the unbound probes should be rapidly eliminated, and they should enable highly sensitive detection.[17] The majority of the currently used imaging probes in clinics are organic molecules or metal-organic compounds, which suffer from photobleaching, weak contrast effect, and short circulation time *in vivo,* which subsequently results in poor targeting efficiency and imaging enhancement.[18]

Nanoparticles are promising candidates for fulfilling the needs of good imaging probes.[19,20] The key advantages of nanoparticle-based probes are their multimodality and multifunctionality. Nanoparticles can be inherently detectable and/or function as carriers for imaging agents, and consequently produce signals for more than one imaging technology (multimodality). Nanoparticles have a large surface area that can be functionalized to introduce several targeting moieties, as well as drugs for theranostic purposes (multifunctionality). Owing to the targeting ability, nanoparticles might even be designed to detect micrometastases usually missed by conventional imaging methods.[21]

However, there are many challenges to overcome in the development of novel imaging probes intended for *in vivo* applications. In order to increase the probability of nanoparticle accumulation at the target site, long blood circulation time is important.[22,23] One of the biological barriers which the nanoparticles need to elude is opsonization by the reticuloendothelial system (RES), also known as mononuclear phagocyte system (MPS).[24] RES is part of the immune system and consists of phagocytic cells, which may bind nanoparticles and increase their clearance from the blood circulation. Biomolecules, such as proteins, may also bind to the surface of the nanoparticles and create a "protein corona" around them, thus also increasing the clearance from the blood circulation via recognition by the immune system. An optimal design of the nanoparticles (size, shape and surface chemistry) are of outmost importance for their *in vivo* behavior, especially for the circulation time.[25] Surface modifications, with e.g. polymers, may provide "stealth" properties to the nanoparticles and thus permit escape from the RES.[26] However, if the target is one of the RES organs (liver, spleen, lymph node, or bone

marrow) the nanoparticles can instead be designed to easily be recognized and internalized by macrophages, abundant in these organs.[27]

Another important aspect to consider is the biocompatibility of the nanoparticles. Biocompatibility is defined by IUPAC as "an ability to be in contact with a living system without producing an adverse effect".[28] The definition is for polymeric systems but can as well be applied for inorganic nanoparticles. A challenge here is the lack of adequate techniques to validate the toxicity from the nanoparticles.[29] Further, most of the toxicology assays are short-term and might not provide a reliable long-term toxicity. Consequently, the long-term toxicity and safety of nanoparticle-based imaging probes need more thorough evaluation by novel or optimized methods. An overall enhanced understanding of the interaction between nanoparticles and biological systems is a challenge that has to be addressed, in parallel with the development of novel multimodal and multifunctional nanoparticle-based imaging probes, to increase the possibility for a successful clinical translation.

2.1.1 Inherently detectable nanoparticles

Inorganic nanoparticles are one of the most studied materials for imaging due to their inherent detectability by various imaging techniques.[18] Superparamagnetic iron oxide nanoparticles (SPIONs) for magnetic resonance imaging, quantum dots for fluorescence imaging and gold nanoparticles for photoacoustic imaging, have been extensively studied.[30] Out of these, the SPIONs are probably the most studied imaging agent and are also available on the market as clinical contrast agent.[31,32] These nanoparticles have primarily been used for negative contrast enhancement by darkening T_2-weighted images in MRI, but have also been proven to provide positive contrast enhancement in T_1-weighted scans and thus offer an advantage over the potentially toxic gadolinium chelates.[33] SPIONS have generally been associated with low toxicity. SPIONs are reported to intracellularly be metabolized in the lysosomes into a soluble non-superparamagnetic form of iron, which is further taken up into the normal iron metabolism pathway and thus becoming part of the normal iron pool.[34] However, there are still some toxicological issues that must be considered, such as oxidative stress, especially after repeated or high doses of SPIONs.[35] With the recent advances in the development of imaging agents, there are also several newer nanoparticle probes, such as upconverting nanoparticles[36] and carbon-based nanomaterials[37,38] (nanodiamonds, carbon dots and carbon nanotubes).

2.1.1.1 Core-shell nanoparticles

One step in the direction towards multifunctional imaging probes is the development of core-shell nanoparticles. These nanoparticles consist of layers of two or

more materials with specific functionalities arising from the different layers.[39] Taking SPIONs as an example, without any surface coating they tend to agglomerate and precipitate in a physiological environment. The three key design considerations for the surface modification of the nanoparticles are the colloidal stability (during both preparation and storage), biocompatibility and blood half-life. SPIONs have mostly been coated with natural polymers (gelatin, dextran, chitosan etc.) or synthetic polymers (such as poly(ethylene glycol) (PEG), poly(vinyl alcohol) (PVA), poly(vinyl pyrrolidone) (PVP), poly(lactic-co-glycolic acid) (PLGA), polyethyleneimine (PEI)).[27]

Lately, inorganic coating materials, such as silica, titania and zeolites, have been highlighted as the most exploitable.[40] Out of these, silica is the material which is most widely used for coating of core-particles, due to its excellent physical and chemical properties.[41,42] Since the silica shell is hydrophilic, it enhances the dispersion of particles in aqueous media, which is critical for most biomedical applications. Owing to the simple and versatile methods for silica synthesis, the silica shell can be either nonporous to protect the core material and serve as a base for further functionalization, or porous to enable loading of bioactive substances such as drugs or imaging agents. However, a problem when designing a multimodal core-shell imaging probe, such as a magnetic-fluorescent nanoparticle, is the risk of quenching of the fluorophore by the magnetite core since it strongly absorbs the transmitted light.[43] Then, a silica shell can be utilized as an effective barrier between the magnetic core and the fluorophores by controlling the thickness of the silica shell. The high surface area of a porous shell may also enhance the degree of further surface functionalization. Moreover, as silica is optically transparent it is suitable for coating of optically active core materials, in the same time as promoting the biocompatibility. Due to the versatility, silica has been widely studied for development of different kinds of nanocomposites. Hollow mesoporous silica nanoparticles have attracted great attention due to their unique features, such as low density, large surface area and high cargo-loading capacity,[44-46] also presented in supporting publication i. The development of core-shell and hollow nanostructures has also recently advanced into a hybrid structure, namely yolk-shell nanoparticles, where a core particle is freely movable inside a hollow shell; thus generally represented as a core-void-shell nanostructure.[47]

2.1.2 Nanoparticles as carriers for molecular imaging agents

Nanoparticles which are not inherently detectable can be utilized as carriers for imaging agents, taking advantage of the same properties as those making these nanoparticles excellent for drug delivery purposes. The imaging agents can be incorporated into the bulk/pore network of the carrier or attached to the surface.

The advantages of using nanocarriers for molecular imaging agents include their ability to overcome problems of solubility and chemical stability, to protect the active compounds from biodegradation or excretion, to improve distribution and targeting, and even to release their payload on-demand.[48] Earlier studies of nanocarriers intended for medical use have mostly involved lipid- and polymer-based nanoparticles. Later there has been a growing interest in inorganic nanocarriers, since these offer the advantage of being extremely robust, and thus very stable and highly resistant to enzymatic degradation.[49]

2.1.2.1 Silica nanoparticles

Silica nanoparticles offer the advantage of being one of the most biocompatible nanocarriers. Other advantages of silica nanoparticles are their well-defined and tunable structures in terms of size, morphology and porosity. They can easily be synthesized from inexpensive starting materials and functionalized by well-established siloxane chemistry.[50] Further, silica nanoparticles are hydrophilic, which is a must for any *in vivo* application. This is due to the extent of silanol groups on the silica surface.[51]

The two major classes of silica nanoparticles are the solid non-porous and the mesoporous (MSNs) nanoparticles. MSNs are ideal platforms for encapsulating traditional organic fluorophores. Due to the large amount of dye molecules which can be entrapped, the signal strength increases and, consequently, also the sensitivity. The encapsulation also improves the dye molecules' resistance to photobleaching, which enables long-duration imaging of tumor cells and tissues.[52,25] However, depending on the design of the silica nanoparticle-platform and the application of it, the possible self-quenching phenomena[53] of the fluorophores upon close contact on the particle surface has to be considered. Dye molecules can be incorporated into the MSNs by postsynthesis methods, either physical adsorption to the pore walls or chemical conjugation. For both non-porous and porous nanoparticles, dye molecules can also be entrapped into the silica matrix by covalently linking the fluorophore to a silica precursor prior to the synthesis. C-dots[54] and FloDots[55] are two examples of imaging probes, where nonporous silica nanoparticles have been doped with fluorescent molecules (both hydrophilic and hydrophobic). However, a drawback with nonporous fluorescent silica nanoparticles is the dye-rich core, with might lead to aggregation-induced self-quenching of the dye. This can be circumvented by using porous nanoparticles, where the dye molecules can be easily separated from each other on the large surface. Nevertheless, the maximum dye loading degree before fluorescence self-quenching starts to occur should be determined.[51] Due to all this flexibility of the silica material, silica nanoparticles are ideal platforms for development of multimodal imaging probes.

2.1.2.1.1 Fabrication of silica nanoparticles

Silica nanoparticles are a type of colloidal amorphous metal oxide. Metal oxide nanoparticles are produced via two main manufacturing methods; top-down (breaking down a bulk material into smaller components) or bottom-up (self-assembly of molecular precursors into larger structures) fabrication. Both of these methods require energy, and the resulting nanoparticles are reactive and might either grow or dissolve (Figure 1).[56] The energy can also be released via aggregation of the nanoparticles or surface adsorption of proteins or polymers.

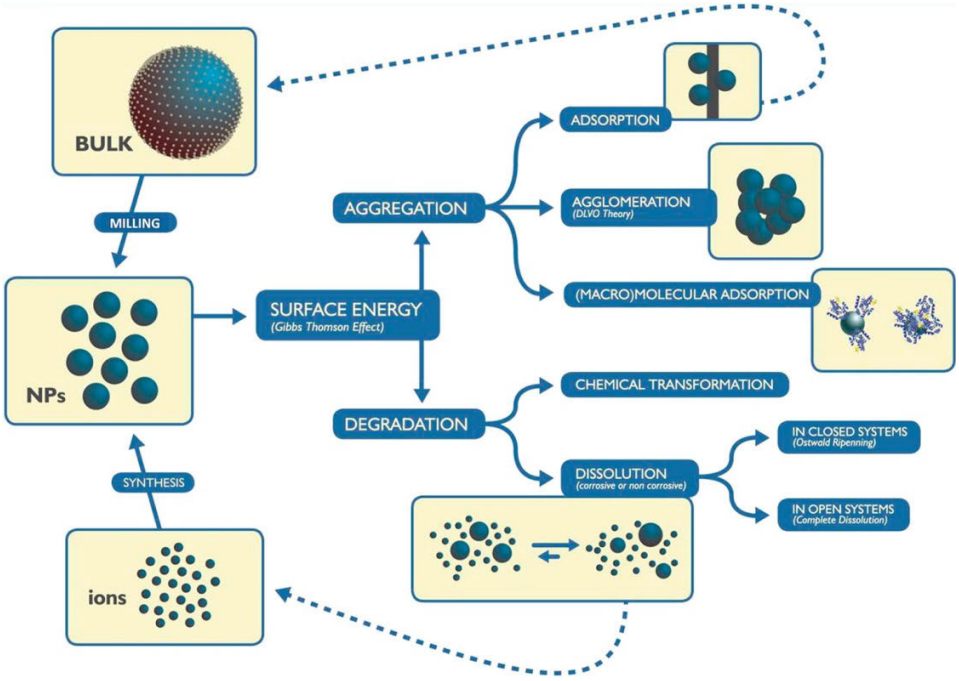

Figure 1. *Overview of the cycle of nanoparticles fabricated through either bottom-up or top-down process. Silica nanoparticles are normally synthesized by a bottom-up, nucleation and growth process in a closed system, thus realized by the so-called Ostwald ripening. Reprinted from Bogart, L. K., et al. ACS Nano 2014, 8 (4), 3107, with permission from ACS. (Further permissions related to the material should be directed to the ACS.)*

Silica nanoparticles are normally synthesized by sol-gel processing, a bottom-up method, which is a wet-chemical technique starting from conversion of molecular precursors into a colloidal solution (sol) which further evolves towards an integrated network (gel) of either discrete particles or network polymers. Non-porous silica nanoparticles are normally prepared through either Stöber, or reverse microemulsion methods.[51] The Stöber method is the most widely used syn-

thetic approach for preparing monodisperse silica nanoparticles involving controlled hydrolysis of a silicon alkoxide precursor (normally tetraethylorthosilicate) into silanol groups using ammonia as catalyst in a mixture of water and alcohol, followed by condensation of the silanol groups or of silanol groups and ethoxy groups into siloxane bridges (Si-O-Si) that form the entire silica structure.[57] It is a one-step process where hydrolysis and condensation (with either alcohol or water as by-product) occur simultaneously via the following reactions (where R is an alkyl group):

$$\underset{hydrolysis}{\equiv Si - OR + H_2O} \rightleftharpoons \underset{esterification}{\equiv Si - OH + ROH}$$

$$\equiv Si - OR + HO - Si \equiv \underset{alcohol\ condensation}{\rightleftharpoons} \equiv Si - O - Si \equiv \underset{alcoholysis}{+ROH}$$

$$\equiv Si - OH + HO - Si \equiv \underset{water\ condensation}{\rightleftharpoons} \equiv Si - O - Si \equiv \underset{hydrolysis}{+H_2O}$$

The microemulsion methods are modifications of the Stöber process. In the reverse microemulsion method the silica nanoparticles are grown inside reverse micelles in a water-in-oil microemulsion.[58] The size of the nanoparticles can be altered by varying the concentration of silica precursor, water/alcohol ratio, temperature, and pH. The hydrolysis reaction can be catalyzed by either acids or bases. Under basic conditions it is easier to obtain homogenous silica particles since the condensation of silica species are reversible. Highly acidic conditions, on the other hand, lead to rapid hydrolysis and precipitation of the particles, which often results in poly-disperse particles.[59]

The formation of silica particles at basic conditions can be divided into two stages: an initial burst of nucleation following a growth of the particles through Ostwald ripening (Figure 1). Oswald ripening is a phenomenon where larger particles in a solution grow from silicic acid dissolved from smaller particles, due to the difference in solubility between different sizes of particles. Smaller particles have higher surface energy due to the high surface-to-volume ratio, thus enabling them to dissolve at an accelerated speed through cleavage of siloxane bridges at the surface. The dissolved material subsequently deposits onto larger particles.

The solubility of silica is highly dependent on both the temperature and pH, where both the silica solubility and dissolution rate are maximized at or above pH 7.[60]

The fabrication of mesoporous silica materials was first reported by Yanagisawa in 1990, and later, in 1992 the more well-known M41S family of periodically ordered mesoporous silica materials was developed by researchers at Mobil Oil Company. The most studied mesoporous silica candidate from the M41S family is the MCM-41 material with a two-dimensional cylindrical hexagonal pore structure (as shown in Figure 2). Here, the use of supramolecular aggregates of ionic surfactants as structure-directing agents (SDAs) leads to the assembly of an ordered mesostructured material during the condensation of the silica precursor under basic conditions with subsequent removal of the SDA by extraction or calcination.[61] The same principles as for the Stöber process employ for the growth of the mesoporous particles.[51]

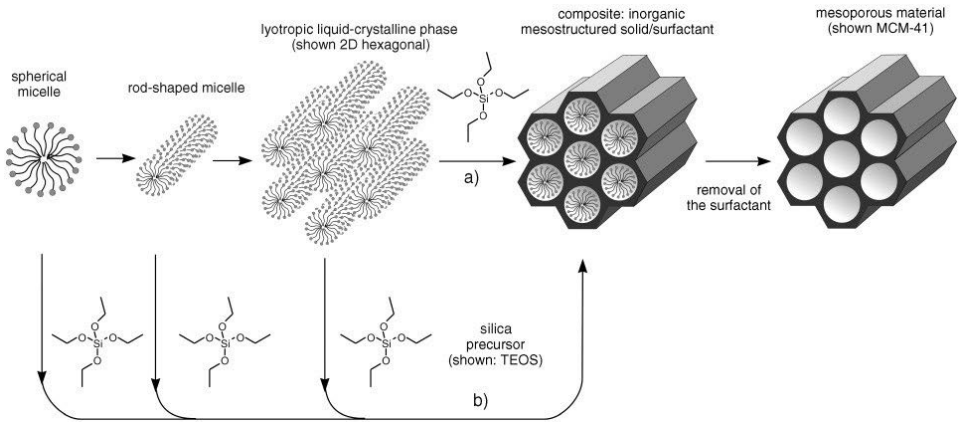

Figure 2. *Formation of mesoporous silica materials by structure-directing agents: a) true-liquid-crystal template mechanism, where the surfactant concentration is high enough to self-assemble into a lyotropic liquid-crystalline phase without the presence of a silica precursor, and b) cooperative liquid-crystal template mechanism, where the already added silica precursor co-assemble with the surfactant molecules. Reprinted from Hoffmann, F., et al. Angewandte Chemie International Edition 2006, 45 (20), 3216, with permission from John Wiley and Sons.*

Based on these early results, MCM-41 type materials are widely studied and synthesized. Mostly tetraethoxysilane (TEOS) has been used as silica precursor and the cationic cetyltrimethyl ammonium bromide (CTAB) as SDA, under alkaline conditions, which leads to materials with mesopore dimensions of 3-4 nm.[62]

The synthesis procedure has also been varied, for example by using triblock co-polymers as SDA under acidic conditions for fabrication of the so-called SBA silica materials.[61]

A lot of effort has been put on increasing the pore size of MSNs (as well as of silica coatings) to efficiently encapsulate larger substances, such as proteins and nucleic acids. This can easily be realized for larger particles, where auxiliary organics such as trimethylbenzene (TMB) has been used as pore swelling agent. For smaller particles it is more challenging, since these syntheses often involve dilute conditions and co-solvents such as alcohols, whereas the swelling agent may be dissolved rather than solubilized in the micelles.[62] Here, SBA-15 type syntheses can be utilized, using polymeric surfactants such as block-co-polymer P123 under acidic conditions.[63]

In order to prevent aggregation of the primary silica nanoparticles during synthesis, the synthesis can either be performed under highly diluted conditions, or by the addition of particle growth quenchers, such as non-ionic surfactants or polymers, fluorocarbon-based cationic surfactants, triethanolamine or propanetriol. Finally, the SDAs are removed by either solvent extraction or calcination. A critical aspect here is the efficiency of template removal, since the most used surfactant, CTAB, is cytotoxic. Calcination is an efficient template-removal process but can easily lead to aggregation of the particles.[62]

2.1.2.1.2 Surface functionalization and bioconjugation of silica nanoparticles

The surface of silica nanoparticles is covered by siloxane groups (≡Si-O-Si≡), with the oxygen on the surface, or one of several forms of silanol groups (≡-Si-OH). Silica surfaces covered with mostly silanols (or hydroxyls, -OH) are highly hydrophilic, which is the case for silica nanoparticles synthesized by standard procedures with subsequent solvent extraction used as template-removal process. If calcination (heat treatment) is used for the template-removal, more siloxane groups are presented on the surface (Figure 3), yielding more hydrophobic properties.[64]

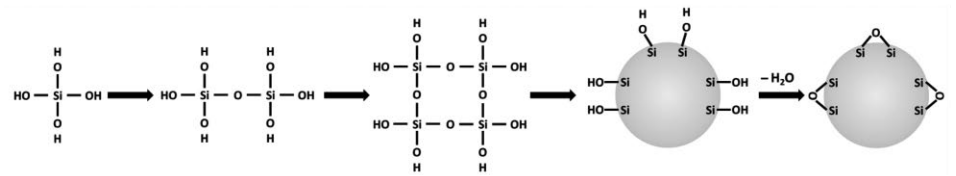

Figure 3. *Condensation polymerization of a silica precursor into silica particles, surface covered by silanol groups. Siloxane groups can form on the surface as a result of dehydroxylation of the silica particles.*

Modification of the silica surface through organic linkers is often necessary for conjugation of biomolecules and contrast agents. Common organic linkers are amino, thiol and carboxyl groups. Amines are positively charged at physiological pH, and primary amino groups can form amide bonds with carboxyl groups, which in turn are negatively charged at physiological pH. The amide bond formation does however not occur spontaneously, and consequently a crosslinking reagent to active the carboxylic acid prior to the reaction with the amino group is needed. The most commonly used reagents for the activation of carboxyl groups are the carbodiimide EDC, 1-Ethyl-3-(3-dimethylaminopropyl)carbodiimide, together with NHS, N-hydroxysuccinimide, which converts the hydroxyl group into a good leaving group.[49] Both amines and carboxylic acids are typically present on biomolecules. Amino groups also offer facile linker chemistry with the frequently used isothiocyanate functionalized molecules, most widely utilized to bind hydrophilic fluorophores. Thiols, on the other hand, are often used to form disulfide bridges. Here a useful reagent is SPDP, N-succinimidyl 3-(2-pyridyldithio)-propionate, which covalently links amino and thiol groups by a redox-cleavable disulfide bond.

The reactive functional groups needed on the silica surface can be introduced by either a co-condensation process or post-synthesis grafting. The inner surface, i.e. the pore walls, of MSNs is normally modified through co-condensation of the silica precursor with an organosilane source, where one or two of the alkoxy arms of silicon are replaced by an organic moiety. The most commonly used silanes have amino or thiol groups at the end of the alkylsilane.[59] Even though co-condensation provides uniform distribution of functional groups, both on the inner and outer silica surface, post-synthesis surface modification (organosilanes grafted onto free silanol groups), is preferable in order to maintain the size-distribution and morphology of the nanoparticles during synthesis.

Except for the co-condensation and post-grafting methods to introduce amino groups on the silica surface, it can also be modified with surface grown poly(ethylene imine) (PEI),[65-67] which yields much larger amount amino-groups on the surface. With this method PEI is grown directly from the surface silanol groups in a one-step acid catalyzed hyperbranching polymerization, where the highly reactive molecule aziridine is used as precursor (Figure 4). In addition to the large amount of reactive sites for further bioconjugation that the hyperbranched PEI-layer provide, it also enhances suspension stability. Since the PEI polymer is covalently attached on the surface, it is also ensured that it remains there throughout additional functionalization steps as well as during application,

in comparison to the widely utilized highly branched PEI polymers that are only physically adsorbed on the particle surface.

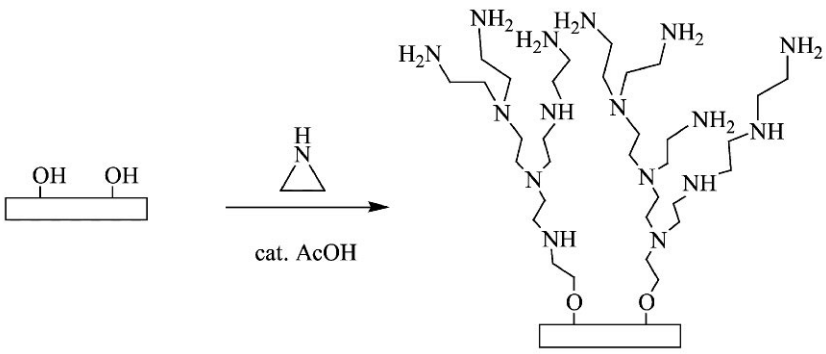

Figure 4. *Schematic representation of the ring-opening polymerization of aziridine on a silica surface, resulting in a hyperbranched PEI layer.*[68] *Reprinted from Kim, C. O., et al. Journal of colloid and interface science 2003, 260 (2), 374, with permission from Elsevier.*

Another widely used polymer for stabilizing nanoparticles in biological fluid, and thus increase the biocompatibility, is polyethylene glycol (PEG) polymer. Two different polymers can also be covalently bound to each other, in order to utilize the specific advantages of both of them. Here PEG-PEI co-polymer is a good candidate. These polymers are discussed more in detail in section 5.1 (PEI) and 5.2.2 (PEG).

Conjugation of biomolecules to nanoparticles can either be covalent, as already described, or noncovalent. Noncovalent conjugation includes electrostatic attachment, other forms of adsorption, and encapsulation. The five general procedures routinely used for bioconjugation are compiled in Figure 5, with a peptide as a model compound. In the case of electrostatic interaction, opposite charges on the particle surface and the peptide are interacting to mediate a charge-based assembly. Direct interaction includes covalent and dative chemistry, where dative bonds are not as strong as covalent ones and can be compromised by for example changes in pH. Thiol groups are an example of a functional group that provides an efficient mean of utilizing dative covalent bonding due to their electronegativity. Secondary interactions involve the specific ligand-receptor interactions, out of which biotin-streptavidin interaction is the most well-known. Covalent chemical attachment to surface ligands utilizes the classical bioconjugation chemistry as discussed above. Encapsulation incorporates the compound, the peptide in this case, into the nanoparticle matrix, either during synthesis or after the nanoparticle is formed.[69]

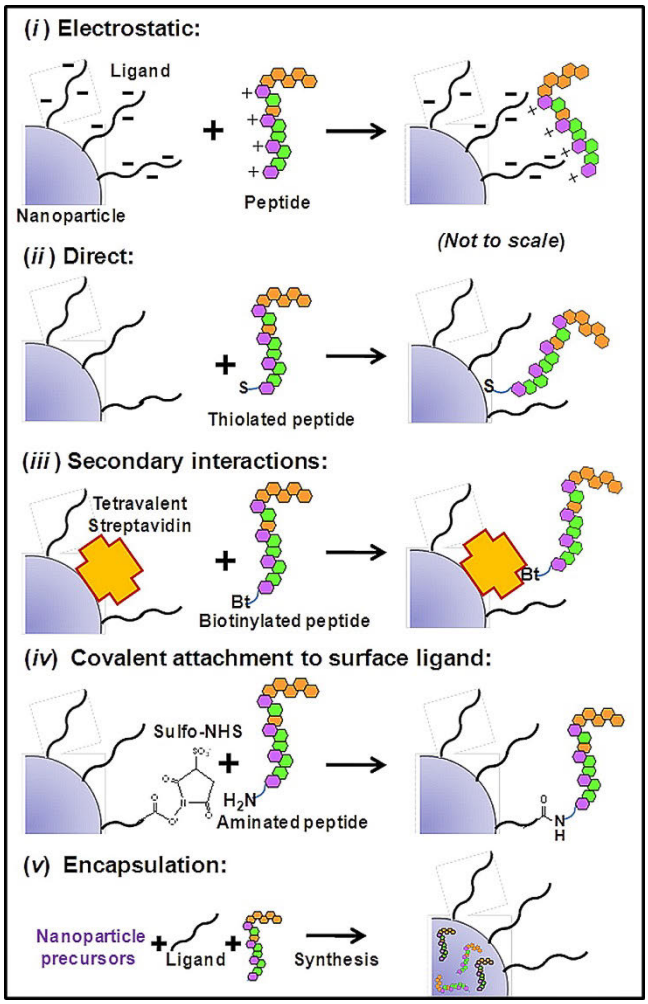

Figure 5. *Schematics of the commonly used bioconjugation methods, here illustrated by the use of a peptide. Reprinted from Sapsford, K. E. et al. Chemical reviews 2013, 113 (3), 1904, with permission from ACS. Copyright 2013 American Chemical Society.*

2.2 Imaging modalities

Non-invasive bioimaging techniques are a powerful tool for diagnosis of various diseases, as well as the disease progression and eventual drug response. With the help of imaging modalities, whole *in vivo* systems can be visualized to provide anatomical, physiological, and molecular information. A range of different imaging modalities are available and the selection of the right modality for a specific study is dependent on the biochemical processes one wants to visualize or the type of data one wants to obtain. The classical imaging modalities include optical imaging, magnetic resonance imaging (MRI), computed tomography (CT), ultrasound

(US) and positron emission tomography (PET) or single photon emission computed tomography (SPECT). Since the modalities are based on different underlying physical principles, each of them has its own unique advantages and disadvantages with respect to sensitivity and specificity to contrast agents, tissue contrast, spatial resolution, quantitativeness, tissue penetration and cost. The characteristics of the imaging modalities frequently used in the clinical practice or preclinical research are shown in Figure 6.[70]

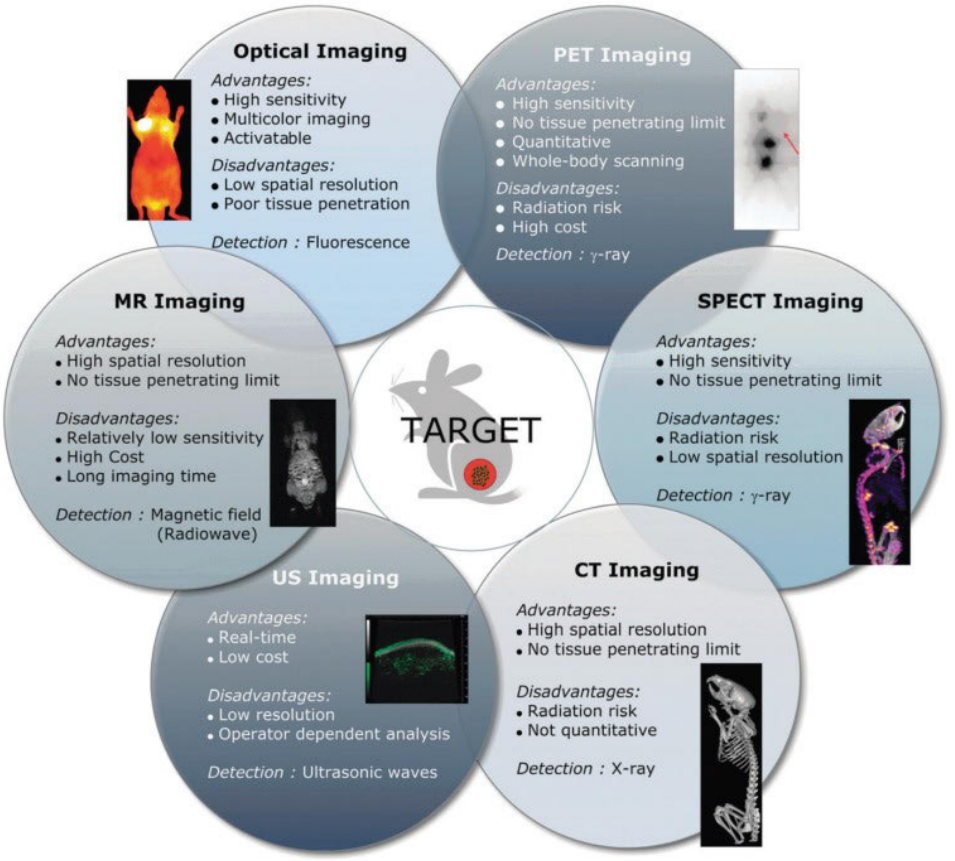

Figure 6. *Characteristics of non-invasive imaging modalities used for biomedical applications. Reprinted from Lee, D.-E., et al. Chemical Society Reviews 2012, 41 (7), 2656, with permission from RSC.*

MRI is one of the most versatile and powerful diagnostic tools due to its high spatial and anatomical resolution. MRI uses a powerful magnet and radiofrequency energy to image the internal structure and soft tissue morphology in the body, by visualizing the spins of specific atomic nuclei. It has enough penetration depth to image the whole human body. However, MRI does not have the most

favorable sensitivity, the quantification procedures are relatively difficult, and it is also relatively expensive and time-consuming to use.[71,72] Optical modalities are used to image more local processes and can readily make use of multiple labels. The most commonly used optical technique is fluorescence imaging, which might be the next widespread imaging technique after MRI.[73] Optical techniques have been the fastest growing way to image small animals, especially for evaluating the biodistribution of nanomedicines, and it is an emerging field in the clinics. The drawback with this technique is that light is scattered and adsorbed quickly within the body, which also limits the spatial resolution and tissue penetration.[74]

CT is an X-ray-based imaging technique and generates anatomical images when tissues in the body absorb X-rays differentially, depending on the density of the different tissues. Unlike the traditional two-dimensional X-ray examinations, CT creates three-dimensional anatomical images.[75] CT scans can clearly visualize highly electron dense (hard) tissues, such as the skeletal structure of the body, and distinguish these from soft tissue and air cavities. However, the differentiation of morphological structures between normal and pathological tissues, such as tumors, is limited without contrast agents.[76] The current CT contrast agents are usually based on iodinated small molecules. These are generally safe, but due to the fast renal clearance of these molecules, large dosages have to be used, which may cause serious renal toxicity. Due to that, nanoparticles loaded with the iodinated organic compounds have been designed, to prolong the *in vivo* circulation time and enhance the localized concentrations.[72] Also the use of nanoparticles with a high atomic number, such as gold, as CT contrast agents is emerging. Overexposure to X-rays can be harmful, thus also limiting the number of scans that can be performed, which is therefore a limitation of the CT technique. However, the advances in the X-ray detector sensitivity will allow for significant dose reductions.[71]

PET and SPECT are radionuclide-based imaging techniques that enable evaluation of biochemical changes such as metabolic parameters, and can be sensitive to detection of high-metabolism tumors and infections.[76] Both of the techniques build up the three-dimensional images by detecting gamma-rays (γ-rays) emitted from the radioactive isotopes, without external excitation. The main difference between PET and SPECT imaging is the type of radionuclides used. While SPECT scans detect single gamma rays ("single photon emission", SPE), the decay of the radionuclides used in PET imaging produces positrons ("positron emission", PE).[77] The emitted short-lived positron collides with an electron, an event known as annihilation. This annihilation produces energy in the form of two photons, both with the same energy of 511 keV, that shoot off in opposite directions. Many isotopes have short half-lives, and since the isotopes mostly are produced

in a cyclotrone, a cyclotrone source needs to be located near the imaging facility, which makes it more costly.[76] Different radioisotopes are used for SPECT imaging, which all emit different γ-rays of different energies, making it possible to image multiple biochemical targets simultaneously. Both of the techniques have limitless depth of penetration and enable whole body imaging with high sensitivity. Since SPECT is less costly as compared to PET, it is generally less sensitive and has a lower spatial resolution. Both techniques have a clear diagnostic advantage over anatomical techniques (such as CT and MRI), since biochemical changes normally occur before anatomical changes in the disease progression. In addition, unlike MRI and optical imaging, both PET and SPECT only require very small mass amounts of the radionuclide-based imaging agent, and due to that the imaging agents are normally nontoxic and unlikely to exert pharmacological effects. However, due to the ionizing radiation, there is a limit to how many scans a subject can have per year.[71]

US imaging is based on backscattered signals from high-frequency sound waves, as they travel through biological tissue. Depending on the deviations in reflection by the different tissues, a clear two-dimensional image can be generated.[72] The resolution of the images can be improved significantly by using higher frequencies, but then at the cost of the penetration depth. Thus, the operator needs to consider resolution versus depth, depending on the required data.[71] Contrast agents are needed for enhancing the reflection signal-to-noise ratio. Gas-filled (air or perfluorocarbon) microbubbles encapsulated by lipids or biopolymers are normally used as US contrast agents. The difference in refractive index between gas and liquid phase cause the microbubbles to appear brighter than the background. However, the microbubbles with soft shell persist only for a short time interval in the tissues. Also, their large sizes and broad size distribution limit their use. Here, hollow mesoporous silica nanoparticles are emerging as US contrast agents.[78,79] Advantages of US include its relative cost effectiveness and good safety profile.

Newer imaging technologies, such as intravital microscopy (IVM),[80] photoacoustic imaging (PAI),[81] and magnetic particle imaging (MPI),[82] are also developing. IVM is an optical imaging platform similar to the traditional fluorescence microscopy, but with modified instrumentation allowing visualization and real-time examination of a living animal. PAI is an imaging technique that integrates optical and ultrasound imaging based on the photoacoustic affect, which can be described as the production of sound waves resulting from the absorption of light. MPI is a technique by which it is possible to determine the location of magnetic nanoparticles. The nanoparticles emit a time-dependent magnetization under an

external magnetic field, and these electromagnetic signals are detected and converted into MPI images. MPI is a quantitative technique because the signal intensity is directly proportional to the concentration of nanoparticles. MPI has no background signal. MPI is used in combination with MRI, as a multi-modal technique using only magnetic nanoparticles as contrast.[83]

2.2.1 Optical imaging

Optical imaging methods, such as fluorescence and bioluminescence imaging, are widely used in preclinical work because of its ease of use and cost effectiveness. While bioluminescence relies on photon emission based on natural biochemistry, such as enzymatic reactions found in different organisms, fluorescence needs photons as energy source. External light is used to excite fluorescent molecules at a certain wavelength. When the molecule absorbs these photons, its electrons are excited to a higher energy level. As the electrons return from the excited state to the ground state, vibrational energy is lost, and subsequently the emitted light is shifted to longer wavelengths (Stokes' shift).[84] Fluorescent molecules have long been used as contrast agents for fluorescence imaging, but due to their problems of photobleaching, nanoparticles doped with organic dye molecules have been developed. Silica nanoparticles are ideal for this application, and have been widely studied,[85-87] since the silica matrix is transparent in the UV-vis and NIR regions of the electromagnetic spectrum thus not interfering with the dyes.

A large variety of fluorescence imaging techniques and methodologies have been developed, including confocal microscopy, near-infrared fluorescence (NIRF) imaging, two-photon microscopy, and fluorescence resonance energy transfer (FRET) imaging, to name a few. Confocal microscopy is a specialized form of normal fluorescence microscopy that uses specific optical components to generate high-resolution three-dimensional images.[88] However, the utility of *in vivo* fluorescence imaging has been limited by the poor penetration depth of light in tissues, as well as the decreased spatial resolution due to autofluorescence and light scattering within the body. To overcome these problems, excitation light in the near-infrared (NIR) spectral range can be used, since living tissues have increased optical transparency at NIR wavelengths.[89] In an experiment of whole-mouse illumination, photon counts in the NIR range where about four orders of magnitude higher than those in the green light range under similar conditions.[84] NIRF imaging can thus improve the imaging depth along with sensitivity and specificity. Compared with other imaging techniques, NIRF imaging possesses several advantages such as user-friendliness, low cost, and utilization of nonionizing radiation.[90] Therefore, development of NIR probes and techniques for applications in fluorescence imaging is important for successful *in vivo* optical imaging

and future clinical applications. Two-photon microscopy is an example of an imaging technique where NIR light can be utilized. Two-photon imaging is based on the anti-Stokes' emission process, which generates emission light with a shorter wavelength than that of the excitation light, by simultaneous absorption of two photons (see Figure 7). In addition to the already mentioned advantages of using NIR light, it also significantly reduces the photoinduced damage of the fluorophores used.[89]

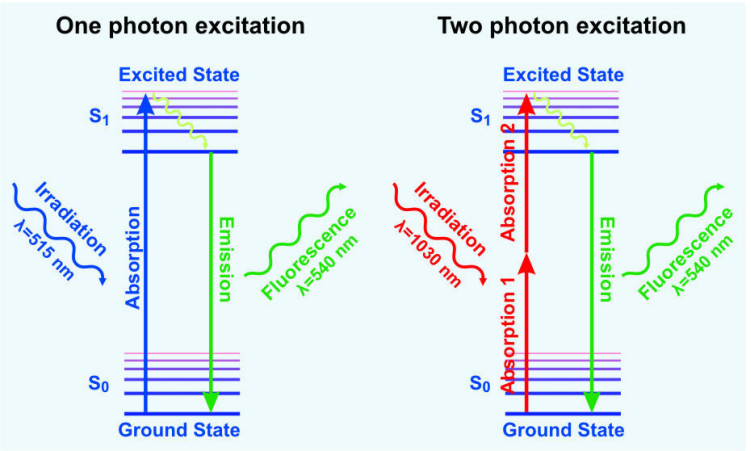

Figure 7. *Schematic illustration of one vs. two photon excitation. Adapted from Candle, Synchrotron Research Institute, www.candle.am.*[91]

FRET imaging is a well-established fluorescence technique used to study molecular interactions below the optical resolution limit of microscopes, by utilizing non-radiative energy transfer from an excited donor molecule to an acceptor molecule. The efficiency of this process depends on distances of typically 1–10 nm, and is thus one of few tools available for measuring changes in distances on a nanometer level. Among many applications of this technique, it has extensively been used for studying cleavage of covalent bonds by intracellular processes.[92,93]

When it comes to clinical applications, fluorescence imaging can still not compete with the other imaging modalities (MRI, CT, PET, SPECT), due to the limitations in tissue penetration and problems with both excitation and emission light getting scattered and absorbed within the body. However, the advantages, such as its user- and cost-friendliness, sensitivity, safety due to no use of radioactive materials, have made it very popular and useful within preclinical studies. Fluorescence imaging has emerged as a real-time modality for the visualization, localization, and measurement of bioactive molecules and molecular processes and

thus having a big impact on the understanding of disease progression and therapeutic response.[84]

2.2.2 Magnetic resonance imaging

MRI is considered one of the foremost diagnostic whole-body imaging modalities and is widely used in the clinics. The advantages of MRI include high spatial resolution and strong soft tissue contrast, without any radiation risk (unlike CT, PET and SPECT) since only radiation in the radiofrequency range is used. However, the inherently poor sensitivity of MRI is a limiting factor, and in order to improve the detection of small biological targets, various exogenous MRI contrast agents have both been applied in the clinics and are being further developed.

During an MRI scan, a living subject is placed inside a tube surrounded by a circular magnet. The magnet creates a strong magnetic field that aligns the proton nuclear spins of hydrogen atoms parallel with the direction of the magnetic field. This generates longitudinal magnetization. The hydrogen atoms are then exposed to a beam of radiofrequency pulses, and as a result, the proton nuclear spins are resonantly excited and aligned antiparallel with the magnetic field. This induces transverse magnetization while decreasing the longitudinal magnetization. When removing the beam of radio waves, the hydrogen protons relax to their ground state by emitting a signal (a radio wave) and align parallel with the magnetic field. The protons in different tissues relax at different rates and are thus measured in two ways. The relaxation proceeds either via T_1 longitudinal relaxation, which is the time taken for the magnetic vector to return to its resting state (longitudinal magnetization recovery), or T_2 transverse relaxation, which is the time needed for the axial spin to return to its resting state. These relaxation processes are detected and T_1-weighted (bright contrast) and T_2-weighted (dark contrast) images are generated. Since the different types of biological tissues, such as fat and water, have different relaxation times the signal strength is varying which causes the tissues and organs to show characteristically distinct contrast. Often this natural contrast difference between the target (pathological) tissue and the surrounding is not enough, and has to be increased by MRI contrast agents, which can accelerate the T_1 or T_2 relaxation rate.[83,94]

The contrast agents influence the MRI signal intensities around them by changing the T_1- and T_2-relaxivities by nearby protons. T_1 agents increase the signal intensities around them, showing bright contrast, and are therefore called positive contrast agents. T_2 agents, on the other hand, decrease the signal intensities, showing dark contrast, and are thus called negative contrast agents.[76] The relaxivity values, r_1 and r_2, are the parameter used to quantify the effect of the contrast

agents, and is the change in $1/T_1$ and $1/T_2$ or protons per concentration of the contrast agent.[49]

Paramagnetic metal ions commonly used for contrast in MRI are gadolinium (Gd^{3+}), manganese (Mn^{2+}), and iron (Fe^{3+}). Gadolinium-containing nanoprobes are the most popular T_1-contrast agents, and have mostly been used as chelates with DTPA (diethyltriamine pentaacetic acid) and DOTA (tetraazacyclododecane tetraacetic acid).[49] In order to achieve a contrast enhancement out of these ions, a relatively large local concentration is needed, and there is a major concern of toxicity of released gadolinium ions. To overcome the problems of toxicity and still have a high dose, a large amount of the ions can be incorporated into nanoparticles. For this purpose, MSNs are an ideal platform, which has been studied in detail by Sen Karaman et al.[95] Preclinical studies have also used manganese oxide nanoparticles as alternatives to Gd-based agents[96] due to the concerns of the conventional gadolinium-contrast agents.

SPIONs, having an iron oxide core, are the most studied T_2-contrast agents both in preclinical and clinical MRI and have undergone or are in the middle of clinical trials in cancer patients.[34,97] One of the SPION used for the trials, ferumoxytol, is an already FDA-approved drug for anemia treatment.[98] The advantages of SPIONs are their low toxicity, large-scale production of diverse core sizes, and their superparamagnetic behavior, which is a necessary property for T_2 contrast agents. Due to the superparamagnetism, the nanoparticles can also be dragged by an external magnet.[99] Even if SPIONS have predominantly been used as T_2-contrast agents, they may also be customized to provide T_1-contrast enhancement, and offer an advantage over gadolinium-based agents due to their nontoxicity.[100] The magnetism of the nanoparticles can be controlled via size, composition, and shape, to enhance the MRI contrast effect. While large magnetization values are necessary for strong T_2-contrast effects, T_1-contrast effects arise from the magnetically disordered spin layers at the surfaces of the magnetic nanoparticles. The various numbers of unpaired electrons of metal ions at the nanoparticle surface effectively accelerate the T_1-relaxation process.[83]

Conventional MRI contrast agents typically serve as single-mode contrast agents, enhancing either the bright (T_1) or dark (T_2) signal. However, accurate interpretation of the images is yet difficult due to artifacts in the body, which can affect the MRI signals originating from the contrast agents.[99] Therefore, T_1-T_2 dual mode contrast agents have also been introduced,[101] for simultaneous acquisitions of positive and negative contrast. An advantage of these dual-mode contrast agents is that they enable self-confirmation of their signal enhancement. A T_1-T_2

dual-mode contrast agent can be constructed by conjugation of paramagnetic metal ions, such as gadolinium and manganese, to iron oxide nanoparticles.[102]

2.2.3 Multimodal imaging

Multimodal imaging is a powerful method that can provide more reliable and accurate information about the target. By combining advantages from two or more imaging modalities, and in the same time compensating for limitations from a single imaging modality, images with high sensitivity and high resolution can be accomplished.[70] There are many possible combinations for dual-mode and tri-modal imaging modalities, including MRI-optical, MRI-PET, PET-CT, optical-PET, MRI-CT, and MRI-PET-optical. Out of these, PET-CT imaging is frequently used in the clinics, with PET-MRI following as the next-generation technology.[103]

A promising dual-mode imaging strategy is to combine MRI and optical imaging. While MRI provides anatomical and physiological images with high spatial resolution, but low sensitivity, optical imaging provides physiological and molecular information with high sensitivity. Another advantage of such combination is that it is safe to be used in humans (even though the technique is still limited to small animal models), since both MRI and optical imaging are free from harmful radiation.[76] By using specific nanoparticle-based contrast agents for MRI-optical dual-mode imaging, much more information can be provided. Especially MRI-NIRF dual-mode nanoparticles are a promising combination. These contrast agents are made by incorporating iron oxide or gadolinium for MRI and NIRF imaging probes, such as synthetic fluorophores, fluorescent semiconductor nanocrystals, or upconverting nanomaterials, into the same nanoparticle.[104,105] The most studied approach to the formation of dual-mode imaging agents for MRI-optical imaging is via conjugation of an organic dye to the surface of an iron oxide nanoparticle. Except for the excellent MRI contrast effect of the iron oxide nanoparticles SPIONs, they have several advantages for nanomedicine, such as for hyperthermia. SPIONs also have low toxicity.

Diagnosis by MRI following by NIRF image-guided surgery has been reported, since MRI does not have enough sensitivity to delineate tumor margins during surgery. Key et al.[106,107] constructed multicomponent nanoparticles by conjugating glycol chitosan nanoparticles with the NIRF dye cyanine 5.5, and then physically loading SPIONs into the core of the nanoparticles. The contrast effect of the particles was evaluated in a murine bladder tumor in mice by both NIRF imaging and MRI and showed potential for dual-modality *in vivo* imaging with MRI detection of tumors and NIRF-guided surgery. Kircher et al.[108] studied the same concept, by labelling cyanine 5.5 to an iron oxide nanoparticle coated with cross-linked dextran. The dual imaging capability was demonstrated *in vivo* with

high sensitivity. Cha et al.[109] reported on an enzyme-triggered activatable MRI-optical imaging probe system, by utilizing the fluorescence quenching effect of SPIONs. An alternative approach for the formation of optical-MRI multimodal agents, which has been extensively reported in the literature, is through the use of a combination of quantum dots and SPIONs.[110,111]

When designing multimodal nanoparticle-based contrast agents, the differences in sensitivity of each modality must be considered to keep the amount of imaging agents in the nanoparticles at a suitable level. The contrast agents used for MRI and CT are needed at relatively high concentrations, while PET and NIRF agents can be used in extremely low concentrations.[70] However, bringing several imaging modalities together in the clinics can be far from straightforward. The magnetic fields of MRI interfere with the radioactivity of PET and SPECT, as an example. When it comes to combinations including optical imaging, the fluorescent labels must first be activated by light, which must also be accounted for. The imaging time is also a factor to consider. While optical imaging can be completed in a minute, an MRI scan can take hours. Despite these issues, multimodal imaging is a revolutionary technique where the advantages of using nanoparticles as contrast agents are maximized.[74] Multimodal imaging is also a very useful tool for drug development.[112]

2.3 Nanoparticles as drug delivery systems

Nanoparticles are not only used for imaging purposes, they are also applied to deliver therapeutic agents at the disease site. The same properties as making nanoparticles good carriers for imaging agents are utilized for creating excellent drug delivery systems. Nanoparticle-based carrier systems can improve the pharmacokinetic and pharmacodynamic profiles of conventional drugs and may thus optimize their efficacy.[48] When both the diagnostic and therapeutic agents are combined into a highly sophisticated carrier system for simultaneous imaging and therapy, it is called theranostics.[113] Theranostics is the recently emerged type of companion diagnostics,[114] and is an important step toward more effective and personalized therapy. Such diagnostic tests can identify and thus pre-screen patients that are most likely susceptible to a specific drug, with subsequent personalized-tailored targeted drug therapy, based on the outcome. The aim of the emerging advanced theranostics is to monitor the response of the drugs in patients in real-time during treatment, in order to reduce the toxicity and enhance the safety, as well as to prevent patients from going through unnecessary treatments.[115]

When designing nanoparticles for drug delivery purposes, detectable (normally fluorescent) model drugs are often used to study and optimize the delivery

and subsequent release of the drug from the carrier.[116-119] However, in case of delivery of larger biomolecules, the molecule itself can be labeled. Controlled drug delivery systems are designed to deliver an active agent at a predetermined rate, for a specific time period,[120] and such a system aims to control the concentration of the drug in the blood. The release can be triggered by specific stimuli, either external (variations in temperature, magnetic field, ultrasound intensity, light or electric pulses) or internal (changes in pH, redox potential, or enzyme concentration).[121] Drug release from magnetically responsive nanoparticle-systems has several advantages, since these can also be magnetically guided by a permanent magnetic field and/or increasing the temperature of the environment when an alternating magnetic field is applied.[99,121] When magnetic nanoparticles are placed in an oscillating or alternating magnetic field, they transform the magnetic field to heat and have thus been extensively used for selective heating of tumors, known as thermal ablation or hyperthermia. However, this phenomenon can also be utilized as a trigger to control the release of therapeutic molecules, by using thermolabile linkers[122] or nanoparticle-coatings of thermosensitive polymers[123]. In addition to these advantages, the use of magnetically responsive systems gives the possibility of performing magnetic resonance imaging.

Drug compounds are usually not inherently detectable, and consequently the drug release has typically been measured indirectly based on the drug´s cytotoxic action. However, theranostic carrier systems with integrated real-time monitoring abilities are emerging.[59] When using real drugs, it is a prerequisite to have a detectable carrier system in order to follow the fate of the nanoparticle-drug complex. Silica nanoparticles are good candidates as drug carriers, since they are biocompatible, bioerodible (often referred to as biodegradable, which is defined as the disintegration of materials by a biological agent such as an enzyme or microbe,[124] and thus bioerodible is a more suitable term for silica),[125] and very flexible delivery platforms when it comes to further functionalization for detectability and targeting.

2.4 Targeted nanoparticle-based imaging and drug delivery

Targeting is defined as the ability for a nanoparticle to identify a tissue of interest and selectively accumulate with it.[25] Through targeting, both contrast agents and drugs can be delivered to the target at higher doses, thus decreasing the side effects of toxic agents. Additionally, the higher contrast differences between the targets and the surrounding tissues can give more detailed information about malignant or abnormal tissues. In general, there are two ways of targeting: passive and active targeting (illustrated in Figure 8). Passive targeting utilizes the leaky vasculature

of tumors, since the blood vessels of tumors have gaps or fenestrations at the borders of endothelial cells. The discovery of this enhanced permeation and retention (EPR) effect, first described by Matsumura and Maeda in 1986,[126] was a great breakthrough for targeted antitumor therapy. Due to the EPR effect, nanoparticles can extravasate into the tumor tissues, allowing for an enrichment of nanoparticles at the tumor sites.[127] This effect is a combination of the increased permeability of the blood vessels, which is characteristic of rapid and defective angiogenesis (production of new blood vessels from already existing ones), and the poor lymphatic drainage retaining the accumulated nanoparticles.[128]

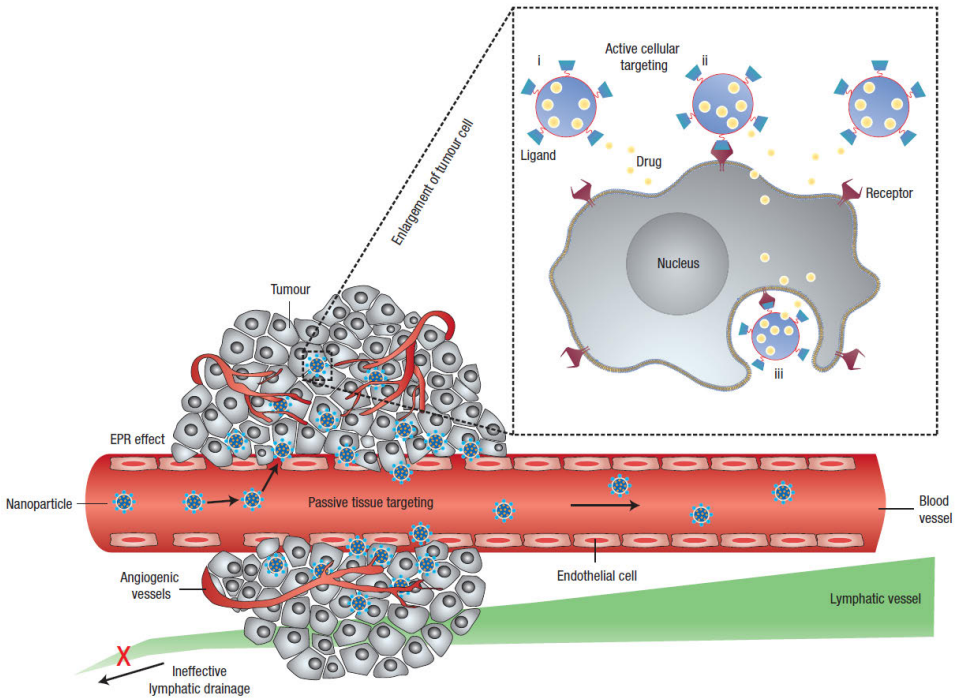

Figure 8. *Overview of the different mechanisms by which nanoparticles can deliver their cargo to cancer cells. Passive tissue targeting utilizes the increased permeability of the tumor vasculature and ineffective lymphatic drainage (EPR effect). Active cellular targeting (inset image) can be realized by attaching targeting ligands on the nanoparticle surface that specifically promote recognition and binding by the cancer cells. The nanoparticles can then release the cargo when close to the target cells (i), attach to the cell membrane and function as an extracellular sustained-release reservoir (ii), or internalize into the cell. Reprinted from Peer, D., et al. Nature nanotechnology 2007, 2 (12), 751, with permission from Springer Nature.*

The passive targeting strategy is limited because the permeability of blood vessels may not be the same throughout a tumor site. Further, the random nature of this strategy makes it difficult to control the process.[26] Due to these limitations, it is preferable to add an active targeting component to the nanoparticles to selectively bind to the target cells. This binding may be achieved by attaching ligands to the surface of the nanoparticles. Ligands are molecules that bind to specific receptors on the cell surface and may include proteins such as antibodies, nucleic acids, and other receptor ligands such as peptides, vitamins, and carbohydrates.[128] The targeting ligands can be attached to the nanoparticle surface via the common bioconjugation methods, as illustrated earlier in Figure 5. In the ligand-based targeting, the receptor should be overexpressed on the target cells relative to normal cells, to maximize the targeting specificity. However, even though many functionalities can be added onto the nanoparticles, the main challenge *in vivo* is the residence time in the systemic circulation, as well as the safety of the nanoparticles.[23] In order for the EPR effect to take place, a long residence time is essential, which might be achieved by reducing the opsonization and thus possibly decreasing the clearance by the immune system.

3 AIMS OF THE STUDY

The overall aims of this thesis were to design, develop and optimize different silica-based nanocomposites, porous and core-shell structures, for application as carriers of active compounds. An overview of the studies included in the thesis is schematically summarized in Figure 9. The specific aim of the first part of the thesis was to focus on **"Means of controlling the bio-behavior of particles by surface-functionalization"** (see Figure 9). In the two studies (publication I and II) included in this part of the thesis, the importance of a surface coating on nanoparticles intended for biomedical applications was demonstrated. A detailed investigation of the widely used copolymer PEI-PEG was presented, including the copolymer's interaction with both the particle surface and biological environment, as well as the significance of choosing the right ratio of the polymers comprising the copolymer (publication II). Further the problems associated with fluorescence-based detection of nanomaterials lacking a stabilizing functionalization was shown, by using magnetite core-shell particles endowing for different means of intracellular detection (publication I). The benefit of a magnetic core for magnetically-aided cellular labeling was also presented here, in addition to the functionality of surface-optimized magnetic core-shell particles as contrast agents for MRI.

The aims of the second part of the thesis were to verify the applicability of nanoparticles both in terms of delivery of active substances (drugs/imaging agents) by different means, as well as to remove a tracer compound *in vivo* by using nanoparticles as scavengers. The loading and delivery of the compounds followed two different routes; either the guest molecules were incorporated inside the porous nanoparticle matrix, (Figure 9: **"Means for *in vitro*/*in vivo* delivery of active substances"**); or the molecules were attached as satellites to the surface of the particles (Figure 9: **"Means of functional utilization of photonic interaction"**). The aim of the study in publication III was to design and evaluate a scavenger-tracer system for removing a specific tracer compound (contrast agent) in the blood circulation, for consequently quenching the background signals and thus benefit for enhanced imaging, while the objective for publication IV was to develop a reporter-system for monitoring redox-induced compound cleavage intracellularly, by using labile bonds that can detach upon cell entry, both of these by utilizing photonic interactions (in terms of FRET) for the visualization in real-time. In publication V and VI the goal was to design and optimize carrier particles for delivery of a large amount of imaging agent, for cellular labeling and tracking over a prolonged time (publication V), or a high amount of drug, especially intended for administration to the lungs (publication VI).

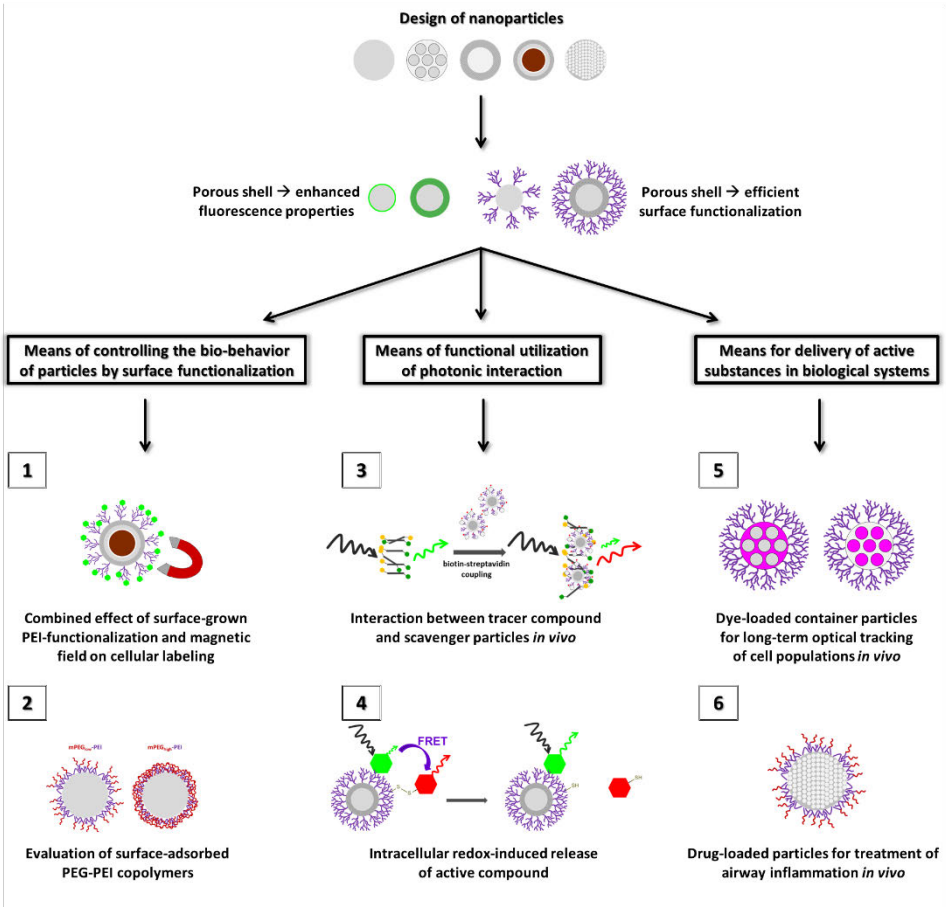

Figure 9. *Outline of the studies included in the thesis. The numbers, 1-6, represent the publications (I-VI) comprising this thesis.*

4 CHARACTERIZATION TECHNIQUES

There is a great benefit in comparing multiple analytical methods to characterize nanomaterials and their interactions with the environment. Possible errors with one technique can easily be sorted out if comparing the measurement with another technique. The interpretation of the results is not either always straightforward, why there is a need of several methods. For the studies presented in this thesis, different techniques have been used to characterize the nanomaterials and to evaluate them for specific applications in a biological environment, as presented in Table 1. In this chapter, the most used techniques will be briefly explained in order to understand the results obtained from them.

Table 1. *Summary of the characterization techniques used for obtaining the results presented in this thesis.*

Characterization technique	Properties/phenomenon studied
Dynamic light scattering	Hydrodynamic size, dispersability, and magnetically-induced aggregation behavior of particles
Electrokinetic measurement	Net surface charge (zeta potential) to confirm surface-functonalization
Electron microscopy	Particle size, particle/pore morphology, and thickness of silica shells
Thermogravimetric analysis	Amount surface functionalization
Fluorescence spectrophotometry *(fluorescence measurements explained in literature review part)*	Fluorescence intensities of particles Shift in maximum wavelength as a function of dye amount
Flow cytometry	Intracellular uptake (based on fluorescence or reflection) and cellular retention of particles
Confocal microscopy (in some cases two-photon imaging or *in vivo* imaging)	Optimization of dye-amount on particles for FRET Intracellular uptake (based on fluorescence or reflection) and cellular retention of particles Distribution of particles on cells Intracellular redox-induced cargo release from particles Visualization of particles and their photonic interactions *in vivo* Visualization of tumor growth
Magnetic resonance imaging *(MR imaging explained in literature review part)*	Cellular uptake of particles with subsequent efficacy as MRI contrast agents

4.1 Dynamic light scattering

Dynamic light scattering (DLS), also known as photon correlation spectroscopy (PCS), is a technique for measuring hydrodynamic size and size distribution of particles. The overall particle size (i.e. hydrodynamic size) is measured, since DLS can not differentiate between inorganic and organic material. Thus the diameter obtained from a DLS measurement is in general higher than the particle size calculated via TEM.[129] However, the advantage of DLS is that the hydrodynamic size can be determined under specific conditions, to get an idea of the stability of the particles in the relevant environment.[130] DLS measures Brownian motion (random movement) of the particles by recording the rate of the intensity fluctuations of the scattered light. The size of the particles is directly related to the speed with which they are being moved by Brownian motion. Large particles move slowly, while smaller particles move more rapidly.

The detected light scatter intensity is passed to a correlator, which determines the degree of similarity between two signals at successive time intervals (nanoseconds to milliseconds). The intensity signal at one point in time (t=0) compared to the signal a short time later are strongly correlated; the correlation is close to one. If the signal at t=0 is compared to a signal after a bit longer time the correlation will not be as good anymore, which means that the correlation is reducing with time. If the original signal is compared to a signal at a much later time, t=∞, the two signals will have no relation to each other and the correlation reaches zero. A typical correlation function for small and large particles is shown in Figure 10, and demonstrates the much faster rate of decay for smaller particles. The recorded correlation function is further used to calculate the size distribution of the particles, which is normally shown in a histogram with the distribution of size classes presented on the x-axis and the relative intensity of the scattered light on the y-axis.[131,132]

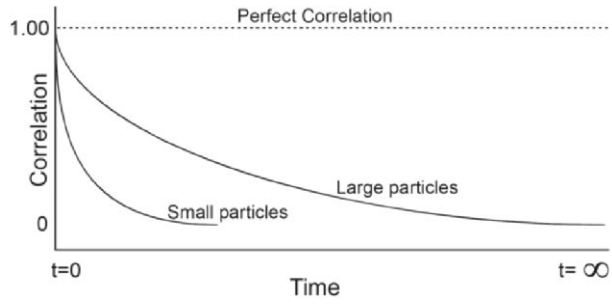

Figure 10. *Typical DLS correlation functions for small and large particles. The diffusion rate of the particles is directly related to the time delay at which the correlation function decreases. Thus, the intensity signal for smaller particles fluctuates more rapidly and as a result the correlation decreases at a faster rate. Adapted from Malvern Instruments Ltd, www.malvern.com.*[131]

4.2 Electrokinetic zeta potential measurements

Zeta potential is a physical property that is exhibited by any particle in suspension and is an important marker of the stability of a colloidal dispersion. Each dispersed particle affects the ionic environment of the suspension media, with an increased concentration of oppositely charged ions close to the particle surface. This is explained as the electrical double layer (Figure 11). The double layer is divided in two parts; an inner region called Stern layer and an outer region called diffuse layer. In the Stern layer ions from the surrounding media are strongly bound to the surface of the particles. Outside this layer is the diffuse cloud-like area where the ions are less firmly attached. The zeta potential is the potential difference measured at the slipping plane, which is the boundary between the bulk solution and the stationary layer of charged ions attached to the dispersed particle. The magnitude of the zeta potential gives an indication of the stability of the particle system, with higher magnitude potentials exhibiting increased electrostatic repulsion and therefore increased stability. The most important factor that affects zeta potential is pH, since the magnitude of the charge on the particle surface depends on that. At a specific pH, the net surface charge will be zero. This is referred to as the isoelectric point and is normally the point where the particles are least stable.

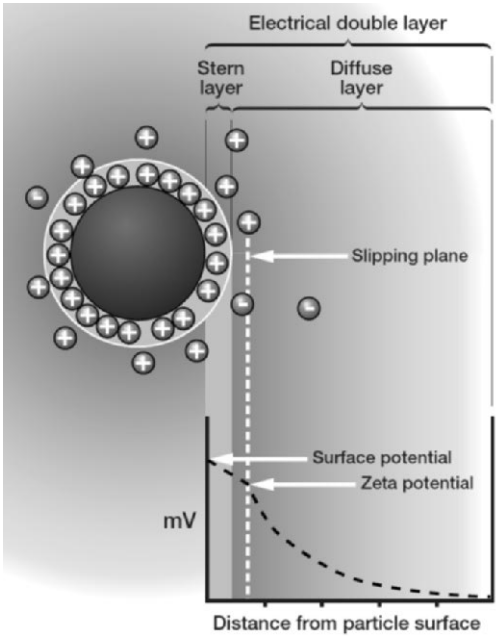

Figure 11. *Schematic of the electrical double layer, showing the potential difference as a function of distance from a dispersed particle. Adapted from Malvern Instruments Ltd, www.malvern.com.*[131]

The zeta potential is often determined by electrophoresis. Charged particles dispersed in a solution are added to a cell with an applied electrical field, which makes the particles move towards the electrode of opposite charge. The velocity of the particles is commonly referred to as the electrophoretic mobility and is measured by light scattering. Particle speed at various voltages is measured, and the zeta potential can be determined by applying the Henry equation:

$$U_E = \frac{2\varepsilon\zeta f(\kappa a)}{3\eta}$$

where U_E = electrophoretic mobility, ε = dielectric constant of the liquid, ζ = zeta potential, η = viscosity, and f(κa) = Henry's function. Two values are normally used as approximations of f(κa); either 1.5 (Smoluchowski) or 1.0 (Hückel). For particles suspended in aqueous media at moderate electrolyte concentration the Smoluchowski approximation is most commonly used.[131,133]

4.3 Electron microscopy

In electron microscopy an electron beam is used to illuminate the sample, in contrast to the light beam used in conventional optical microscopy. The resolving power of an optical microscope is mainly limited by the wavelength of the photons and does not give enough resolution for imaging of nanomaterials. Electron beams can be produced with wavelengths much smaller than that of photons, and thus greatly extend the resolution.

Scanning electron microscopy (SEM) is a powerful characterization technique which provides information about surface topology, surface morphology and, depending on the instrument, also chemical composition. In SEM a finely focused electron beam is used to scan the sample and produce an image of the surface. When the electron beam hits the sample surface, the sample itself emits secondary electrons while also some part of the electrons from the electron beam will be absorbed by the sample or reflected as back-scattered electrons. All these electrons give different information about the sample. The detection of secondary electrons gives high spatial resolution and strong topographic contrast. The process has to operate under vacuum conditions to avoid collisions between electrons and gas molecules in the air. SEM offers an image resolution down to about 1 nm.[133,134]

Transmission electron microscopy (TEM) is providing more detailed morphological information, with a high resolution which enables objects to be studied down to 0.1 nm. In addition, TEM affords structural information via electron dif-

fraction. The major difference between SEM and TEM is that TEM detects transmitted electrons. The sample has to be very thin in order to allow the electrons to penetrate it. The contrast of the images depends on the atomic number of the atoms forming the sample. Materials containing heavy atoms provide a higher contrast due to the higher electron density which results in more interactions between the electrons in the primary beam and those in the sample. Thus, organic samples often need to be stained with heavy metals to enhance the contrast in the resultant image.[133,134]

4.4 Thermogravimetric analysis

Thermogravimetric analysis (TGA) is a technique which provides information about the amount and rate of change in mass of a material as a function of temperature or time, as the sample is subjected to a controlled temperature program in a controlled atmosphere. TGA can be used to determine the composition of a material by analyzing the quantitative weight changes that occur in specific temperature regions. It also gives information about the thermal stability of the sample, the purity of the material, and the kinetic parameters for chemical reactions which might occur in the sample. A TGA consists of a precision balance holding a sample pan inside a furnace, which is heated or cooled during the experiment according to a predetermined thermal cycle. The mass of the sample is monitored during the experiment. The atmosphere in the sample chamber is controlled with a purge gas (inert or reactive depending on the application).[135,136]

4.5 Flow cytometry

Flow cytometry is a widely used method for simultaneously measuring multiple physical characteristics of cells, such as size, granularity (cellular density), as well as fluorescence emitted from stained cells. One of the fundamentals of flow cytometry is that it measures the properties of individual cells (or particles, down to about 200 nm depending on the setup). This contrasts with other methods, for instance fluorescence spectroscopy in which fluorescence is measured for a bulk volume of a sample.

When a cell suspension is injected into a flow cytometer, sheath fluid is used to order the sample into a stream of single cells. The tiny stream of fluid passes through a small nozzle and takes the cells past a laser beam one cell at a time (Figure 12). Scattered and emitted light from the cells are detected and converted to electrical pulses by the different detectors. One detector is placed in front of the light beam and measures light scattered at small angles, i.e. forward scatter (FSC). FSC gives information about the size of the cells. Several detectors are placed at a

90° angle to the laser beam. One of them measures side scatter (SSC), which correlates with the density of the cells, and the others are fluorescence detectors. The most common type of detector is the photomultiplier tube (PMT). These are converting the light into electrical pulses, which are further processed by a series of linear and log amplifiers. The measured voltage pulse area will correlate directly to the fluorescence intensity for the specific cell. Logarithmic amplification is most often used when measuring fluorescence in order to expand the scale for weak signals. The final data is usually shown either as single parameter histograms or as two parameter correlated plots (cytograms).[137,138,139]

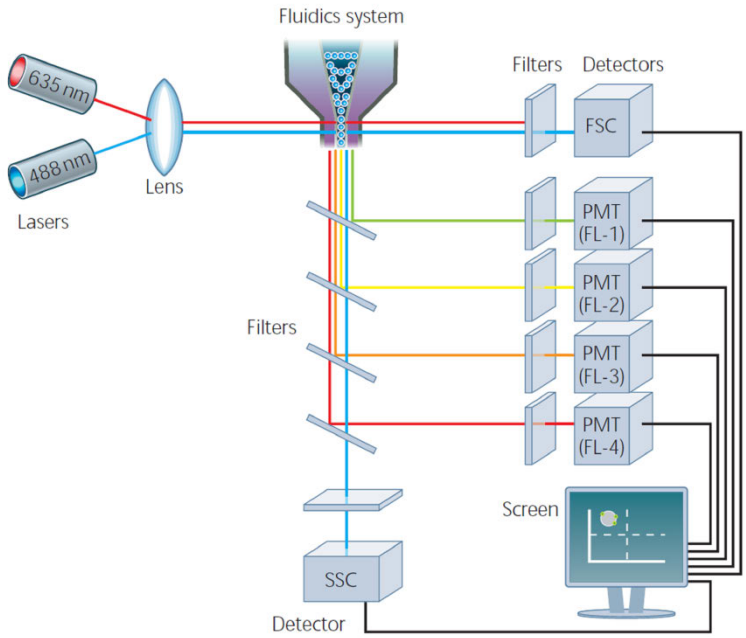

Figure 12. *Schematic diagram of the flow cytometry setup. Adapted from Rahman, M., Serotec. Ltd.*[140]

4.6 Confocal microscopy

Confocal microscopy is a technique in optical imaging which provides high-resolution images with fine details and more contrast, compared to conventional microscopy. This is achieved by point-by-point illumination of the sample and rejection of out-of-focus light. Thus, a thin cross-section of the sample is reconstructed as a 2D image one pixel at a time. By assembling a series of such slices at different depths, a 3D reconstruction of the sample can be performed.

In confocal microscopy both reflected light and fluorescent light can be used to image the sample. The incoming light beam is usually provided by a laser

to generate high intensities of fluorescence or reflectance from the sample. A schematic diagram of a confocal microscope is shown in Figure 13. The laser beam is directed by a dichroic mirror towards a pair of mirrors which send the light further through the microscope objective and excites the sample. The same objective collects the fluorescent (or reflected) light coming back from the sample, and the light is further directed by the mirrors through the dichroic mirror and a small pinhole placed in the confocal plane of the sample. The pinhole allows only the light emitted (or reflected) from the desired focal spot to pass through; all out-of-focus light coming from the sample is rejected. The light that makes is through the pinhole is finally measured by a sensitive light detector, a photomultiplier tube (PMT). This method allows the sample to be imaged one point at a time. By rapidly scanning the sample, a computer collects all the imaged points of a thin planar region of the sample and constructs the 2D image one pixel at a time. This is referred to as optical sectioning. By combining a number of these optical sections the 3D reconstruction can be made, which is one of the main advantages with confocal microscopy. It is also this sectioning ability that allows for the sharpness of the images.[141-143]

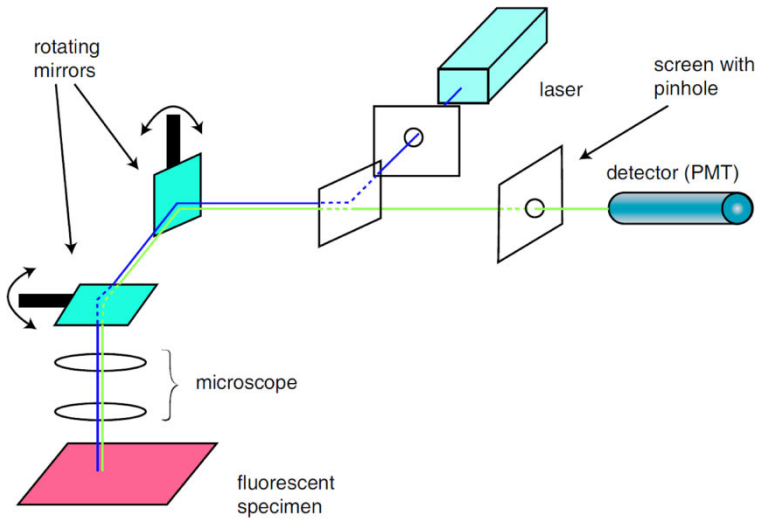

Figure 13. *Schematic overview of the basic setup of a confocal microscope. Adapted from Semwogerere, D., et.al. Encyclopedia of Biomaterials and Biomedical Engineering 2005, 23, 1.*[142]

5 SUMMARY OF RESULTS

5.1 Design of functional core-shell particles

Depending on the intended application of a nanomaterial, a range of different design aspects must be considered in order to provide for a nanomaterial with the desired properties. Nanoparticles can be produced with wide variations when it comes to combinations of different types of materials, size and shape.[144,145] The development of inorganic nanoparticles intended for biomedical applications goes towards more complex structures, such as core-shell particles which will be presented in the following chapter, and hollow particles that were developed in **supporting publication i.**

Core-shell particles, with a solid silica core or a magnetite cluster core, and additional non-porous and porous silica shells, were produced for the studies presented in **publication I, III and IV**. The core-shell particles having a silica core were used as model particles for any inorganic core material, while the particles synthesized with a magnetite core were used specifically to study magnetically enhanced cellular labeling as well as to demonstrate the aggregation behavior of particles not being surface-functionalized. A schematic illustration of a surface-functionalized core-shell particle with magnetite core is presented in Figure 14.

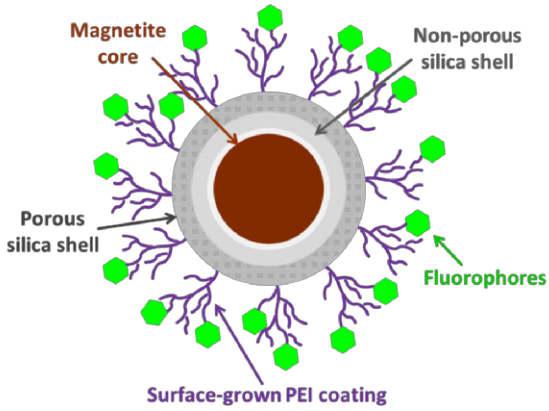

Figure 14. *Schematic presentation of a fluorescent magnetic core-shell particle.*

The magnetite cores were first coated with a non-porous silica shell in order to provide for a protective barrier between the cores and the fluorophores subsequently labeled on the surface, considering the risk of fluorescence quenching by the magnetite core, via an energy transfer process, since it strongly absorbs the transmitted light.[43] To demonstrate the role of this protective silica shell, the fluorescence intensity of magnetite cores before and after non-porous silica coating

was measured (Figure 15). The particles were labeled with same amount of FITC with respect to the mass of the magnetite core. The pure magnetite cores (Mag) were already coated with a very thin silica shell in order to protect the core and keep the core surface hydrophilic, but this thin layer was not sufficient for protecting the fluorophores from quenching by the cores, resulting in a low fluorescence intensity. A 1.5-fold increase in fluorescence intensity could be obtained when increasing the thickness of the nonporous silica shell (Mag@*n*SiO_2). The intensity was further greatly enhanced after coating of a porous silica shell on the particles (Mag@*n*SiO_2@*m*SiO_2). A porous silica shell helps in keeping the fluorescent molecules more apart due to the large surface area and porous structure, and as a result, the possible self-quenching of the fluorophores upon close contact on the particle surface decreases drastically which promotes the high increase in intensity.

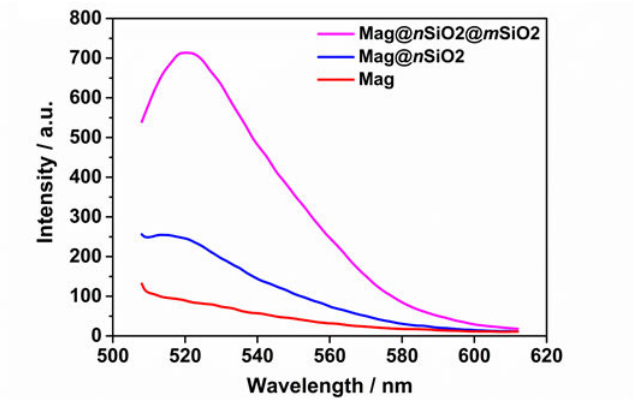

Figure 15. *Fluorescence intensities of similarly FITC-labeled magnetic core particles or magnetic core-shell particles, with increasing number of silica layers, in HEPES buffer (pH 7.2). Adapted from Paper I.*

Figure 16 shows scanning electron microscopy (SEM) and transmission electron microscopy (TEM) images of the Mag@*n*SiO_2@*m*SiO_2 particles. SEM reveals an average diameter of almost 300 nm. The average size of the magnetite cluster core is 120 nm and the thickness of the nonporous and mesoporous silica shell is about 60 nm and 30 nm, respectively. The Mag@*n*SiO_2@*m*SiO_2 particles were further fully dispersible in water (Figure 16c), given a high-quality dynamic light scattering (DLS) peak at 550 nm and a low polydispersity index (PdI) of 0.15. The difference between the size of the dried particles measured from SEM images and the hydrodynamic diameter measured by DLS is a known phenomenon that can be ascribed to the drawbacks with the DLS technique.[146-150] Magnetite particles

give rise to large light scattering and absorbance, which may here have resulted in errors in the size calculation.

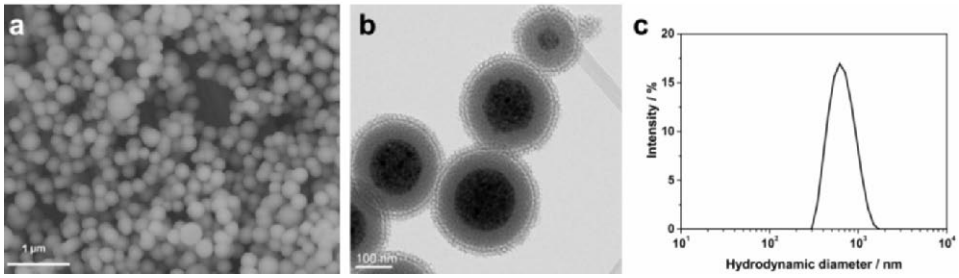

Figure 16. *Characterization of the magnetic core-shell particles, by (a) SEM, (b) TEM, and (c) DLS. Modified from Paper I.*

The mesoporous coating was synthesized under neutral conditions in order to protect the magnetite core.[151] Since this mild procedure avoids both high and low pH synthesis conditions that could lead to dissolution of cores, it can be suitable for various inorganic cores. As model core, a solid silica particle of Stöber type was used, representative of any inorganic colloidal material. To stand as a model for the Mag@*n*SiO_2 (ca 240 nm) a silica core of 270 nm was chosen. Figure 17a and b present SEM and TEM images of the silica core-shell particles *n*SiO_2@*m*SiO_2. The size of the *n*SiO_2@*m*SiO_2 particles is about 300 nm as determined by SEM. The particles were further functionalized with a surface-grown hyperbranched PEI-layer. A well-defined peak at 400 nm with a low PdI of 0.11, measured by DLS, indicated that the functionalized particles were completely dispersible.

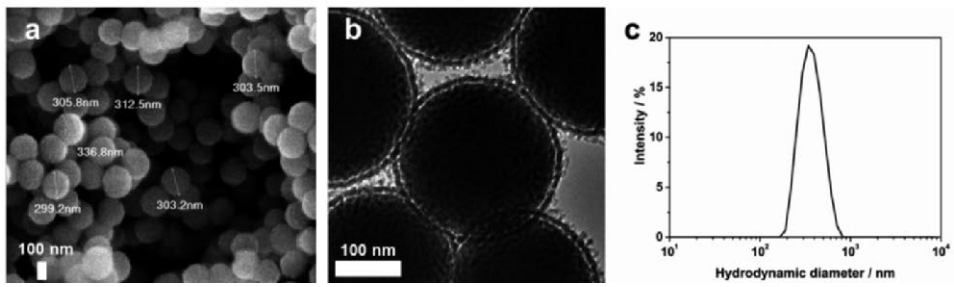

Figure 17. *Characterization of the model silica core-shell particles, by (a) SEM, (b) TEM, and (c) DLS. Modified from Paper IV.*

The mesoporous shell obtained via the synthesis route used here is characterized by mesopores larger than the "standard" size (3-4 nm) and is consequently

more suitable for accommodating larger molecules such as biomolecular cargo. In the present case, the porous layer allowed for efficient organic modification by the surface hyperbranching polymerization of PEI. A high density of surface-grown PEI is beneficial since it provides a number of advantageous properties,[152] such as a large amount of reactive surface groups for further attachments of active molecules, high particle suspension stability via electrostatic (and steric) stabilization, charge tuning ability which can be utilized to overcome unspecific biointeractions, as well as possible endosomal escape via its characteristic "proton sponge" or "endosomal buffering" ability[153]. Even though amines catalyze silica dissolution, it has been demonstrated that PEI modification of core-shell particles retard the total degradation of the silica shell by re-adsorbing the dissolved negative silicates and provide for a favorable environment for further condensation of the adsorbed silicates.[154] This is especially true for porous shells which are more susceptible to hydrolytic degradation due to their exposed nature. Electrokinetic measurements (zeta potential) as well as thermogravimetric analysis (TGA) confirmed successful PEI-functionalization of the core-shell particles (Table 2). The PEI-functionalized particles, nSiO$_2$@mSiO$_2$@PEI, obtained a high positive net charge (+45 mV), while the plain core-shell particles (nSiO$_2$@mSiO$_2$) exhibited a negative net charge characteristic of its silica surface (-30 mV). For comparison, the silica cores were PEI-functionalized directly (nSiO$_2$@PEI), which also resulted in a high positive net charge (+44 mV). While the core and core-shell particles displayed a similar net surface charge after PEI-functionalization, TGA analysis revealed a ten-fold increase in the PEI-content of the nSiO$_2$@mSiO$_2$@PEI particles as compared to the nSiO$_2$@PEI particles. The PEI-content of the functionalized nSiO$_2$@mSiO$_2$ particles was 7.3 wt%, whereas the obtained PEI amount for the cores was only 0.7 wt%, which clearly shows that a thin porous silica shell can significantly enhance the degree of PEI-functionalization.

Table 2. *TGA and zeta potential measurements confirmed that a thin porous silica coating can increase the efficiency of the surface-grown PEI-polymer ten-fold.*

Particle	Mass loss / %	Zeta pot. / mV
nSiO$_2$@mSiO$_2$	0.0	- 30
nSiO$_2$@PEI	0.7	+ 44
nSiO$_2$@mSiO$_2$@PEI	7.3	+ 45

5.2 Means of controlling the bio-behavior of particles by surface functionalization

Surface functionalization of nanoparticles is essential for a successful utilization of these materials in biological systems, such as for use as drug delivery vehicles through different *in vivo* administration routes, as well as to pre-label cells and tissues.[155] Labeling of i.e. stem cells is a promising application to noninvasively monitor the distribution and fate of transplanted stem cells.[156-158] Gene transfection is another growing field of study where the design of the optimal surface functionalization is highly important,[159] as has also been demonstrated in **supporting publication ii and iii**. Except the desire to expand the nanoparticles' biocompatibility, their undesired interactions with components in the biological environment can also be reduced with help of the right surface modification and/or surface charge.[152] Polymer constructs are often used to increase the biomedical applicability of the nanoparticles by providing adequate dispersion stability.[160] Simultaneously, these polymers can endow for reactive sites for further attachment of bioactive molecules.

The high degree of PEI-functionalization demonstrated above is advantageous both for its high particle suspension stability, but also for its ability to boost the cellular uptake of silica particles by interacting with the cell membrane.[161,162] The here presented surface-grown PEI has also a considerably higher surface concentration of reactive amino-groups as compared to corresponding silica materials prepared by classical silanization reactions, like co-condensation and post-synthesis grafting of amino-silanes.[66]

In the two studies presented below different means of controlling the bio-behavior of particles by surface functionalization has been studied. In the first study, the unique role of PEI-functionalization was utilized for cellular labeling of nanoparticles. Here, magnetic core-shell particles were developed and used in order to simultaneously enhance the degree of cellular labelling by a magnetic field, and further study the consequences of lacking a stabilizing functionalization of the nanoparticles and the subsequent errors in analyzing the nanoparticle uptake by fluorescence-based techniques. Finally, the synergistic effect of PEI-functionalization and a magnetic field on cellular uptake was validated by MR-imaging of labeled cells. In the second study, PEG-PEI copolymers were investigated in-depth to be utilized for stabilizing/dispersing silica nanoparticles. Even if widely used, the interaction of these copolymers with the environment where they are intended to be used, as well as with their behavior on the particle surface, is rarely studied in detail. Thus, also an optimization of the ratio between the two polymers is left out. Here, we have attempted to find the optimum range for the PEG-PEI ratio

and studied the interaction mechanisms for the surface adsorption process with subsequent dispersion ability, with a final demonstration of the impact of the surface coating on the particle-uptake in cells.

5.2.1 Combined effect of surface-grown PEI-functionalization and magnetic field

The synergistic effect of surface PEI-functionalization and an external magnetic field on cellular labeling efficiency of magnetic core-shell particles was studied in **publication I**. Further, the problem of aggregation of non-functionalized particles, which is strongly enhanced under a magnetic field, was demonstrated. The aggregation led to difficulties in correctly analyzing the degree of particle uptake by fluorescence-based techniques (flow cytometry and microscopy), which were overcome by employing reflection-based assessments. An overview of the study is presented in Figure 18.

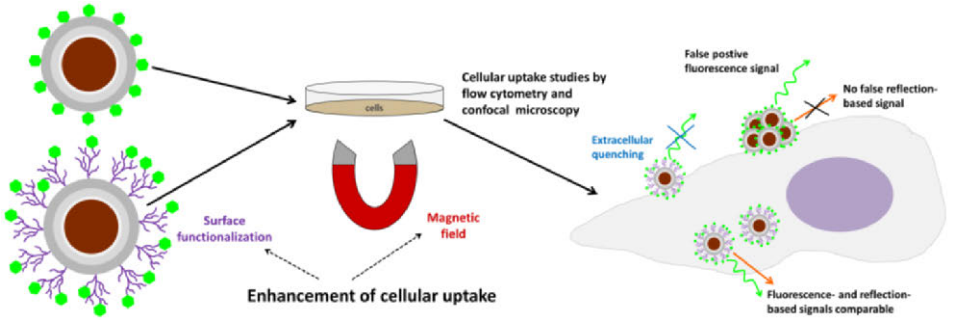

Figure 18. *Schematic illustration of the study, where the effect of surface functionalization and an external magnetic field on cellular labeling of magnetic core-shell particles was investigated. Both fluorescence- and reflection-based methods were used in order to study the aggregation behavior of the non-functionalized particles. Adapted from Paper I.*

The influence of a magnetic field on the cellular uptake of non-functionalized (Mag@nSiO$_2$@mSiO$_2$) and PEI-functionalized (Mag@nSiO$_2$@mSiO$_2$@PEI) magnetic core-shell particles was investigated both by flow cytometry and microscopy. HeLa (human cervical cancer) cells were incubated with 10 µg/ml particles for a short time period of only one hour with or without the presence of a magnetic field (0.3 T), whereafter the extracellular fluorescence was quenched by trypan blue in order to detect only internalized particles. Flow cytometry analysis (Figure 19a) reveals apparent higher uptake of the non-functionalized Mag@nSiO$_2$@mSiO$_2$ particles (III, +magnet IV) than the positively charged functionalized Mag@nSiO$_2$@mSiO$_2$@PEI particles (I, +magnet II), which is contradic-

tory to what was expected since it is well known that positively charged silica particles are more extensively taken up by HeLa cells. Since it is also widely known that there are a considerable number of problems with fluorescence-based tracking of internalized particles, the particle uptake measured by flow cytometry was re-analyzed by scattering intensities (reflection). The result is presented in Figure 19b, where the graph clearly shows lower uptake of the Mag@*n*SiO_2@*m*SiO_2 particles, regardless of whether the magnetic field was applied or not. As expected, an approximately 5 times higher uptake of Mag@*n*SiO_2@*m*SiO_2@PEI particles was found and the internalization was further increased by a factor of 2 when a magnetic field was applied. To confirm these results, the cellular uptake was also investigated by reflection-based confocal microscopy (Figure 19c). Thin confocal slices were imaged with the focus set in the middle of the cell nuclei and, as seen, the Mag@*n*SiO_2@*m*SiO_2 particles are mostly distributed outside the cells, with no significant difference seen when a magnetic field was applied. The positively charged Mag@*n*SiO_2@*m*SiO_2@PEI particles, on the other hand, are much more extensively taken up by the cells, and the particles have accumulated close to the cell nuclei. In the presence of a magnetic field a significantly increased reflection signal was found, which set the results obtained from microscopy in good agreement with the reflection-based flow cytometry data.

The conflicting result obtained from fluorescence-based flow cytometry analysis was further investigated by fluorescence-based microscopy, as presented in publication I. The extracellular quenching was left out in order to study how the particles "behave" on the cell surface. The microscopy images clearly revealed that the Mag@*n*SiO_2@*m*SiO_2 particles were aggregated on the cell surface, and formed even larger aggregates when a magnetic field was applied. On the contrary, the Mag@*n*SiO_2@*m*SiO_2@PEI particles were well dispersed over the cells, also when a magnetic field was applied, which also readily enhanced the cellular uptake. Since the non-functionalized particles formed large aggregates on the surface of the cells, these aggregates could probably not be effectively quenched, and false high fluorescence intensity, from nearly 100% of the cells, was detected by flow cytometry.

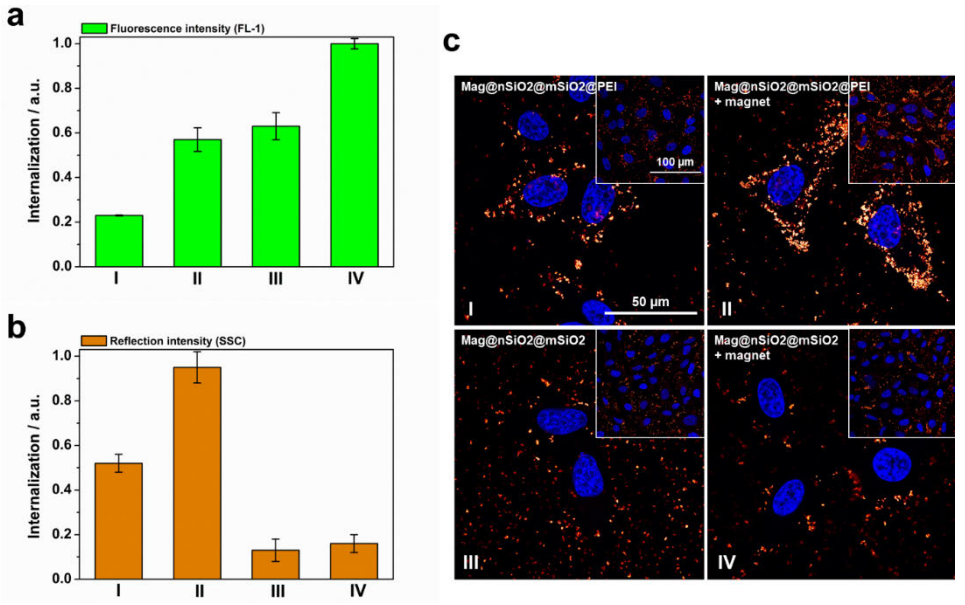

Figure 19. *Comparison of fluorescence- and reflection-based analysis of the cellular uptake of core-shell particles. (a) and (b) cellular uptake of Mag@nSiO_2@mSiO_2@PEI (I, +magnet II) and Mag@nSiO_2@mSiO_2 (III, +magnet IV) particles, as determined by flow cytometry and analyzed by either fluorescence (FL-1) or reflection (side scatter of cells, SSC). The cells were incubated with particles for 1 h, with the addition of a magnetic field for the "+magnet" samples. Trypan blue was used to quench the extracellular fluorescence. "Internalization" in the graphs corresponds to the intensity, FL-1/SSC, per cell multiplied with the fraction of positive cells. (c) Reflection-based confocal microscopy images of the corresponding samples as presented in (a) and (b). The cell nuclei were stained with DAPI (blue). Modified from Paper I.*

To explore the aggregation phenomena of the particles in more detail, both Mag@*n*SiO_2@*m*SiO_2 and Mag@*n*SiO_2@*m*SiO_2@PEI were dispersed in cell media and the autocorrelation function of the particle suspensions was measured and compared by DLS before and after being placed in a magnetic field for one hour (Figure 20a). The autocorrelation function decay, which is related with particle diffusion rate in solution, is a useful tool to study the aggregation behavior of particles.[163-165] As the time at which the correlation starts to decay is an indication of the size of the particles, both the Mag@*n*SiO_2@*m*SiO_2 and Mag@*n*SiO_2@*m*SiO_2@PEI have the same hydrodynamic size in the beginning. After the particles were placed in a magnetic field for one hour, the correlation curve for the non-functionalized Mag@*n*SiO_2@*m*SiO_2 particles is significantly shifted to the right with remarkably longer decay time (τ, 10^6 µs), compared to the curve for the PEI-functionalized particles (10^4 µs). This indicates that large aggregates of the

non-functionalized particles have formed, since the signal will decay more slowly if the particles are large and the correlation will persist for a longer time before decaying. The additional plateau in the decay time range from 10^4 µs to 10^6 µs before the correlation reaches zero, further affirms the presence of large aggregates. The same result could be observed visually in Figure 20b, with a more rapid sedimentation of the Mag@nSiO$_2$@mSiO$_2$ particles, again confirming magnetically induced aggregation of these particles to large clusters with, as a result, a faster sedimentation and separation rate by the magnetic field.

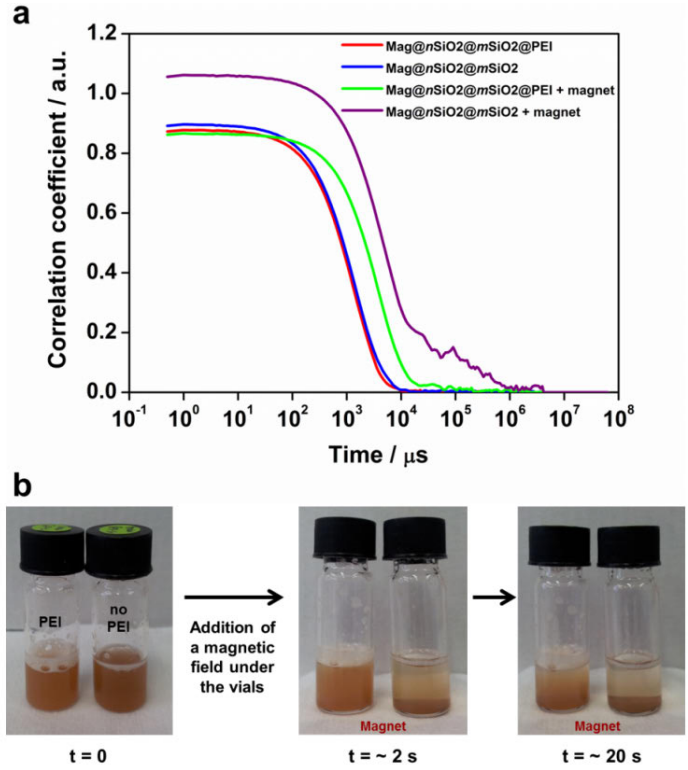

Figure 20. *Magnetically induced aggregation of Mag@nSiO$_2$@mSiO$_2$ in cell media as compared to Mag@nSiO$_2$@mSiO$_2$@PEI. (a) Autocorrelation function, measured by DLS, for both of the particles before and after being in contact with a magnetic field for one hour. (b) Mag@nSiO$_2$@mSiO$_2$@PEI ("PEI") and Mag@nSiO$_2$@mSiO$_2$ ("no PEI") as freshly dispersed in cell media, and after being placed on a magnetic field for 2 s and 20 s. Adapted from Paper I.*

In order to demonstrate that results obtained from fluorescence- and reflection-based measurements are comparable if no particle aggregation occurs, HeLa cells were incubated with the well-dispersable Mag@nSiO$_2$@mSiO$_2$@PEI particles

and analyzed by flow cytometry after various internalization times, as presented in Figure 21. The external magnetic field could greatly enhance the cellular uptake especially after short incubation times. Nevertheless, even after three hours of incubation, the effect of the magnetic field was significant. After 24 h of incubation, no difference owing to the magnetic field could be detected, since the amount positive cells even without a magnetic field reached 100%. On the basis of the results obtained, it is apparent that particle aggregation led to the erroneous determination of cell internalization in the case of Mag@nSiO$_2$@mSiO$_2$. Aided by PEI-functionalization, Mag@nSiO$_2$@mSiO$_2$@PEI particles can maintain high suspension stability even under biologically relevant conditions. The hyperbranched PEI-layer acts to slow down and/or prevent aggregation of the particles also in the presence of a magnetic field. At the same time, previous studies[161,162] have as well shown that the positively charged PEI-coating enhances the cellular uptake by its alleged strong interaction with the cell plasma membrane. Hence, in the present case, the surface PEI-functionalization possesses a dual functionality for the cellular labeling of the particles.

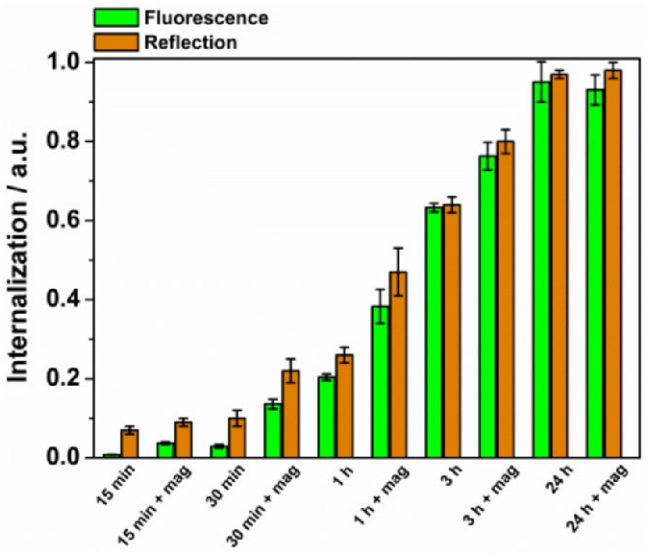

Figure 21. *Time-dependency, of the magnetically induced cellular uptake of the nicely dispersed Mag@nSiO$_2$@mSiO$_2$@PEI particles, demonstrates the ability to compare measurements based on both fluorescence and reflection when no particle aggregation occurs. Adapted from Paper I.*

The Mag@nSiO$_2$@mSiO$_2$@PEI particles were further evaluated by MRI. HeLa cells were again labeled with the particles at a concentration of 10 μg/ml for different time intervals with/without the presence of an external magnetic field,

and measured on a clinical 3 T MRI instrument. T_2-weighted phantom images (Figure 22a) clearly show the T_2 shortening effect (signal loss), which demonstrates that the Mag@*n*SiO_2@*m*SiO_2@PEI particles were efficiently taken up by HeLa cells and served as a contrast agent for the labeled cells being visualized by MRI. Moreover, the extent of T_2 shortening shows the same trend (Figure 22b) of dependency on the labeling time and the magnetic field, as already demonstrated with flow cytometry. A 6-fold increase in $1/T_2$ value, for the labeled sample compared to the control sample, is seen after only 30 min when a magnetic field is applied. The $1/T_2$ value increased to almost 7-fold compared to the control cells after 1 h of treatment time, whereafter no significant further enhancement caused by the magnetic field can be observed at the 3 h time-point, revealing a saturated enhancement of MRI signal at this particle concentration. An incubation time of 24 h was most often presented in similar MRI studies where cell labeling were involved.[166-168] This further confirms the significant advantage of a magnetic field, for efficiently enhancing the cellular labeling and decreasing the incubation time, in the same time as demonstrating the core-shell particles functionality as contrast agents for MRI.

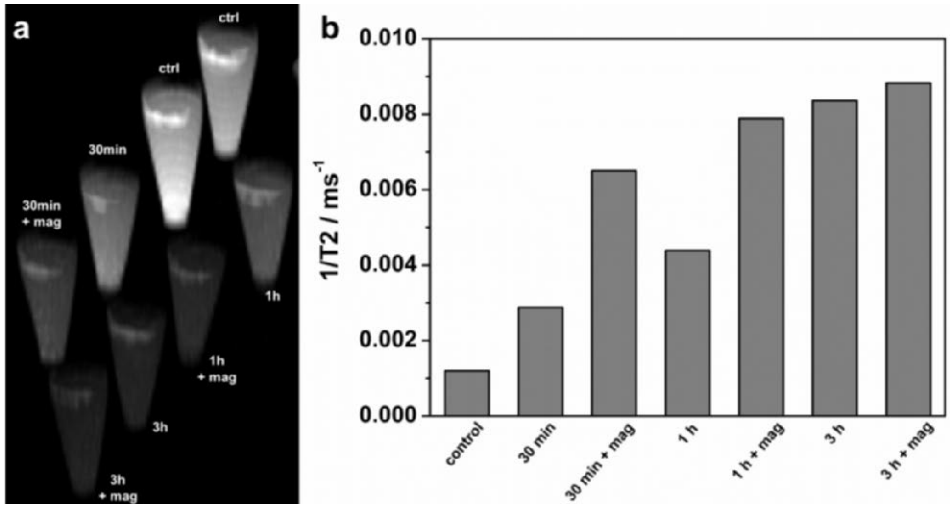

Figure 22. *MR imaging of labeled cells as a function of treatment time with and without the presence of an external magnetic field. (a) MRI phantom images and (b) $1/T_2$ values, derived from the images, as a function of various labeling time points. The same concentration of HeLa cells (1.5 x 10^6 cells/tube) were used for all of the samples. Adapted from Paper I.*

5.2.2 Evaluation of surface-adsorbed PEG-PEI copolymers

As demonstrated above, surface modification of nanoparticles is essential in order to prevent aggregation of particles and thus increase their biocompatibility, as well as enhance the cellular affinity. Except the already discussed surface-grown hyperbranched PEI-polymer, also adsorbed polymers such as PEI and PEG (polyethylene glycol) are used either separately or as block-copolymers. Especially PEG polymers are widely applied since they have been shown to prolong the circulation time in the blood stream as a result of their so-called 'stealth' properties,[169,170] which means that they help in reducing the amount of plasma protein adsorption on the particle surface, which further reduces the probability of the particles being removed by the body's defense mechanisms.[171] PEG has a neutral charge and thus prevents aggregation by providing a steric barrier.[172,173] The PEG polymers have not shown any toxicity *in vivo* (shown for PEG with a molecular weight ≥1 kDa),[174] and several PEG-coated drugs are used in the clinics or are in clinical development.[175] PEI-polymers are also commonly applied due to a number of advantageous properties, as already discussed in section 5.1. Commercial high molecular weight PEI (25 kDa) is thus well-known to be cytotoxic,[176,177]however, it has been demonstrated that PEI in combination with silica nanoparticles is readily reducing the cytotoxicity, even at very high particle concentrations.[152] Even though these two polymers are often used together as block-copolymers, these copolymers and their interaction with the particle surface as well as the environment are often not investigated in detail. In **publication II** two PEG-PEI copolymers with different grafting ratios have been synthesized and comprehensively studied to provide a solid rationale for utilizing these as surface modifiers and stabilizing agents of nanoparticles with focus on biomedical applicability.

Non-porous silica particles, with a size of 100 nm, were used as model particles for this study in order to reduce the complexity of the adsorption process that would occur on porous surfaces. Copolymers were prepared from PEI (25 kDa) grafted with PEG (5 kDa) at two different grafting ratios. The PEG-PEI grafting ratios for the two synthesized copolymers, abbreviated $mPEG_{low}$-PEI and $mPEG_{high}$-PEI, were studied and shown to be 2 and 30, respectively. For both of the copolymers a concentration of 7.5 wt% was found to be the optimal level for dispersing and stabilizing the silica particles. The adsorption mechanism of the copolymers on the particles, in comparison to plain PEI, were studied and revealed a clear difference between high and low PEG grafting ratios. Weaker interaction was observed for $mPEG_{low}$-PEI than for plain PEI adsorption, which was shown to be due to lower amine accessibility. The weakest interaction was thus observed for

$mPEG_{high}$-PEI adsorption as a result of further decay of free amine groups with increasing PEG ratio. This demonstrates that the electrostatic adsorption provided by the amine groups of PEI is stronger compared to hydrogen bonding provided by PEG. Besides this, the architecture of the adsorbed copolymers changes from PEG chains stretching out from the surface to PEG chains contributing to the adsorption (Figure 23a), and as a result, this portion of PEG does not take part in the steric stabilization as polymer chains extended from the particle surface do. Consequently, higher PEG grafting ratio does not enhance the colloidal stability of the particles, as was further investigated in the presence of salt and serum protein to mimic physiological conditions (Figure 23b and c). No significant difference in flocculation behavior were observed between particles coated with $mPEG_{low}$-PEI and $mPEG_{high}$-PEI in presence of salt, and both were colloidally stable up to 0.15 M NaCl, which is equivalent to the ionic strength of physiological media. On the contrary, aggregation was observed for particles coated with plain PEI, as also expected, due to the ionic shielding of the charges that contribute to the electrostatic stabilization. Furthermore, the acclaimed 'stealth' effect of PEG was studied for both of the copolymer coatings in comparison to plain PEI coating, with Bovine Serum Albumin (BSA) as protein source. The result showed that PEG reduced the adsorbed amount of protein compared to PEI only. However, a clear-cut effect in the degree of protein adsorption prevention by PEG could not be observed, even due to a 15 times higher PEG ratio of the $mPEG_{high}$-PEI polymer than the $mPEG_{low}$-PEI. This is in line with the study by D. Desai et al.,[152] who also concluded that a PEGylation of a PEI-grafted silica particle lead to very slight reduction in serum protein adsorption.

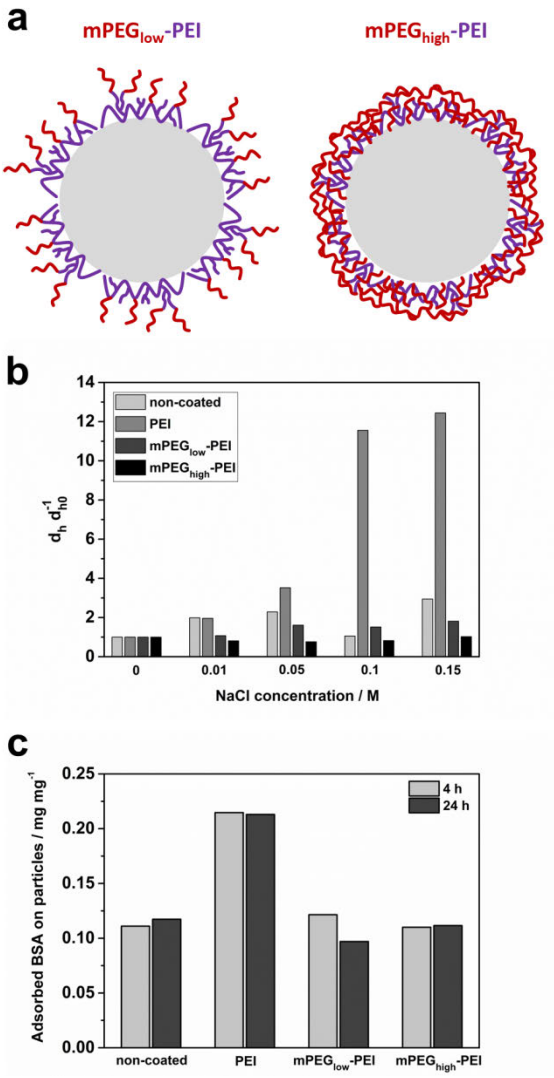

Figure 23. *Presentation and characterization of mPEG$_{low}$-PEI and mPEG$_{high}$-PEI coated particles in comparison to plain or PEI-coated particles. (a) Schematic illustration of the mPEG$_{low}$-PEI and mPEG$_{high}$-PEI polymers adsorbed on the particles, (b) change in hydrodynamic diameter of the particles with the different coatings as a function of NaCl concentration, and (c) adsorbed BSA amount on the particles at two different time points. Modified from Paper II.*

Finally, confocal microscopy imaging of HeLa cells incubated for 4 h with non-coated and copolymer-coated FITC-labeled particles was carried out in order to compare the findings from the detailed characteristic investigation with the particle behavior in real cellular conditions. A clear difference in intracellular patterning after uptake was observed (Figure 24), where the final dispersibility of particles

coated with $mPEG_{low}$-PEI was significantly higher than those coated with $mPEG_{high}$-PEI. One reason for this might be the difference in the net surface charges, as the particles coated with $mPEG_{high}$-PEI are close to neutral both in the absence and presence of proteins, while the $mPEG_{low}$-PEI coated particles are negatively charged in the presence of proteins and this also contributes to electrostatically stabilize the particles. Another explanation might be due to the PEG chains taking part in the adsorption process in the case of higher PEG grafting ratio and hence not stretching out from the particle surface, which consequently might lead to a less efficient molecular cushioning effect. Also, the non-coated particles appeared aggregated, which confirms the need of surface functionalization for particles intended for applications in biological systems.

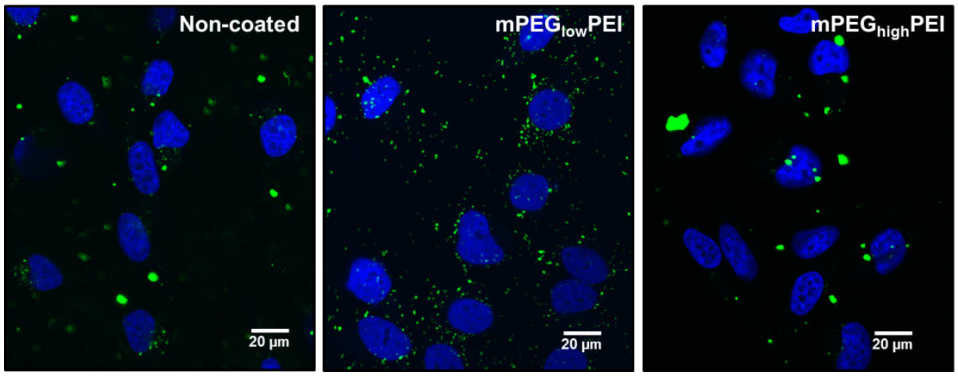

Figure 24. *Confocal fluorescence images of cells labeled with plain or copolymer-coated fluorescent particles. The cell nuclei were stained with DAPI (blue). Modified from Paper II.*

These results clearly demonstrate that it is the effective amount of PEG chains exposed on the particle surface with the correct conformation that is important rather than the total concentration of PEG, which further suggest that an optimal amount of PEG for a specific system exists. The PEI amount of the copolymer is also crucial in order to provide efficient electrostatic stabilization. The electrostatic interaction of PEI is the reason for the highest protein amount adsorbed on PEI-coated particles. Adsorption of such charged species can either counteract or aid in the electrostatic stabilization mechanism and consequently, in the best-case scenario, benefit the cellular internalization process. Thus, careful tuning of the surface functionalization and its subsequent interactions with the nanoparticles and the environment, under the conditions presenting the milieu of the intended application, is required for evaluation of the utilization of a specific surface coating.

5.3 Means of functional utilization of photonic interaction

Non-invasive bioimaging techniques are powerful tools for *in vivo* imaging, and are successfully applied in academic research and clinical trials, as discussed in the literature review part of this thesis. In research, fluorescence imaging is the most widely applied visualization method,[178] and is often applied to monitor biological processes as they take place, such as the tracking of specific cells and interaction of biological macromolecules. Also processes like cell signaling have been documented in real-time, by combining pairs of fluorescent proteins able to undergo fluorescence resonance energy transfer (FRET).[179] Further, fluorescence methods are widely applied to track and evaluate nanoparticles in biological systems, such as in cells. The emerging field of molecular imaging[180-183] has enabled visualization of molecular processes in living organisms on cellular level, and proved its efficiency for diagnosis of various diseases. Molecular imaging techniques require administration of a contrast agent prior to an imaging procedure in order to improve the quality of the generated images.[25] These contrast agents, which are suitable for recognizing structural alterations (lesions) in tissues, are typically small molecules capable of crossing the blood-tissue barriers.[71] However, a major drawback associated with conventional imaging methods is the failure to accurately differentiate between the signals originating from the contrast agent still circulating in the blood stream and the signals originating from surrounding tissue. A method allowing for *in vivo* differentiation between these signals would allow for a radically improved contrast between tissue and blood. In order to increase the range of these kinds of biological questions that can be tackled, experimental approaches and labeling methods have to continually be improved.

In the two following sections two different means of functional utilization of photonic interactions are presented. In the first study a FRET-system was implemented, to study the feasibility of using nanoparticles to catch and remove/quench (i.e. scavenge) a specific tracer compound directly in the blood circulation in an animal model. As discussed above, the background signal from the main portion of imaging agent that has not crossed the blood-tissue barrier can severely hamper the imaging, and in order to clear these background signals from the blood circulation, the "scavenger particles" were developed. In the second study, the efficacy of photonic interaction was demonstrated intracellularly, for redox-induced delivery of an active compound from a nanoparticle-based platform. Normally it is not possible to monitor the intracellular release of non-toxic compounds (such as siRNAs) directly, where an indirect read-out based on the

cytotoxic action cannot be measured. This hampers the validation of novel delivery platforms. Thus, a reporter system based on the FRET-approach was presented here, for in-real-time monitor the compound cleavage intracellularly.

5.3.1 Interaction between tracer and scavenger for enhanced molecular imaging

Contrast agents utilized for imaging purposes are substances that temporarily change the way electromagnetic radiation interact with internal structures or tissues,[184] thus making any structural changes in a damaged organ's tissue clearly distinguished from the surrounding healthy tissue. A multitude of different contrast agents already exist, which have the ability to provide for a high contrast that consequently help in correctly diagnosing a medical condition. Certain contrast agents are capable of crossing an intact blood-tissue barrier, but leakage of the contrast agent from blood to surrounding tissue is significantly more pronounced when the blood-tissue barrier is disrupted. Since disruption of a barrier occurs locally at disease sites,[185,186] such as in tumors or due to inflammation, leakage and accumulation of the contrast agent at the particular site is indicative of a pathological condition. Due to the problem of discerning the emitted signals from the contrast agents in the blood flow and in the tissue, an efficient detection of tissue changes is restricted to places where the structural changes have already affected relatively large regions. Consequently, specific pathological conditions, such as cancer or Alzheimer's disease, are often medically diagnosed at a rather late stage.[187-190] There is an extensive research going on for developing new molecules and particles for use as contrast agents, as highlighted in the literature review part of this thesis. A lot of attention is also focused on making these new compounds able to cross blood-tissue barriers, such as the blood-brain barrier which is especially known for not being permeable to a variety of molecules.[191,192] As a result, there is a need for a novel method of removing/decreasing the excess contrast agents from the blood circulation, which could increase the contrast between tissue and blood, and consequently, increase the probability of early diagnosis of various diseases.

To address this issue, a tracer-scavenger system was developed in **publication III** to investigate the potential of silica nanoparticles to scavenge a specific tracer compound (and quench its fluorescence) directly in the blood circulation in mice. For this study, the PEI-functionalized silica core-shell particles, $n\mathrm{SiO_2}@m\mathrm{SiO_2}$, were utilized to provide for a flexible nanoparticle-platform where the silica core can be exchanged to some other inorganic colloidal material, such as a magnetic core for a magnetic tracer-removal system that could itself be traced with MRI, or any other inherently detectable core for imaging. In case of a magnetic core, the size of the core is optimal for both a strong magnetization and a

high contrast in MRI, as demonstrated in **publication I**. To choose the right size of the particles intended for a specific application is crucial in many ways, not least for the biodistribution of the particles.[193] As commonly known, particles with a diameter less than 200 nm tend to have prolonged blood circulation time and are more favorable for crossing disrupted blood-tissue barriers ("passive targeting") via the enhanced permeation and retention (EPR) effect.[194]

Thus, particles with a size of approximately 200 nm were chosen, to support optimum circulation time, but large enough to rather stay in the blood circulation than easily extravasate into the leaky vasculature through disrupted blood-tissue barriers. The core-shell particles were further functionalized with a high degree of surface-grown PEI, as demonstrated and evaluated in **publication IV**. These *n*SiO_2@*m*SiO_2@PEI particles obtained a high positive charge (+41 mV) in HEPES buffer (25 mM, pH 7.2), and were fully dispersible with a hydrodynamic diameter of 350 nm.

The high surface-concentration of reactive amino-groups was utilized for further surface-functionalization with streptavidin. The high affinity biotin-streptavidin binding system was selected to be used as model molecular linker for the scavenger-system, since this interaction is one of the strongest non-covalent bond known in nature,[195] and has been successfully used for many bioapplications.[196-198] However, the bacteria-derived streptavidin has a disadvantage of being immunogenic,[199,200] which may hamper the translation of this specific system into the clinics. Streptavidin has several functional groups, including carboxylic acids (-COOH), which makes it well-suitable to be covalently linked to the primary amines (-NH_2) on the PEI-polymer, via amide bonds. Since streptavidin is negatively charged at physiological pH, it can also be adsorbed on the positively charged PEI-functionalized particles. The adsorption approach was utilized to get an insight on the amount of streptavidin that can be attached to the particle surface. By titration of streptavidin onto the particles, a maximum labeling concentration of 2.5 wt% streptavidin was determined by UV-absorbance. 2.5 wt% streptavidin was subsequently used for covalently labeling the particles, resulting in *n*SiO_2@*m*SiO_2@PEI@STV particles. Biotin-labeled dextran was chosen as model tracer compound. The streptavidin and the dextran were both fluorescently labeled as a FRET-pair, with Dylight 549 and fluorescein in the form of FITC. The photonic interaction between the scavenger particles, *n*SiO_2@*m*SiO_2@PEI@STV, and the biotin-labeled dextran tracer was first evaluated by stepwise addition of particles to dextran suspended in HEPES buffer solution, as schematically described in Figure 25a. The results presented in Figure 25b show a clear correlation between the interaction (I_{FRET} /I_{FITC}) and the amount of free dextran tracer, where the photonic interaction readily increases when the

amount of free tracer approaches zero. The circled point, after which the photonic interaction becomes pronounced as evidenced by the steep rise in the slope, correlates to a molar ratio of 2:1 of dextran and streptavidin. Streptavidin has four biotin binding sites,[201] but since it here is conjugated to a particle it is expected that not all of the biotin binding sites will be accessible.

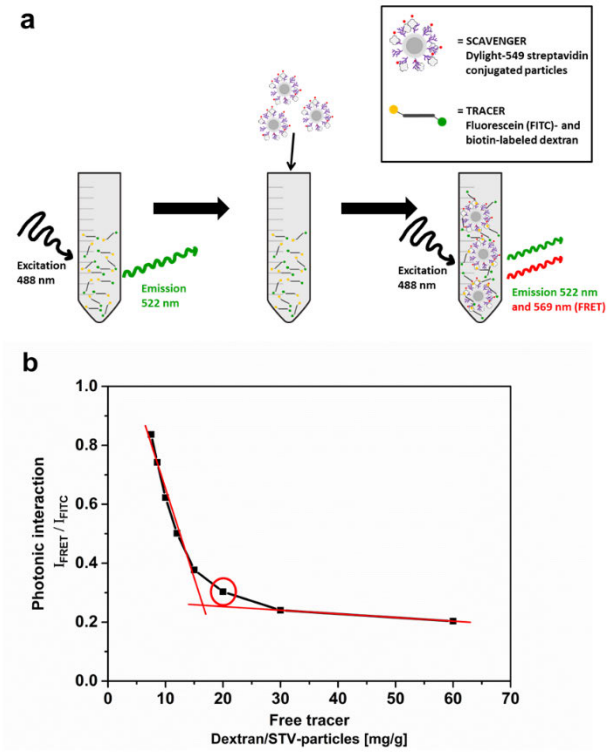

Figure 25. *Photonic interaction between dextran tracer and silica scavenger particles by streptavidin-biotin binding in vitro, as measured by FRET. (a) A schematic illustration of the process, where the initial solution of fluorescein- and biotin-labeled dextran give rise to green emission only, while after addition of Dylight 549-streptavidin conjugated particles the green emission decreases and red emission increases. (b) The photonic interaction (I_{FRET} / I_{FITC}) increases with higher amount of particle-bound tracer. The circled point correlates to a molar ratio of 2:1 of dextran and streptavidin. Adapted from Paper III.*

In the literature, it has been demonstrated that functionalizing the PEI-coating with succinic acid groups ("succinylation") decreases protein adsorption on the particles,[202] since the zwitterionic nature of this coating provides better stealth properties. Thus, succinylation was also investigated for the scavenger par-

ticles, and is presented in detail in **publication III**. However, the succinylated particles were not as good scavengers for the dextran tracer as the ones only PEI-functionalized, and therefore they were not considered for the *in vivo* study.

After intravenous injection of the dextran tracer in mice, with subsequent injection of the scavenger particles, the chemical and photonic interaction of the two compounds could be visualized (as schematically illustrated in Figure 26a). Chronic cranial windows were implanted over mouse somatosensory cortex, and shortly after injection, the scavenger particles as well as their interaction with the tracer was imaged. As nanoparticles moved in the blood circulation with a high speed, the best approach for detection was by using line-scans (Figure 26b). The tracer fluorescence was more pronounced than the scavenger fluorescence, due to the fact that the dextran tracer filled most of the available volume of blood vessels. Consequently, the best approach for detection of the interactions between tracer and scavenger was to observe the increase in the ratio of fluorescence between the Dylight549 and fluorescein channels on individual nanoparticles. This is analog to the increase in acceptor fluorescence observed in the FRET photonic interaction, in environments where the conditions for FRET are optimal. Microscopy images in Figure 26c represent examples of nanoparticles detected with line profile scanning. The red color, in the lower image, confirm the strong photonic interaction between the scavenger and the tracer labeled with biotin, as compared to only yellow color, in the upper image, when the tracer was not labeled with biotin and thus no interaction occurred. A statistically significant shift in fluorescence was detected, towards the scavenger fluorescence (Dylight549 channel) in experiment with biotin-fluorescein-labeled tracer, set against experiment where the tracer was only labeled with fluorescein and no biotin ($p=0.00377$), as can be seen in Figure 26d. This means that the streptavidin-functionalized particles could recognize and bind the biotin-labeled dextran tracers, and the strong interaction between these led to an in real-time detectable physico-chemical interaction in the blood circulation in mice. This study shows the capability of the produced nanoparticles to scavenge specific tracer compounds *in vivo*, which subsequently can provide for an efficient method to remove and/or quench excess contrast agents from the blood circulation prior to an imaging session. Such a method would allow for better contrast of signals originating from the tissue area of interest and the signals originating from the blood circulation. As a result, this kind of system could enhance the probability of earlier diagnosis of various diseases.

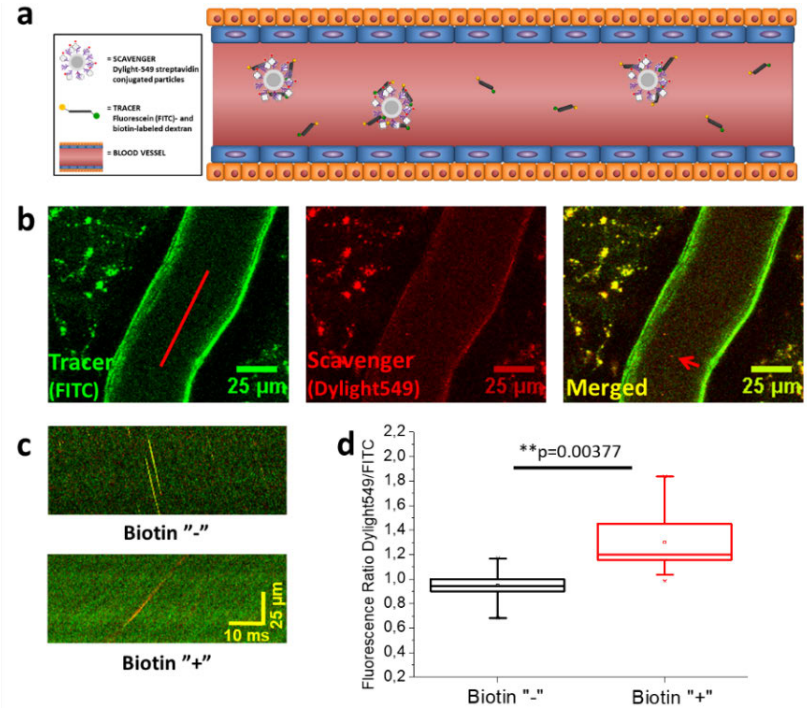

Figure 26. *Photonic interaction between dextran tracer and silica scavenger particles in vivo. (a) Schematic illustration of the interaction between tracer and scavenger in a blood vessel. (b) Examples of mouse cortical vessels used for visualization of tracer; fluorescein (FITC)- and biotin-labeled dextran (left panel), and scavenger; Dylight549- and streptavidin-labeled nanoparticles (middle panel) in vivo. Merged image is shown in the right panel. Red line in the left panel represents a line-scan along the vascular lumen used to detect and analyze nanoparticles. Red arrow in the right panel shows example of nanoparticle detected in the typical 2D plane image. (c) Examples of nanoparticles detected with line profile scanning, where the tracer (FITC) and scavenger (Dylight549) channels are superimposed. The images comprise stacks of individual line-scans (as shown in (b)), with time shift on the x-axis and distance on y-axis, resulting in nanoparticles detected in the form of lines. The lower image represents an experiment where the dextran tracer is labeled with biotin (Biotin "+"), while the upper image presents a control experiment where the tracer has no biotin (Biotin "-"). A more reddish hue of nanoparticles in the presence of biotin is noted. (d) Analysis of the change in the ratio between FITC and Dylight549 channels in experiments with (Biotin "+") and without (Biotin "-") biotin. In the presence of biotin on the dextran tracer we observed statistically significant shift of ratio towards scavenger (STV-Dylight549) channel highlighting physical and chemical interaction between dextran tracer and silica scavenger particles in vivo. Adapted from Paper III.*

5.3.2 Intracellular redox-induced release of active compound

As demonstrated above, photonic interactions can be used as a convenient tool for studying and evaluating processes in biological systems, which can be very challenging to study by other means. Especially in the recently emerging field of intracellular delivery of active compounds by nanoparticles, the release is typically measured indirectly, normally by determining the cellular response, such as the viability of the treated cells. Thus, the evaluation of non-cytotoxic cargo release as well as the time-course of it is limited. A method allowing for directly monitoring of the intracellular release would be highly desirable, since the release mechanisms determined under *in vitro* conditions rarely can be directly translated to actual biological or physiological (*in vivo*) conditions. Thus, in **publication IV**, a FRET-reporter system was developed to directly follow the time-course of intracellular release of a redox-cleavable model drug compound from a nanoparticle platform.

Here, the same PEI-functionalized silica core-shell particles, $n\mathrm{SiO_2}@m\mathrm{SiO_2}$, as used in the study presented above, were synthesized and utilized as delivery platform. The FRET-reporter system was established by covalently attaching two fluorophores, a donor and an acceptor acting as a FRET-couple, to the particle surface, by employing a redox-cleavable bond for the acceptor compound. The donor molecule, FITC (fluorescein isothiocyanate), was coupled through a stable isothiocyanate bond to amino-groups on the PEI-polymer. Subsequently, the acceptor molecule, sulfo-rhodamine (sulforhodamineamidoethyl mercaptan), was coupled to the particle surface through a redox-labile disulfide bond. This was introduced using SPDP (Succinimidyl-3-(2-pyridyldithio)-propionic acid) as a linker between sulforhodamine and the amino-groups. Thus, a decrease in FRET signal intensity reported on redox-induced acceptor compound release. A schematic illustration of the coupling and cleaving procedures is presented in Figure 27.

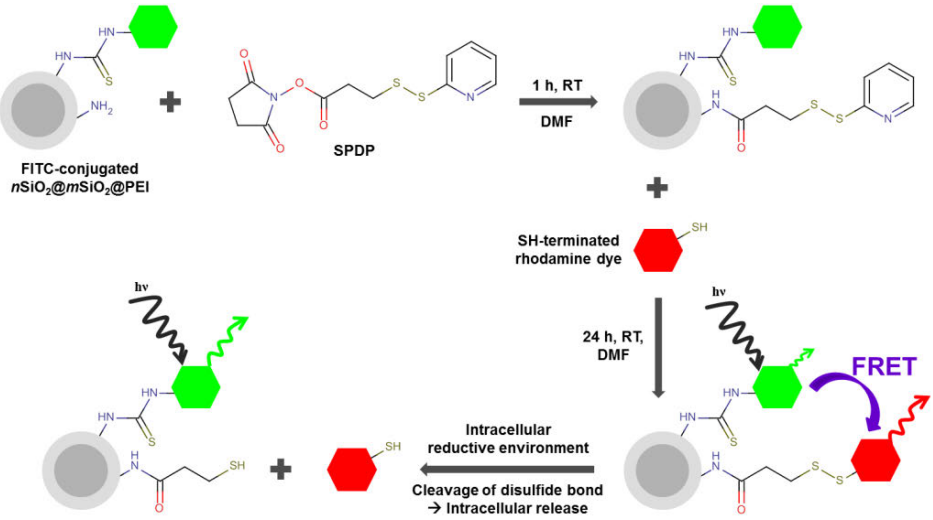

Figure 27. *A schematic diagram representing the coupling procedure for the acceptor compound, with subsequent detection, as well as loss, of the FRET-signal. The donor compound fluoresceine (as FITC) was stably coupled to the amino-functionalized particle surface, while the acceptor rhodamine (Rh-SH) was covalently linked via a redox-sensitive disulfide linker. The redox-induced disulfide cleavage inside the cell, endowed for the loss of FRET-signal. Adapted from Paper IV.*

The surface concentration of the donor and the acceptor molecules were evaluated in order to optimize the degree of FRET signal. At first, particles were conjugated with a range of different FITC concentrations between 0.0001 wt% and 1 wt% and the recorded fluorescence intensity was compared to establish the highest concentration that does not lead to self-quenching (Figure 28a). The fluorescence intensity rapidly increased up to 0.1 wt%, afterwards it dropped due to a too high density of FITC molecules. The FITC concentration was therefore fixed at 0.01 wt%, which was one order of magnitude below the concentration that led to self-quenching, to also leave enough space for the acceptor molecules. Next, the optimal concentration of acceptor sulfo-rhodamine molecules was evaluated by confocal microscopy, to in the same time validate the sensitivity of this instrument for the following cell study. Particles with decreasing donor:acceptor ratios were imaged, and the FRET level determined as a FRET-ratio index. Increasing the amount of acceptor relative to the donor up to 10-fold increased the FRET successively (Figure 28b). In order to have a high starting FRET-level and thus better dynamic range for detecting compound cleavage, the particles with the highest donor:acceptor ratio of 1:10 were chosen for further study.

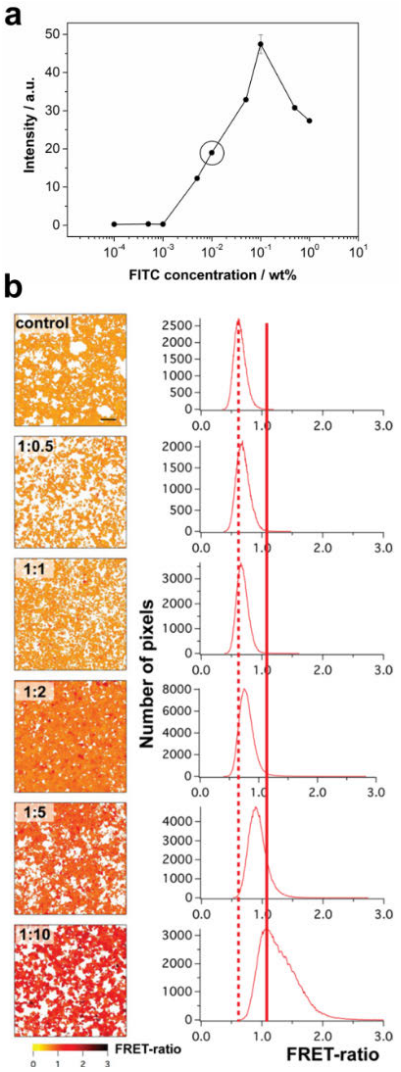

Figure 28. *Optimization of the donor and acceptor concentrations on the particle surface. (a) The fluorescence intensity of particles labeled with different concentrations of FITC was determined in order to establish an optimal FITC concentration for the final labeling. If a too high concentration of FITC-molecules were conjugated, the intensity dropped due to self-quenching. The circle represents the FITC-donor concentration chosen for the labeling of the subsequent FRET-reporter particles. (b) Microscopy images, with corresponding histograms, of particles labeled with different donor:acceptor ratios. The control sample is a 1:1 mix of particles labeled with only donor or acceptor-fluorophore. High-FRET levels are shown in black and low-level FRET in yellow. The dotted vertical line in the histograms represents the control FRET-ratio level, while the solid line marks the high FRET maximum of the histogram of the particles with highest relative acceptor-concentration. Modified from Paper IV.*

HeLa cells were incubated with the high-FRET (1:10) particles at a concentration of 20 μg/ml for different time intervals to investigate the intracellular cleavage by FRET imaging. Figure 29a reveals a significant loss of FRET over time, while particles with a non-cleavable FRET-pair did not show changes in the FRET even after 24 h (as shown in publication IV). To relate this to the rate of particle internalization, Hela cells were incubated with the same concentration of particles at the same time intervals, and the extracellular fluorescence was quenched by trypan blue prior to flow cytometry analysis (Figure 29b). A complete shift of the histogram shows that most of the cells had internalized particles already after one hour. After 24 h of incubation the intensity histogram had shifted approximately 4-fold. The correlation between the time-courses of particle internalization and compound cleavage revealed that, for this particle system, internalization depends linearly on the incubation time after the first hour of incubation, while cleavage from internalized particles occur much faster and is even most pronounced within the first hour (Figure 29c). With such a FRET-reporter system presented here, cargo-compound release could be directly monitored upon particle internalization, benefiting the indirect read-outs that are based on the cytotoxic cellular effects from the released compounds.

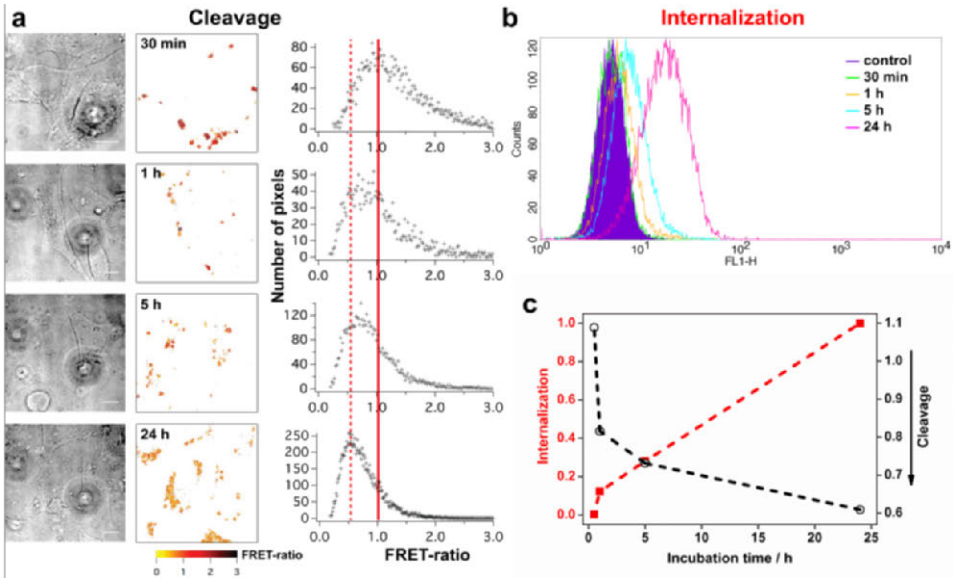

Figure 29. *Intracellular evaluation of the developed high-FRET particles. (a) Microscopy images, bright-field and FRET in parallel, with corresponding histograms of the FRET-ratio per pixel, of cells incubated with particles labeled with a donor:acceptor ratio of 1:10. A clear loss of FRET over time can be distinguished from the histograms. (b) Cellular uptake of particles, measured by flow cytometry, at corresponding time intervals as presented in Figure (a). The shaded area represents the control cells without particles. An increasing particle uptake is seen by higher fluorescence intensity values (right-shift) of the histograms, over time. (c) In order to facilitate the correlations between internalization, i.e. the particle uptake presented in (b), and acceptor compound cleavage, determined from the FRET-ratio values of the histogram peaks in (a), these are plotted on the same time axis. The graph shows that particle uptake into cells is highly efficient and that intracellular redox-mediated cleavage occurs shortly after internalization. Modified from Paper IV.*

5.4 Means for delivery of active substances in biological systems

As discussed in the literature review part of this thesis, the encapsulation of drugs and imaging agents into porous inorganic nanoparticles has expanded as a field of study, due to the realization that they can carry a large amount of cargo and protect it from degradation or loss of activity in the biological environment, as well as in some cases provide for a sustained release. Especially silica nanoparticles have attracted much attention as being one of the most biocompatible drug carriers. Silica has a high surface area that makes it possible to incorporate an amount of drug equal to the particle's own weight.[203] Since silica is a hydrophilic material, and the dispersability of such nanoparticles can further be enhanced by the right surface functionalization, mesoporous silica nanoparticles (MSNs) have recently been highlighted as ideal carriers for poorly water-soluble molecules.[204-206]

In the two following studies, different means of delivery of active substances by MSNs in biological systems have been highlighted. In the first study, we have designed a range of different MSN-dye formulations and evaluated their potential as optical probe systems intended for long-term labeling and tracking of cells. After thoroughly investigation of the dye-incorporated MSNs in cellular models, with focus on arriving at an optimal design, the most suitable candidates were evaluated and followed over time on the chorioallantoic membrane (CAM) of developing chicken embryos, as well as in mice, by xenotransplantation of labeled cells. The CAM model is emerging as a useful *in vivo* model system to assess tumor angiogenesis, progression and metastasis.[207] Still, the mouse is one of the most widely used model organism, due to its similarity to humans, and pre-labeled human cells can be transplanted into these animals by xenotransplantation, which currently is the only experimental system for tracking human cells in animals.[179] In the second study in this chapter, the possible beneficial treatment effect of MSNs loaded with the hydrophobic anti-inflammatory drug dexamethasone was investigated on two differently induced lung inflammation models in mice by inhalation of the particles.

5.4.1 Dye-loaded container particles for long-term optical tracking of cell populations

Dye-incorporated MSNs were comprehensively investigated in **publication V** for long-term detectability and cellular retention. The cell populations labeled with the here developed fluorescent optical probes were followed for one week *in vitro* and up to one month *in vivo*. Two different sizes of MSNs (Figure 30) were used as carriers for commercially available hydrophilic and hydrophobic fluorophores, MSN_{100} (approx. 100 nm in diameter) and MSN_{300} (approx. 300 nm in diameter). MSN_{100} particles were utilized as carriers for hydrophobic dyes, while MSN_{300} particles were employed as carriers for hydrophilic dyes in order to be comparable to earlier studied MSNs of similar designs.[65,67,116] In order to provide a more compatible environment for the hydrophobic dye cargo, the MSN_{100} particles were hydrophobized via two different routes. The particles were further PEI-functionalized to ensure proper dispersability and enhance the cellular internalization. The particle designs are briefly summarized in Figure 30g.

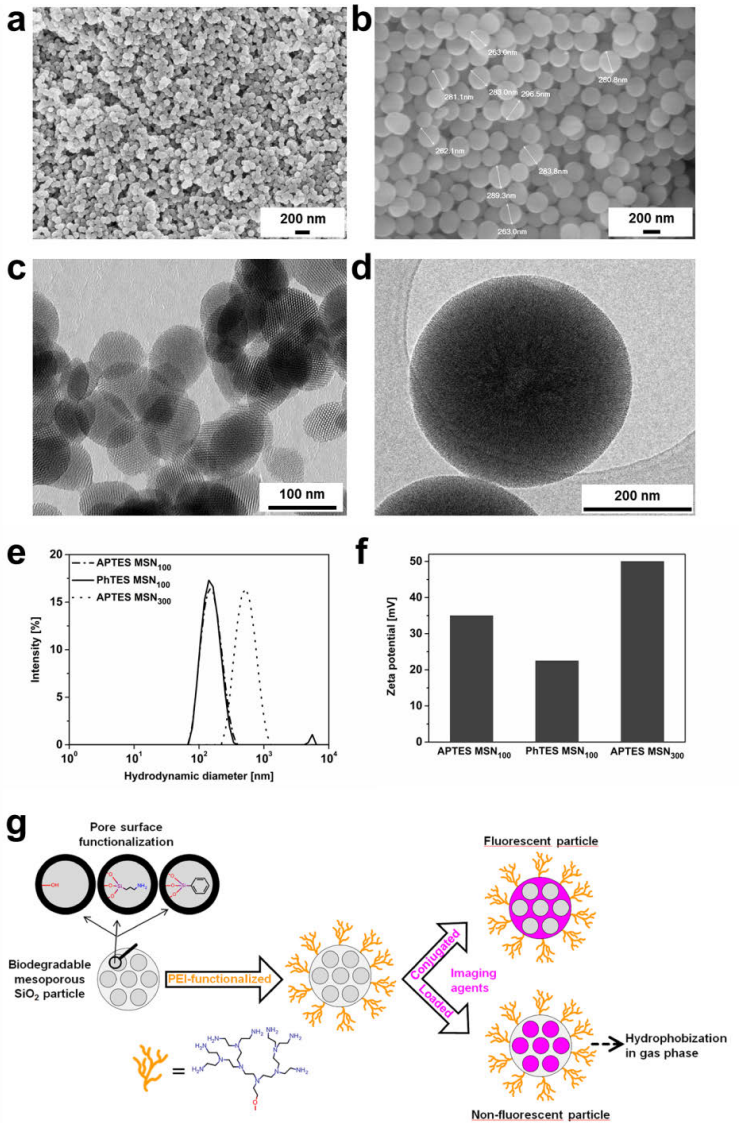

Figure 30. *Characterization of the two differently sized MSNs. (a) SEM image of MSN_{100}, (b) SEM image of MSN_{300}, (c) TEM image of MSN_{100}, (d) TEM image of MSN_{300}, (e) hydrodynamic size distributions of the MSNs, (f) zeta potential measured in HEPES buffer at pH 7.2, (g) schematic representation of the particle designs. Modified from Paper V.*

Commercially available fluorophores, which are widely used in bioscientific research, were chosen for the study. As hydrophilic dyes, fluorescein and rhodamine were used in the form of free fluorescein and rhodamine B, as well as in their amine-reactive forms, FITC (fluorescein isothiocyanate) and TRITC (tetramethylrhodamine isothiocyanate). As hydrophobic counterparts, lipophilic carbocyanine dyes of similar emission wavelengths were chosen, namely DiO and

DiI. Different routes of incorporating the fluorophores were employed, as summarized in Scheme 1. The hydrophilic dyes were either incorporated in the silica matrix already in the synthesis step of the particles (F-1,2,3 and R-1,2), adsorbed in the porous particles before (F-5,6 and R-3,4,5) or after PEI-functionalization (F-4 and R-6,7), or conjugated to PEI-functionalized particles (F-7,8 and R-8,9). The hydrophobic dyes were adsorbed into the porous particles after or during PEI-functionalization. The starting particles used for the hydrophobic dye cargo were either all silica (MSN_{100}: I-3,5 and O-5), aminofunctionalized (MSN_{100}APTES: I-1,4,6,8,9 and O-1,3,6,7,8,9,11), or phenylfunctionalized (MSN_{100}PhTES: I-2,7 and O-2,4,10) to gain hydrophobic properties. As a last step, hydrophobization in gas phase was carried out for those hydrophobic dye carriers that had not been loaded into already hydrophobized MSNs (I-4,5,8,9 and O-6,7,8,11).

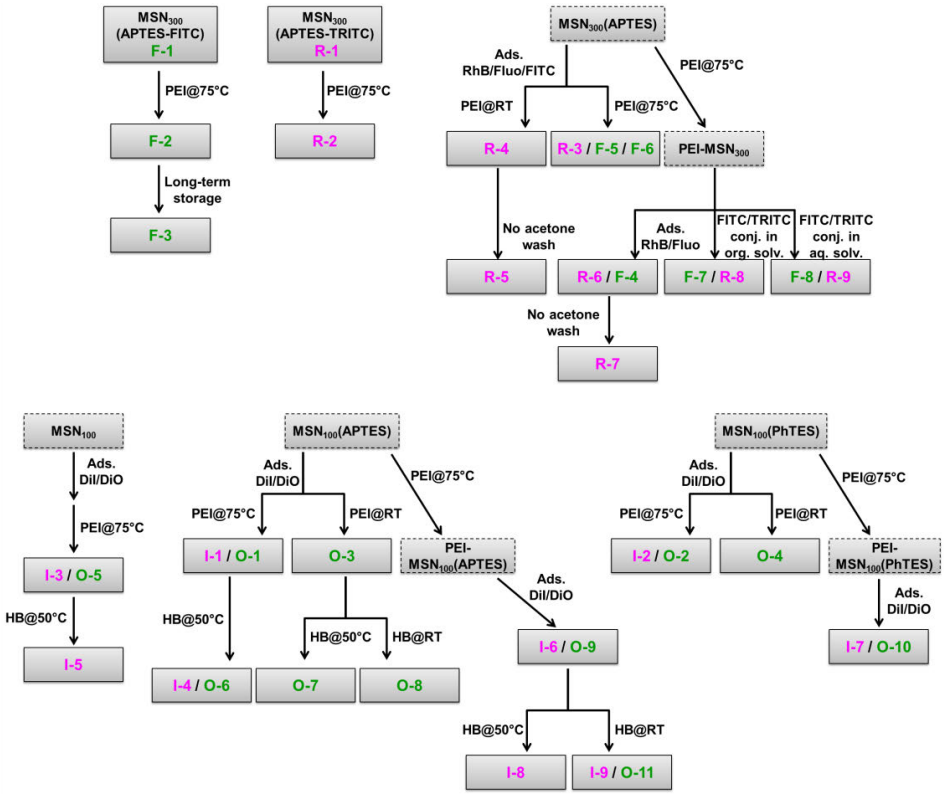

Scheme 1. *Overview of the dye incorporation and surface functionalization procedures. Modified from Paper V.*

All the different MSN-dye formulations were characterized based on fluorescence to assess the limitations and considerations with fluorophores as well as to serve as a basis for further studies. The particles were dispersed to 1 mg/ml in HEPES buffer and their maximum peak intensity was recorded on a fluorescence spectrometer (Figure 31a-d). The maximum fluorescence intensities are not correlated to the loading degrees of the dyes, as demonstrated by comparing to the amount loaded dye (Figure 31e). The loading degree was determined for the most interesting samples based on UV-vis absorbance after complete elution of dye for loaded fluorophores, or dissolution of the MSN-dye conjugates for covalently attached fluorophores. The large difference in fluorescence intensity between sample F-1 and F-2, though same amount of fluorophore (same base particle), can be explained by the surface coating of F-2 with PEI, which creates a local pH-effect that lowers the fluorescence intensity of fluorescein.[152] Too high dye loading degrees result in self-quenching phenomena. This is thus not the case for samples F-4 and R-5, where fluorescein and rhodamine have been adsorbed into MSNs (fluorescein into ready-made PEI-MSN which allows for high loading degree), and as consequence leading to a rapid desorption of the dyes in aqueous solution since the solvent-dye interactions become more favorable. In this case the self-quenching effect is absent, since it is the free dyes being measured and giving rise to high fluorescence intensity. The samples F-7 and R-8, where FITC and TRITC have been conjugated to PEI-MSNs, give rise to fluorescence intensities in line with the amount conjugated dyes. The hydrophobic dye molecules are not expected to leach out from the MSNs in aqueous solvents, as also evidenced by the nearly non-existent fluorescence intensities of the pure dyes at corresponding dye concentrations under aqueous conditions (samples "pure"). For samples O-4 (DiO) and I-7 (DiI) hydrophobized (MSN_{100}PhTES) carriers were used, which provided a highly favorable environment for the dyes to fluoresce, thus exhibiting a high fluorescence intensity despite a low loading degree. On the contrary, the dye loading degree was higher for the sample I-4 (MSN_{100}APTES carrier), which resulted in self-quenching of the dye molecules, and a lower fluorescence intensity. Apparently, the phenyl-functionalized MSNs did not enhance the loading of the hydrophobic dye molecules (O-4 and I-7) as compared to the amino-functionalized MSN (I-4) suggesting that hydrophobic interactions may not be dominant in the adsorption process.

Consequently, amino-functionalized MSNs were chosen to investigate at which loading degree the self-quenching effect becomes critical. A range of dye concentrations were loaded into the MSNs and the recorded fluorescence

intensity compared (Figure 31f). At low dye loading degrees, the resulting fluorescence intensity of the suspension rapidly increased up until 0.5 wt%, and after 1 wt% dramatically decreased to very low intensity values when exceeding 5 wt%. Each increase in loading degree was also accompanied by a shift in maximum intensity wavelength (Figure 31g,h). This suggests that self-quenching phenomena occur also at low loading degrees, as a shift to higher wavelength is associated with an energy drop, i.e. less energy states are allowed to emit. This can also be understood, since a doubling in loading degree does not lead to a doubling in resultant intensity. The outcome here can be compared to the results obtained when the surface concentration of FITC was evaluated, as presented in Figure 28a, in order to establish the highest concentration that did not lead to self-quenching. There, the fluorescence intensity rapidly increased up to 0.1 wt%, whereafter it dropped due to self-quenching. A reason for the ten-fold increase in the dye-amount that did not lead to self-quenching in this present study, is ascribed to the difference in the high internal surface of a porous particle, compared to the much lower surface area available on the outer particle surface, which consequently places the dye molecules in closer proximity. This, in addition to reasons attributed to the differences in dye properties.

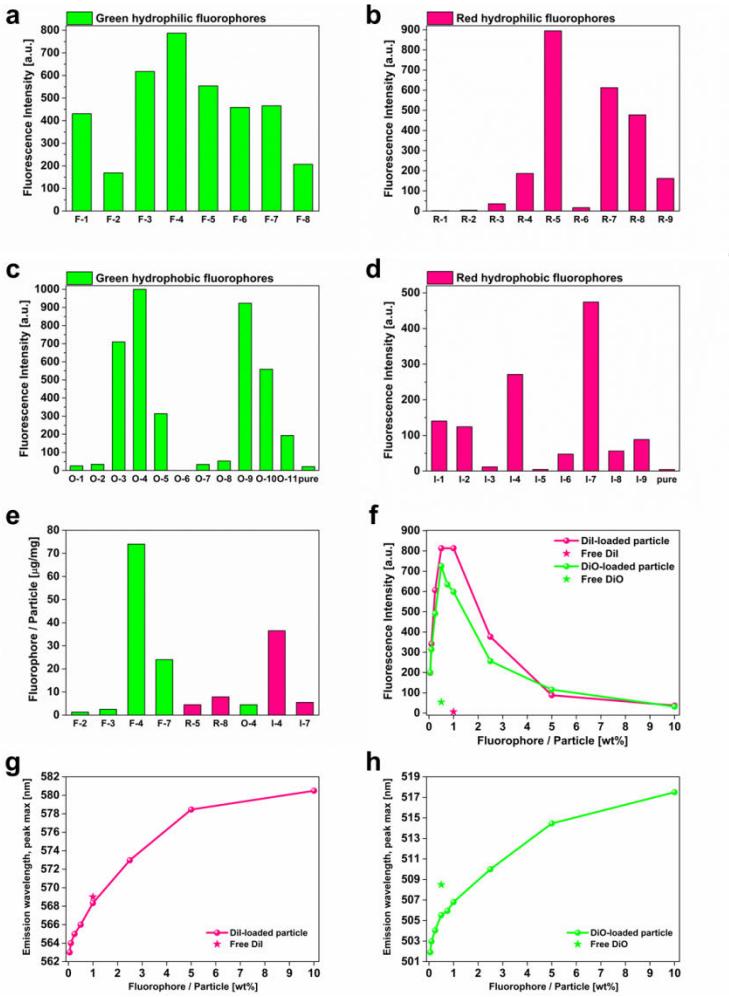

Figure 31. *Fluorescence characterization of the dye-loaded MSNs presented in Scheme 1. (a)-(d) Fluorescence intensities for particle suspensions, (e) fluorophore content per particle mass, (f) fluorescence intensity as a function of hydrophobic fluorophore loading into amino-functionalized particles, (g) and (h) shift in maximum emission wavelength as a function of fluorophore loading into the MSNs presented in (f). Modified from Paper V.*

To further investigate how the different MSN-dye formulations behave as cellular labeling agents, the most promising candidates were used to label human breast cancer MDA-MB-231 cells, followed by flow cytometry assessment for five days. Due to the laser option of the specific instrument used, the MSNs loaded with green hydrophilic and hydrophobic dyes were chosen for this part of the study. Both the %positive cells as well as the mean fluorescence intensity (MFI) were considered to get an idea of the intracellular retention of label versus the di-

lution of label upon cellular division. For the hydrophilic series, most of the samples followed typical cell proliferation behavior with dilution upon division. The MDA-MB-231 cell line is an aggressive type with a high proliferation rate (cell population doubles in 24-36h), which were clearly reflected in their %positive cells versus time profiles as S-shaped curves, in line with the MFI versus time graph where the fluorescence intensity decreases to about half each day. The most promising samples from the hydrophilic series were sample F-3 and F-6. F-3 was a co-condensed MSN where the conjugated dye was introduced in the synthesis step, which results in a homogenous distribution of dye molecules in the silica matrix, and low possibility of leaching of dye. Sample F-6 was loaded with FITC prior to PEI-functionalization which most probably led to both efficient encapsulation of dye molecules as well as conjugation of dye molecules to the PEI-polymer. The cellular labeling efficiency of the hydrophilic series in comparison to the hydrophobic series are investigated and discussed in more detail in publication V.

The most promising MSN-dye formulations in the hydrophobic series were further compared to a commercially available cellular labeling agent, namely quantum dots (QDs). The cellular retention and labeling efficiency of these were followed for one week by flow cytometry complemented with three days of confocal microscopy studies (Figure 32). The QDs chosen for the experiment were of corresponding wavelength as the DiO-MSNs and were reported to have free amines on the surface. The three selected DiO-MSNs were also the ones which gave rise to highest fluorescence intensity as stock suspensions (Figure 31c). The concentration of QDs chosen to label the cells were adjusted to match with the fluorescence intensity of the DiO-MSN suspensions. The QDs were hardly detectable over the control level in flow cytometry, as also complemented by the microscopy evaluation where a few green dots were discernible on day one (Figure 32c). The hydrophobic dye-loaded MSNs showed a distinctly different fluorescence intensity profile over time than what was observed for the hydrophilic series. As expected, the result indicated slow intracellular release of dye, which further accumulates in the hydrophobic parts of the cell, which leads to an enhancement in fluorescent properties. Due to this even an increase in MFI can be observed from day one to day two, even though the cells have doubled during the same time, which also can be seen from the microscopy images. After the first 24 hours the MFI starts to decrease due to further cell division. The %positive cells is still very high up to day five, since the prospective sustained release of dye can continue also after the transfer to daughter cells. This implies a considerably extended retention effect than what can be accomplished for inherently detectable optical probes, as for the hydrophilic series.

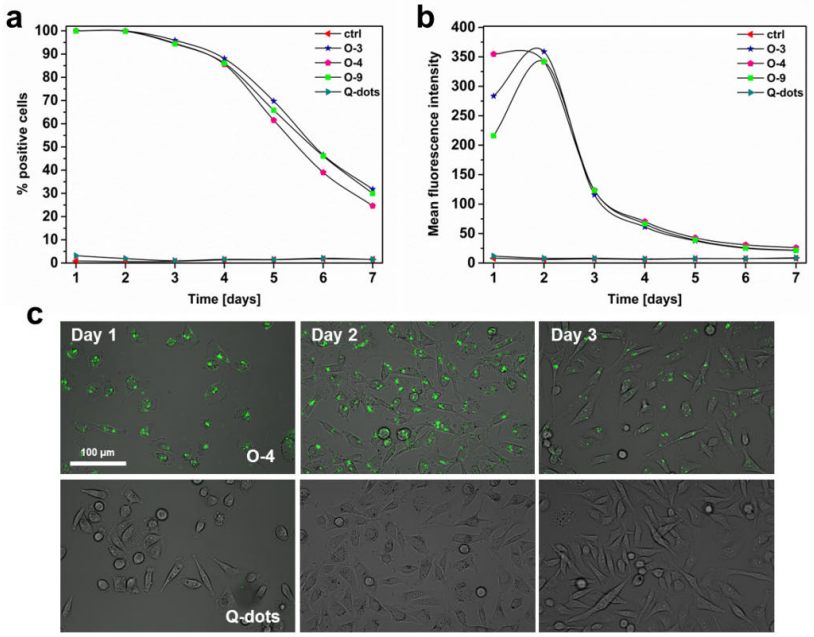

Figure 32. *Cellular labeling efficiency of MSNs loaded with hydrophobic dye, in comparison to quantum dots. The particles were followed by flow cytometry up to 7 days (a) and (b), and by microscopy up to 3 days (c). Adapted from Paper V.*

Prior to the *in vivo* part of the study, the rate of exo-endocytosis of the particles was evaluated in co-culture assays, in order to evaluate the risk of cellular exchange of particles between cell populations. The results indicated that although exo-endocytosis occurred, the rate of the cellular exchange was very low, and will thus not give rise to enough false positives to significantly hamper the cell tracking *in vivo* (presented in publication V). The MSNs were then further characterized with the *in vivo* imaging system (IVIS) both as particle suspensions and labeled MDA-MB-231 cells to choose the best candidate to study the evolution of the fluorescence signal *in vivo*. Cells labeled with sample I-6 (corresponding to sample O-9) gave rise to a bright signal with this specific setup, and where thus chosen for the *in vivo* studies. This sample was dye-loaded as a last step in the MSN-preparation process whereby complete adsorption (5 wt%) is attained. This high dye loading should provide for long intracellular release ability over time, which was already confirmed in the flow cytometry analyses on shorter time scales. MDA-MB-231 cells were labeled with the selected MSNs, and xenotransplanted subcutaneously into both flanks of 6 nude mice. Tumor growth was followed for 32 days with optical *in vivo* imaging, after which the animals were sacrificed, and the organs further analyzed *ex vivo*. To verify that cancer cells in the tumor core were also labeled, the tumors were cut in half prior to image analyses. The tumors were clearly visible during the course of the

experiments, and still after 32 days the signal was easily detectable (Figure 33a). *Ex vivo* analyses confirmed that labeled cells existed throughout the tumor tissue (Figure 33b). Interestingly, fluorescent cell colonies were detected in the lymph node and the rib of one mouse, which was later confirmed by histological analysis by unbiased pathologist (Figure 33c). To further visualize tumor cells in the vasculature in real-time, labeled cells were transplanted on the chorioallantoic membrane (CAM) of a developing chicken embryo. CAM allows for imaging of cancer cell invasion and circulation in the blood stream during approximately one week, and is therefore a valuable *in vivo* model system. The labeled cells were readily detectable in real-time as circulating in the blood stream. MSNs loaded with hydrophobic dye followed by a sustained release were here proven to be an efficient optical probe system suitable for long-term labeling and tracking of cells. Different dye incorporation strategies led to considerably deviating cellular labeling efficiency in terms of detectability and sustainability of the provided signal, than what may have been expected from characterization of particle suspensions only. The results emphasized the importance of all preparation and modification steps to be carefully considered depending on the final application.

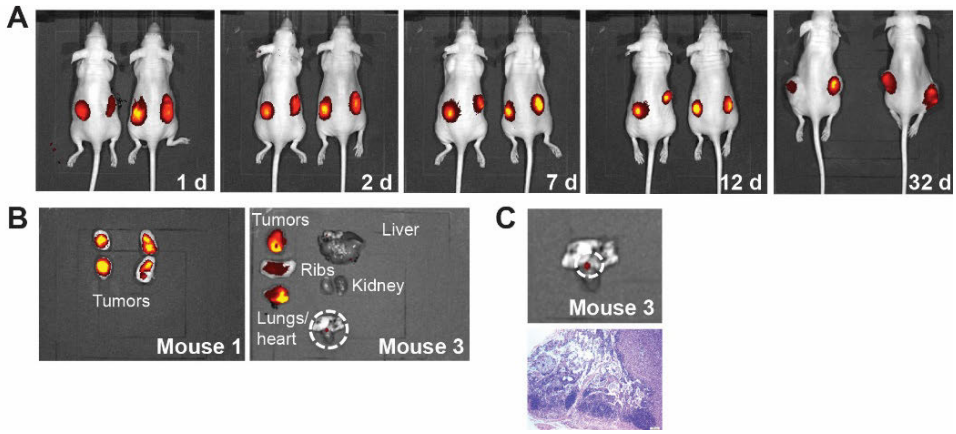

Figure 33. *In vivo imaging of tumor growth of breast cancer cells, labeled with dye-loaded MSNs, in mice. (A) The xenotransplanted cells were followed for a period of 32 days, (B) and (C) ex vivo imaging of the isolated organs verified the tumor labeling, and further allowed for detection of metastatic colonies in lymph node and rib. Adapted from Paper V.*

5.4.2 Drug-loaded particles for treatment of airway inflammation by pulmonary delivery

Numerous benefits can be attained by incorporating molecular agents into carrier particles for *in vivo* systems. In **publication VI** we investigated the feasibility of using mesoporous silica particles (MSPs) as carriers for anti-inflammatory drugs in

the treatment of airway inflammation. Corticosteroids, such as dexamethasone (DEX) used in this study, are well-known to decrease the number of inflammatory cells in airways and to improve the respiratory function; however, DEX can also cause unwanted side effects particularly when used at high doses.[208-211] Since DEX is practically insoluble in water (0.1 mg/ml)[212] it would be expected that a silica particle-formulation can enhance the solubility and dissolution rate of the drug.

Two different sizes of particles on the micron and nanoscale (1 μm and 200 nm) were produced (Figure 34) and loaded with DEX to a loading degree of 1:1 DEX:MSP. Both the larger (L-MSP) and the smaller (S-MSP) particles were produced with modifications from the synthesis reported in Kumar *et al.*[213], which yields highly porous particles composed of a random close packing of smaller primary nanoparticles. The particles were further surface functionalized with the PEG-PEI copolymer developed in **publication II** (presented in chapter 5.2.2) for optimal aqueous dispersibility also after high drug loading, and in addition, to potentially promote favorable and suppress unfavorable interactions upon administration via the airways. The amount of DEX in the particles after surface functionalization was measured by elution of DEX from the particles in methanol. DEX has a high solubility in methanol and is rapidly eluted from the silica matrix. The amount of drug in the supernatant could thus be calculated through UV-Vis measurement of the supernatant and reached about 100 wt% for both L-MSP and S-MSP, which shows that the drug was still retained in the silica matrix during the PEG-PEI functionalization done in buffer solution.

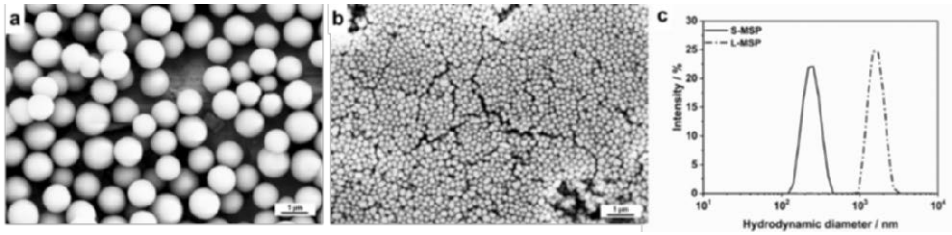

Figure 34. *Characterization of the large (L-MSP) and small (S-MSP) particles. (a) SEM image of the L-MSP, and (b) SEM image of the S-MSP, reveal spherical mono-dispersed particles with the larger particles sized around 1 μm and the smaller less than 200 nm (c) Hydrodynamic size distributions of the particles. The peak for the S-MSP is centered at 230 nm with a PdI of 0.03, while the peak for the L-MSP is at 1500 with a PdI of 0.05. Modified from Paper VI.*

Two different mice models of airway inflammation were utilized; chemical-induced airway inflammation provoked by exposure to the cytotoxic compound melphalan (MEL), and endotoxin-induced pulmonary inflammation induced by

exposure to lipopolysaccharide (LPS). Both of the models give rise to a rapid inflammatory process in the acute phase, which peaks within 24 h. The mice were treated with aerosolized free DEX or MSPs with and without loaded DEX, 1 h after exposure to MEL or LPS. The DEX-loaded L-MSPs were administered in two different concentrations—10 mg/mL (which corresponds to 5 mg/mL free DEX), and 5 mg/mL (corresponds to 2.5 mg/mL free DEX). As controls, empty L-MSPs were used in the concentrations of 5 mg/ml and 2.5 mg/mL, respectively, to keep the number of L-MSPs on the same level as the DEX-loaded L-MSPs. For the S-MSPs, only the lower concentration was chosen; 5 mg/mL DEX-loaded S-MSPs and 2.5 mg/mL empty S-MSPs. Both the drug-loaded and the empty MSPs were surface-coated with the PEG–PEI copolymer.

Mice were evaluated for treatment effects 24 h after exposure by analyzing inflammatory cells in bronchoalveolar lavage fluid (BALF), as presented in Figure 35. Both MEL- and LPS-exposure cause a neutrophilic inflammatory response in the lung and in the progression of the neutrophilic inflammatory response, specific pro-inflammatory mediators such as MPO, KC and MMP-9 are indicators of activation and recruitment of neutrophils to the airways.[214,215] The analysis of these (MPO, KC and MMP-9) is presented in publication VI. The results of the treatment effects of the MEL-induced lung inflammation is presented in Figure 35a, and reveal that the highest concentration of L-MSP loaded with DEX (L-MSP+DEX 10) provided a similar effect to the MEL-induced lung inflammation, as a single aerosol of free DEX (5 mg/mL, "DEX only"). This was indicated by the reduced influx of neutrophils 24 h post exposure. Furthermore, the S-MSPs (S-MSP + DEX 5 mg/mL) reduced the cellular inflammation ($p = 0.08$) and neutrophils ($p = 0.07$) almost to the same degree, even though the administered amount of these particles carried only half of the amount DEX (2.5 mg/mL) compared to free DEX (5 mg/mL). In the LPS-model, the inflammatory response was significantly reduced in all of the MSP-treated groups. Regardless of the DEX-loading in the MSPs or not, all of the treated animals showed a reduced number of total cells and neutrophils 24 h after exposure (Figure 35b).

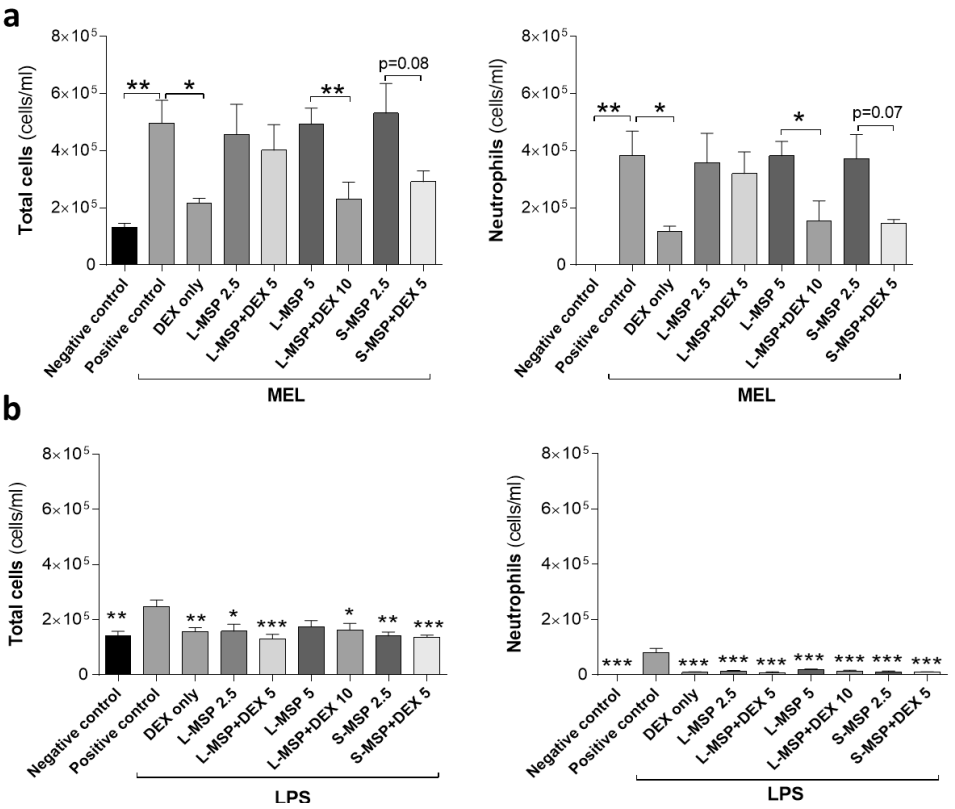

Figure 35. *Total leukocytes and the total number of neutrophils in bronchoalveolar fluid (BALF) from mice exposed to (a) melphalan, MEL or (b) lipopolysaccharide, LPS. Values indicate means ± SEM, *p<0.05, **p<0.01, ***p<0.001 compared to control groups. MSP: mesoporous silica particle (L: large; S: small), DEX: dexamethasone. Positive control: HEPES buffer administered to mice exposed to MEL/LPS; negative control: HEPES buffer administered to healthy mice; DEX only: 5 mg/mL (free DEX/HEPES buffer). The numbers on the x-axis denote mg/mL (particles/HEPES buffer). Each bar represents a group of n = 6 animals. Modified from Paper VI.*

In conclusion, the results showed that the MEL-induced airway inflammation could be treated by aerosolized MSP-encapsulated DEX to the same extent as free DEX, and thus indicate that MSPs are viable drug carriers for pulmonary delivery of corticosteroids. Interestingly, in the MEL-induced inflammation, inhaled empty particles had no apparent effect on the inflammation while in the LPS-induced inflammation, inhaled particles significantly down-modulated the inflammatory response regardless of the presence of DEX or not. The mechanism by which empty MSP reduced the LPS-induced airway inflammation is presently not known, but should be the focus of future studies. Hypothetically, this observation could be explained by different magnitudes of inflammation in the two models

and also by possible interactions of MSPs with proteins and cells in BALF.[216] Due to the fact that respiratory diseases rank among the top ten causes of death in the world,[217] and the lungs offer a large surface for drug adsorption, nanoparticle-based drug delivery platforms are gaining importance for use through the pulmonary route. The results presented here, provide a foundation for future studies aimed at identifying new concepts for treatment using MSP-based drug delivery.

6 SUMMARY AND OUTLOOK

The main emphasis of this thesis was to design multifunctional nanoparticles, porous and core-shell, and evaluate them for specific applications within the emerging field of nanomedicine. The nanoparticles, consisting of either pure silica or magnetite-silica composite, were thoroughly characterized, with the focus on controlling their bio-behavior by surface functionalization. The stability of nanoparticles in application-relevant media is highly important, and surface functionalization is thus essential for a successful utilization of these materials in biological systems. Especially if the intended use is intravenous administration *in vivo*, the nanoparticles must have a long systemic circulation time and overcome clearance by the immune system, which further puts the outermost surface coating on top of the list of the most crucial and challenging parameters of the nanoparticles. The feasibility of coating the nanoparticles with a stabilizing polymer have been comprehensively studied in this thesis. It was concluded that a thin porous silica coating on an inorganic core can greatly enhance the degree of surface functionalization, and thus provide for better stability and higher amount of surface-functional groups for conjugation of application-specific active compounds. To further increase the bioavailability of nanoparticles, block-copolymers consisting of two different polymers are often utilized in this field of study, however rarely studied in-depth. In this thesis a detailed investigation clearly suggested that an optimum combination of steric and electrostatic stability for a system exists. Further, the consequences of lacking a stabilizing functionalization of the nanoparticles was demonstrated, with the subsequent errors in tracking the nanoparticles intracellularly by fluorescence-based techniques. The nanoparticles tailored for their specific diagnostic and therapeutic applications were further evaluated here, specifically for cellular labeling and tracking, as well as delivery and scavenging of active substances *in vivo*.

Non-invasive imaging techniques are powerful diagnostic tools, which are applied in both research and clinics. In research, fluorescence imaging is the most widely applied visualization method to monitor biological processes, and to track and evaluate nanoparticles in biological systems. Molecular imaging has enabled visualization of molecular processes in living organisms on cellular level. This imaging technique requires administration of contrast agents, which are typically small molecules capable of crossing the blood-tissue barriers. Thus, the contrast agents easily accumulate in the tissues, especially if the blood-tissue barrier is disrupted, as in the case of tumors or inflammations. However, a major drawback

with the contrast-enhanced molecular imaging is the failure to accurately differentiate between the signals originating from the contrast agent in the blood circulation and the signals originating from surrounding tissue. A method allowing for *in vivo* differentiation between these signals, by developing a "removal-system" which could catch and quench the contrast agent, would allow for a radically improved contrast between tissue and blood. For this purpose, scavenger nanoparticles were produced, for catching and removing a specific tracer compound directly in the blood circulation *in vivo*. Photonic interactions were utilized to visualize the interaction between tracer and scavenger. The obtained results are eventually a first step towards a fast and efficient system for improving the contrast of the tissue area of interest and consequently, such a system could enhance the probability of earlier diagnosis of various diseases. Photonic interactions are widely utilized to study close-molecular interactions, mostly in the form of FRET. The efficacy of FRET was thus further demonstrated intracellularly, for redox-induced delivery of an active compound from a nanoparticle-based platform. Intracellular release mechanisms are especially challenging to study, however highly desired, since release mechanisms measured only in biological/intracellular-relevant conditions rarely represent significant correlation to actual conditions. Normally, an indirect read-out based on the cytotoxic action of an active compound is measured, which hampers the validation of the intracellular release of non-toxic compounds. The reporter-system presented here, demonstrated the potential for real-time monitoring of the compound cleavage intracellularly, by the FRET-approach.

The developed porous nanoparticles were further used for encapsulation of active compounds. Loading of drugs and imaging agents into porous inorganic nanoparticles has expanded as a field of study, due to the realization that the porous nanoparticle matrix can carry a large amount of cargo, and protect it from degradation or loss of activity in the biological environment. In this thesis, different means of delivery of active substances by porous particles have been demonstrated, both i*n vitro* and *in vivo*. A range of different particle-dye formulations were designed, and comprehensively evaluated as optical probe systems suitable for long-term labeling and tracking of cells, with the focus on determining an optimal design. The optimized formulation showed superior characteristics compared to existing cellular labeling probes, with respect to shelf-life, biodegradability, cellular labeling efficiency, fluorescence intensity signal retention *in vivo* up to one month, and possibility of real-time detection of circulating metastatic cells. Further, the same principles were utilized to load a hydrophobic anti-inflamma-

tory drug into both larger micron-sized porous particles and porous nanoparticles, with subsequent administration through the pulmonary route, to investigate the treatment effect on two differently induced lung inflammation models *in vivo*. The results showed that the chemical-induced airway inflammation could be treated by aerosolized drug-loaded particles at least to the same extent as free drug, and the particles are viable drug carriers for pulmonary delivery of corticosteroids. An interesting observation, of a down-modulatory effect on the lung inflammation by empty particles was noted, the reasons of which it naturally would be highly attractive to study further.

The results presented in this thesis contribute to the above-discussed specific applications of the highly diverse field of nanomedicine. The research in this field is rapidly developing, with novel nanoformulations and nanomaterial-based methods continuously being demonstrated. However, more in-depth knowledge is still needed regarding the nanomaterials' interaction with the biological environment *in vivo*. The nanomaterials are easily recognized by the immunological system and they exhibit poor penetration through biological barriers, and significant efforts are needed to solve these disadvantageous properties. Common guidelines for the preparation and utilization of nanomaterials are also lacking. The ultimate goal, for a more comprehensive progress in this area, would be to find a system to combine the knowledge gained from studies across the world. Nevertheless, due to the limitations of conventional diagnostic and therapeutic strategies, the management of diseases is slowly moving towards tailored treatments for individual patients, also known as "personalized medicine". By combining non-invasive imaging and targeted drug delivery into theranostics, patients can be pre-selected, ensuring that only patients susceptible to a specific treatment are included. In the future, theranostics might offer a possibility of early diagnosis and in-real-time response of the efficacy of therapeutic treatments. Even though the expectations of personalized medicine are rather high, novel theranostics are foreseen to have the potential for addressing the challenges in this field.

However, even if rapidly evolving, many biological and clinical characterizations still remain unexplored in the field of nanomedicine. The clinical translation from pre-clinical proof-of-concepts is suffering from the lack of reliable screening platforms for evaluating the toxicity and stability of the nanomaterials *in vivo*. The expectations of a highly efficient and versatile carrier system, which is non-toxic, biodegradable, and in addition to owning specific targeting ability, additionally can deliver its cargo intracellularly, is hard to fulfill. There are also several demands in the manufacturing process to be met, such as reproducibility and scale-up, and the naturally hard-to-overcome three phases of FDA trials will be a

challenge before new nanomedicines can be introduced into the medical practice. Fortunately, challenges are always accompanied by opportunities, which still rise hope and expectations to this field of study, in terms of new and sophisticated diagnostic and therapeutic interventions. By close collaboration between the different disciplines within the academic research and industry, where all these challenges of nanomedicines are carefully considered and evaluated, personalized medicine has potential to revolutionize the treatment of diseases, hopefully in a future not too far.

REFERENCES

1 Zhang, X.-Q.; Xu, X.; Bertrand, N.; Pridgen, E.; Swami, A.; Farokhzad, O. C., Interactions of nanomaterials and biological systems: Implications to personalized nanomedicine. *Advanced drug delivery reviews* **2012,** *64* (13), 1363-1384.

2 Lammers, T.; Rizzo, L. Y.; Storm, G.; Kiessling, F., Personalized Nanomedicine. *Clinical Cancer Research* **2012,** *18* (18), 4889-4894.

3 Xu, X.; Ho, W.; Zhang, X.; Bertrand, N.; Farokhzad, O., Cancer nanomedicine: from targeted delivery to combination therapy. *Trends in molecular medicine* **2015,** *21* (4), 223-232.

4 Rizzo, L. Y.; Theek, B.; Storm, G.; Kiessling, F.; Lammers, T., Recent progress in nanomedicine: therapeutic, diagnostic and theranostic applications. *Current opinion in biotechnology* **2013,** *24* (6), 1159-1166.

5 Joint European Commission, ETN nanomedicine: roadmaps in nanomedicine towards 2020. *Expert Report* **2009,** *2009*, 56.

6 Riehemann, K.; Schneider, S. W.; Luger, T. A.; Godin, B.; Ferrari, M.; Fuchs, H., Nanomedicine—challenge and perspectives. *Angewandte Chemie International Edition* **2009,** *48* (5), 872-897.

7 Ventola, C. L., Progress in nanomedicine: approved and investigational nanodrugs. *Pharmacy and Therapeutics* **2017,** *42* (12), 742.

8 Bashir, M. R.; Bhatti, L.; Marin, D.; Nelson, R. C., Emerging applications for ferumoxytol as a contrast agent in MRI. *Journal of Magnetic Resonance Imaging* **2015,** *41* (4), 884-898.

9 Bobo, D.; Robinson, K. J.; Islam, J.; Thurecht, K. J.; Corrie, S. R., Nanoparticle-based medicines: a review of FDA-approved materials and clinical trials to date. *Pharmaceutical research* **2016,** *33* (10), 2373-2387.

10 Li, Z.; Barnes, J. C.; Bosoy, A.; Stoddart, J. F.; Zink, J. I., Mesoporous silica nanoparticles in biomedical applications. *Chemical Society Reviews* **2012,** *41* (7), 2590-2605.

11 Benezra, M.; Penate-Medina, O.; Zanzonico, P. B.; Schaer, D.; Ow, H.; Burns, A.; DeStanchina, E.; Longo, V.; Herz, E.; Iyer, S., Multimodal silica nanoparticles are effective cancer-targeted probes in a model of human melanoma. *The Journal of clinical investigation* **2011,** *121* (7), 2768-2780.

12 Phillips, E.; Penate-Medina, O.; Zanzonico, P. B.; Carvajal, R. D.; Mohan, P.; Ye, Y.; Humm, J.; Gönen, M.; Kalaigian, H.; Schöder, H., Clinical translation of an ultrasmall inorganic optical-PET imaging nanoparticle probe. *Science translational medicine* **2014,** *6* (260), 260ra149-260ra149.

13 Barbe, C.; Bartlett, J.; Kong, L.; Finnie, K.; Lin, H. Q.; Larkin, M.; Calleja, S.; Bush, A.; Calleja, G., Silica particles: a novel drug-delivery system. *Advanced materials* **2004,** *16* (21), 1959-1966.

14 Wang, Y.; Zhao, Q.; Han, N.; Bai, L.; Li, J.; Liu, J.; Che, E.; Hu, L.; Zhang, Q.; Jiang, T., Mesoporous silica nanoparticles in drug delivery and biomedical applications. *Nanomedicine: Nanotechnology, Biology and Medicine* **2015,** *11* (2), 313-327.

15 Guerrero-Martínez, A.; Pérez-Juste, J.; Liz-Marzán, L. M., Recent progress on silica coating of nanoparticles and related nanomaterials. *Advanced materials* **2010,** *22* (11), 1182-1195.

16 Ehlerding, E. B.; Grodzinski, P.; Cai, W.; Liu, C. H., Big Potential from Small Agents: Nanoparticles for Imaging-Based Companion Diagnostics. *ACS nano* **2018,** *12* (3), 2106-2121.

17 Kiessling, F.; Mertens, M. E.; Grimm, J.; Lammers, T., Nanoparticles for imaging: top or flop? *Radiology* **2014,** *273* (1), 10-28.

18 Kim, D.; Kim, J.; Park, Y. I.; Lee, N.; Hyeon, T., Recent Development of Inorganic Nanoparticles for Biomedical Imaging. *ACS central science* **2018,** *4* (3), 324-336.

19 Foster, C.; Watson, A.; Kaplinsky, J.; Kamaly, N., Improved targeting of cancers with nanotherapeutics. In *Cancer Nanotechnology*, Springer: **2017**; 13-37.

20 Burke, B. P.; Cawthorne, C.; Archibald, S. J., Multimodal nanoparticle imaging agents: design and applications. *Phil. Trans. R. Soc. A* **2017,** *375* (2107), 20170261.

21 Kantamneni, H.; Zevon, M.; Donzanti, M. J.; Zhao, X.; Sheng, Y.; Barkund, S. R.; McCabe, L. H.; Banach-Petrosky, W.; Higgins, L. M.; Ganesan, S., Surveillance nanotechnology for multi-organ cancer metastases. *Nature Biomedical Engineering* **2017,** *1* (12), 993.

22 Wang, Y.-F.; Liu, L.; Xue, X.; Liang, X.-J., Nanoparticle-based drug delivery systems: What can they really do in vivo? *F1000Research* **2017,** *6*.

23 Tamarov, K.; Näkki, S.; Xu, W.; Lehto, V.-P., Approaches to improve the biocompatibility and systemic circulation of inorganic porous nanoparticles. *J. Mater. Chem. B* **2018,** *6*, 3632.

24 Tran, S.; DeGiovanni, P.-J.; Piel, B.; Rai, P., Cancer nanomedicine: a review of recent success in drug delivery. *Clinical and translational medicine* **2017,** *6* (1), 44.

25 Rosen, J.; Yoffe, S.; Meerasa, A.; Verma, M.; Gu, F., Nanotechnology and diagnostic imaging: new advances in contrast agent technology. *J. Nanomed. Nanotechnol* **2011,** *2* (5), 1-12.

26 von Roemeling, C.; Jiang, W.; Chan, C. K.; Weissman, I. L.; Kim, B. Y., Breaking down the barriers to precision cancer nanomedicine. *Trends in biotechnology* **2017,** *35* (2), 159-171.

27 Jin, R.; Lin, B.; Li, D.; Ai, H., Superparamagnetic iron oxide nanoparticles for MR imaging and therapy: design considerations and clinical applications. *Current opinion in pharmacology* **2014,** *18*, 18-27.

28 Vert, M.; Doi, Y.; Hellwich, K. H.; Hess, M.; Hodge, P.; Kubisa, P.; Rinaudo, M.; Schué, F., Terminology for biorelated polymers and applications (IUPAC Recommendations 2012). *Pure and Applied Chemistry* **2012,** *84* (2), 377-410.

29 Agrahari, V.; Hiremath, P., Challenges associated and approaches for successful translation of nanomedicines into commercial products. *Nanomedicine* **2017,** *12* (8), 819-823.

30 Taylor, A.; Wilson, K. M.; Murray, P.; Fernig, D. G.; Lévy, R., Long-term tracking of cells using inorganic nanoparticles as contrast agents: are we there yet? *Chemical Society Reviews* **2012,** *41* (7), 2707-2717.

31 Singh, A.; Sahoo, S. K., Magnetic nanoparticles: a novel platform for cancer theranostics. *Drug discovery today* **2014,** *19* (4), 474-481.

32 Wang, Y.-X. J., Superparamagnetic iron oxide based MRI contrast agents: Current status of clinical application. *Quantitative imaging in medicine and surgery* **2011,** *1* (1), 35.

33 Revia, R. A.; Zhang, M., Magnetite nanoparticles for cancer diagnosis, treatment, and treatment monitoring: recent advances. *Materials Today* **2016,** *19* (3), 157-168.

34 Thakor, A. S.; Jokerst, J. V.; Ghanouni, P.; Campbell, J. L.; Mittra, E.; Gambhir, S. S., Clinically approved nanoparticle imaging agents. *Journal of Nuclear Medicine* **2016,** *57* (12), 1833.

35 Soenen, S. J.; De Cuyper, M., Assessing iron oxide nanoparticle toxicity in vitro: current status and future prospects. *Nanomedicine* **2010,** *5* (8), 1261-1275.

36 Lingeshwar Reddy, K.; Balaji, R.; Kumar, A.; and Krishnan, V., Lanthanide doped near infrared active upconversion nanophosphors: Fundamental concepts, synthesis strategies, and technological applications. *Small* **2018**, *14* (37), 1801304.

37 Bhattacharya, K.; Mukherjee, S. P.; Gallud, A.; Burkert, S. C.; Bistarelli, S.; Bellucci, S.; ...; Fadeel, B., Biological interactions of carbon-based nanomaterials: from coronation to degradation. *Nanomedicine: Nanotechnology, Biology and Medicine* **2016**, *12* (2), 333-351.

38 Chen, D.; Dougherty, C. A.; Zhu, K.; Hong, H., Theranostic applications of carbon nanomaterials in cancer: Focus on imaging and cargo delivery. *Journal of controlled release* **2015**, *210*, 230-245.

39 Ghosh Chaudhuri, R.; Paria, S., Core/shell nanoparticles: classes, properties, synthesis mechanisms, characterization, and applications. *Chemical reviews* **2011,** *112* (4), 2373-2433.

40 Sun, Z.; Zhou, X.; Luo, W.; Yue, Q.; Zhang, Y.; Cheng, X.; Li, W.; Kong, B.; Deng, Y.; Zhao, D., Interfacial engineering of magnetic particles with porous shells: Towards magnetic core–Porous shell microparticles. *Nano Today* **2016,** *11* (4), 464-482.

41 Schärtl, W., Current directions in core–shell nanoparticle design. *Nanoscale* **2010,** *2* (6), 829-843.

42 Guerrero-Martínez, A.; Pérez-Juste, J.; Liz-Marzán, L. M., Recent progress on silica coating of nanoparticles and related nanomaterials. *Advanced materials* **2010,** *22* (11), 1182-1195.

43 Corr, S. A.; Rakovich, Y. P.; Gun'ko, Y. K., Multifunctional magnetic-fluorescent nanocomposites for biomedical applications. *Nanoscale Research Letters* **2008,** *3* (3), 87.

44 Shi, S.; Chen, F.; Cai, W., Biomedical applications of functionalized hollow mesoporous silica nanoparticles: focusing on molecular imaging. *Nanomedicine* **2013,** *8* (12), 2027-2039.

45 Chen, Y.; Chen, H.-R.; Shi, J.-L., Construction of homogenous/heterogeneous hollow mesoporous silica nanostructures by silica-etching chemistry: principles, synthesis, and applications. *Accounts of chemical research* **2013,** *47* (1), 125-137.

46 Chen, F.; Hong, H.; Shi, S.; Goel, S.; Valdovinos, H. F.; Hernandez, R.; Theuer, C. P.; Barnhart, T. E.; Cai, W., Engineering of hollow mesoporous silica nanoparticles for remarkably enhanced tumor active targeting efficacy. *Scientific reports* **2014,** *4*, 5080.

47 Purbia, R.; Paria, S., Yolk/shell nanoparticles: classifications, synthesis, properties, and applications. *Nanoscale* **2015,** *7* (47), 19789-19873.

48 Wicki, A.; Witzigmann, D.; Balasubramanian, V.; Huwyler, J., Nanomedicine in cancer therapy: challenges, opportunities, and clinical applications. *Journal of controlled release* **2015,** *200*, 138-157.

49 Chen, G.; Roy, I.; Yang, C.; Prasad, P. N., Nanochemistry and nanomedicine for nanoparticle-based diagnostics and therapy. *Chemical reviews* **2016,** *116* (5), 2826-2885.

50 Caltagirone, C.; Bettoschi, A.; Garau, A.; Montis, R., Silica-based nanoparticles: a versatile tool for the development of efficient imaging agents. *Chemical Society Reviews* **2015,** *44* (14), 4645-4671.

51 Karaman, D. Ş.; Sarparanta, M. P.; Rosenholm, J. M.; Airaksinen, A. J., Multimodality Imaging of Silica and Silicon Materials In Vivo. *Advanced Materials* **2018**, 1703651.

52 Wu, X.; Wu, M.; Zhao, J. X., Recent development of silica nanoparticles as delivery vectors for cancer imaging and therapy. *Nanomedicine: Nanotechnology, Biology and Medicine* **2014,** *10* (2), 297-312.

53 Ishikawa-Ankerhold, H. C.; Ankerhold, R.; Drummen, G. P., Advanced fluorescence microscopy techniques—Frap, Flip, Flap, Fret and flim. *Molecules* **2012,** *17* (4), 4047-4132.

54 Ow, H.; Larson, D. R.; Srivastava, M.; Baird, B. A.; Webb, W. W.; Wiesner, U., Bright and stable core− shell fluorescent silica nanoparticles. *Nano letters* **2005,** *5* (1), 113-117.

55 Yao, G.; Wang, L.; Wu, Y.; Smith, J.; Xu, J.; Zhao, W.; Lee, E.; Tan, W., FloDots: luminescent nanoparticles. *Analytical and Bioanalytical Chemistry* **2006,** *385* (3), 518-524.

56 Bogart, L. K.; Pourroy, G.; Murphy, C. J.; Puntes, V.; Pellegrino, T.; Rosenblum, D.; Peer, D.; Lévy, R., Nanoparticles for imaging, sensing, and therapeutic intervention. *ACS Nano* **2014,** *8* (4), 3107-3122.

57 Biju, V., Chemical modifications and bioconjugate reactions of nanomaterials for sensing, imaging, drug delivery and therapy. *Chemical Society Reviews* **2014,** *43* (3), 744-764.

58 Rahman, I. A.; Padavettan, V., Synthesis of silica nanoparticles by sol-gel: size-dependent properties, surface modification, and applications in silica-polymer nanocomposites—a review. *Journal of Nanomaterials* **2012,** *2012*, 8.

59 Chen, F.; Hableel, G.; Zhao, E. R.; Jokerst, J. V., Multifunctional nanomedicine with silica: Role of silica in nanoparticles for theranostic, imaging, and drug monitoring. *Journal of colloid and interface science* **2018,** *521*, 261-279.

60 Piletska, E.; Yawer, H.; Canfarotta, F.; Moczko, E.; Smolinska-Kempisty, K.; Piletsky, S. S.; Guerreiro, A.; Whitcombe, M. J.; Piletsky, S. A., Biomimetic Silica Nanoparticles Prepared by a Combination of Solid-Phase Imprinting and Ostwald Ripening. *Scientific reports* **2017,** *7* (1), 11537.

61 Hoffmann, F.; Cornelius, M.; Morell, J.; Fröba, M., Silica-based mesoporous organic–inorganic hybrid materials. *Angewandte Chemie International Edition* **2006,** *45* (20), 3216-3251.

62 Rosenholm, J. M.; Sahlgren, C.; Lindén, M., Towards multifunctional, targeted drug delivery systems using mesoporous silica nanoparticles–opportunities & challenges. *Nanoscale* **2010,** *2* (10), 1870-1883.

63 Siefker, J.; Karande, P.; Coppens, M.-O., Packaging biological cargoes in mesoporous materials: opportunities for drug delivery. *Expert opinion on drug delivery* **2014,** *11* (11), 1781-1793.

64 Zhuravlev, L., The surface chemistry of amorphous silica. Zhuravlev model. *Colloids and Surfaces A: Physicochemical and Engineering Aspects* **2000,** *173* (1-3), 1-38.

65 Rosenholm, J. M.; Penninkangas, A.; Lindén, M., Amino-functionalization of large-pore mesoscopically ordered silica by a one-step hyperbranching polymerization of a surface-grown polyethyleneimine. *Chemical Communications* **2006,** (37), 3909-3911.

66 Rosenholm, J. M.; Lindén, M., Wet-chemical analysis of surface concentration of accessible groups on different amino-functionalized mesoporous SBA-15 silicas. *Chemistry of Materials* **2007,** *19* (20), 5023-5034.

67 Rosenholm, J. M.; Meinander, A.; Peuhu, E.; Niemi, R.; Eriksson, J. E.; Sahlgren, C.; Lindén, M., Targeting of porous hybrid silica nanoparticles to cancer cells. *ACS nano* **2008,** *3* (1), 197-206.

68 Kim, C. O.; Cho, S. J.; Park, J. W., Hyperbranching polymerization of aziridine on silica solid substrates leading to a surface of highly dense reactive amine groups. *Journal of colloid and interface science* **2003,** *260* (2), 374-378.

69 Sapsford, K. E.; Algar, W. R.; Berti, L.; Gemmill, K. B.; Casey, B. J.; Oh, E.; Stewart, M. H.; Medintz, I. L., Functionalizing nanoparticles with biological molecules: developing chemistries that facilitate nanotechnology. *Chemical reviews* **2013,** *113* (3), 1904-2074.

70 Lee, D.-E.; Koo, H.; Sun, I.-C.; Ryu, J. H.; Kim, K.; Kwon, I. C., Multifunctional nanoparticles for multimodal imaging and theragnosis. *Chemical Society Reviews* **2012,** *41* (7), 2656-2672.

71 James, M. L.; Gambhir, S. S., A Molecular Imaging Primer: Modalities, Imaging Agents, and Applications. *Physiological Reviews* **2012,** *92* (2), 897-965.

72 Kunjachan, S.; Ehling, J.; Storm, G.; Kiessling, F.; Lammers, T., Noninvasive imaging of nanomedicines and nanotheranostics: principles, progress, and prospects. *Chemical reviews* **2015,** *115* (19), 10907-10937.

73 Wolfbeis, O. S., An overview of nanoparticles commonly used in fluorescent bioimaging. *Chemical Society Reviews* **2015,** *44* (14), 4743-4768.

74 Baker, M., Whole-animal imaging: The whole picture. *Nature* **2010,** *463* (7283), 977.

75 Massoud, T. F.; Gambhir, S. S., Molecular imaging in living subjects: seeing fundamental biological processes in a new light. *Genes & development* **2003,** *17* (5), 545-580.

76 Key, J.; Leary, J. F., Nanoparticles for multimodal in vivo imaging in nanomedicine. *International journal of nanomedicine* **2014,** *9*, 711.

77 Khalil, M. M.; Tremoleda, J. L.; Bayomy, T. B.; Gsell, W., Molecular SPECT imaging: an overview. *International journal of molecular imaging* **2011,** *2011*.

78 Martinez, H. P.; Kono, Y.; Blair, S. L.; Sandoval, S.; Wang-Rodriguez, J.; Mattrey, R. F.; Kummel, A. C.; Trogler, W. C., Hard shell gas-filled contrast enhancement particles for colour Doppler ultrasound imaging of tumors. *MedChemComm* **2010,** *1* (4), 266-270.

79 Liberman, A.; Martinez, H. P.; Ta, C. N.; Barback, C. V.; Mattrey, R. F.; Kono, Y.; Blair, S. L.; Trogler, W. C.; Kummel, A. C.; Wu, Z., Hollow silica and silica-boron nano/microparticles for contrast-enhanced ultrasound to detect small tumors. *Biomaterials* **2012,** *33* (20), 5124-5129.

80 Nobis, M.; Warren, S. C.; Lucas, M. C.; Murphy, K. J.; Herrmann, D.; Timpson, P., Molecular mobility and activity in an intravital imaging setting–implications for cancer progression and targeting. *J Cell Sci* **2018,** *131* (5), jcs206995.

81 Kim, J.; Park, S.; Jung, Y.; Chang, S.; Park, J.; Zhang, Y.; Lovell, J. F.; Kim, C., Programmable real-time clinical photoacoustic and ultrasound imaging system. *Scientific reports* **2016,** *6*, 35137.

82 Lemaster, J. E.; Chen, F.; Kim, T.; Hariri, A.; Jokerst, J. V., Development of a Trimodal Contrast Agent for Acoustic and Magnetic Particle Imaging of Stem Cells. *ACS Applied Nano Materials* **2018,** *1* (3), 1321-1331.

83 Shin, T.-H.; Choi, Y.; Kim, S.; Cheon, J., Recent advances in magnetic nanoparticle-based multi-modal imaging. *Chemical Society Reviews* **2015,** *44* (14), 4501-4516.

84 Wang, Z. J.; Chang, T.-T. A.; Slauter, R., Use of Imaging for Preclinical Evaluation. In *A Comprehensive Guide to Toxicology in Preclinical Drug Development*, Elsevier: **2013**, 759-775.

85 Wang, K.; He, X.; Yang, X.; Shi, H., Functionalized silica nanoparticles: a platform for fluorescence imaging at the cell and small animal levels. *Accounts of chemical research* **2013,** *46* (7), 1367-1376.

86 Korzeniowska, B.; Nooney, R.; Wencel, D.; McDonagh, C., Silica nanoparticles for cell imaging and intracellular sensing. *Nanotechnology* **2013,** *24* (44), 442002.

87 Cha, B. G.; Kim, J., Functional mesoporous silica nanoparticles for bio-imaging applications. *Wiley Interdisciplinary Reviews: Nanomedicine and Nanobiotechnology* **2018**, e1515.

88 Peterson, D. A., Confocal Microscopy. In *Encyclopedia of Movement Disorders*, Kompoliti, K.; Metman, L. V., Eds. Academic Press: Oxford, **2010**, 250-252.

89 Pansare, V. J.; Hejazi, S.; Faenza, W. J.; Prud'homme, R. K., Review of long-wavelength optical and NIR imaging materials: contrast agents, fluorophores, and multifunctional nano carriers. *Chemistry of materials* **2012,** *24* (5), 812-827.

90 Yao, J.; Yang, M.; Duan, Y., Chemistry, biology, and medicine of fluorescent nanomaterials and related systems: new insights into biosensing, bioimaging, genomics, diagnostics, and therapy. *Chemical reviews* **2014,** *114* (12), 6130-6178.

91 Candle, Synchrotron Research Institute, Multiphoton Laser Fluorescence microscopy. www.candle.am (accessed 5.11.2018)

92 Rowland, C. E.; Brown III, C. W.; Medintz, I. L.; Delehanty, J. B., Intracellular FRET-based probes: a review. *Methods and applications in fluorescence* **2015,** *3* (4), 042006.

93 Yang, J.; Chen, H.; Vlahov, I. R.; Cheng, J.-X.; Low, P. S., Evaluation of disulfide reduction during receptor-mediated endocytosis by using FRET imaging. *Proceedings of the National Academy of Sciences* **2006,** *103* (37), 13872-13877.

94 Berger, A., Magnetic resonance imaging. *BMJ : British Medical Journal* **2002,** *324* (7328), 35-35.

95 Karaman, D. Ş.; Desai, D.; Zhang, J.; Tadayon, S.; Unal, G.; Teuho, J.; Sarfraz, J.; Smått, J.-H.; Gu, H.; Näreoja, T., Modulation of the structural properties of mesoporous silica nanoparticles to enhance the T 1-weighted MR imaging capability. *Journal of Materials Chemistry B* **2016,** *4* (9), 1720-1732.

96 Pan, D.; Caruthers, S. D.; Senpan, A.; Schmieder, A. H.; Wickline, S. A.; Lanza, G. M., Revisiting an old friend: manganese-based MRI contrast agents. *Wiley Interdisciplinary Reviews: Nanomedicine and Nanobiotechnology* **2011,** *3* (2), 162-173.

97 Caster, J. M.; Patel, A. N.; Zhang, T.; Wang, A., Investigational nanomedicines in 2016: a review of nanotherapeutics currently undergoing clinical trials. *Wiley Interdisciplinary Reviews: Nanomedicine and Nanobiotechnology* **2017,** *9* (1), e1416.

98 Bashir, M. R.; Bhatti, L.; Marin, D.; Nelson, R. C., Emerging applications for ferumoxytol as a contrast agent in MRI. *Journal of Magnetic Resonance Imaging* **2015,** *41* (4), 884-898.

99 Lee, N.; Yoo, D.; Ling, D.; Cho, M. H.; Hyeon, T.; Cheon, J., Iron oxide based nanoparticles for multimodal imaging and magnetoresponsive therapy. *Chemical reviews* **2015,** *115* (19), 10637-10689.

100 Tromsdorf, U. I.; Bruns, O. T.; Salmen, S. C.; Beisiegel, U.; Weller, H., A highly effective, nontoxic T 1 MR contrast agent based on ultrasmall PEGylated iron oxide nanoparticles. *Nano letters* **2009,** *9* (12), 4434-4440.

101 Shin, T.-H.; Choi, J.-s.; Yun, S.; Kim, I.-S.; Song, H.-T.; Kim, Y.; Park, K. I.; Cheon, J., T 1 and T 2 dual-mode MRI contrast agent for enhancing accuracy by engineered nanomaterials. *ACS nano* **2014,** *8* (4), 3393-3401.

102 Zhou, Z.; Huang, D.; Bao, J.; Chen, Q.; Liu, G.; Chen, Z.; Chen, X.; Gao, J., A synergistically enhanced T1–T2 dual-modal contrast agent. *Advanced materials* **2012,** *24* (46), 6223-6228.

103 Cherry, S. R. In *Multimodality imaging: Beyond pet/ct and spect/ct*, Seminars in nuclear medicine, Elsevier: **2009**, 348-353.

104 Nam, T.; Park, S.; Lee, S.-Y.; Park, K.; Choi, K.; Song, I. C.; Han, M. H.; Leary, J. J.; Yuk, S. A.; Kwon, I. C., Tumor targeting chitosan nanoparticles for dual-modality optical/MR cancer imaging. *Bioconjugate chemistry* **2010,** *21* (4), 578-582.

105 Kircher, M. F.; Mahmood, U.; King, R. S.; Weissleder, R.; Josephson, L., A multimodal nanoparticle for preoperative magnetic resonance imaging and intraoperative optical brain tumor delineation. *Cancer research* **2003,** *63* (23), 8122-8125.

106 Key, J.; Kim, K.; Dhawan, D.; Knapp, D. W.; Kwon, I. C.; Choi, K.; Leary, J. F., In *Dual-modality in vivo imaging for MRI detection of tumors and NIRF-guided surgery using multi-component nanoparticles*, Nanoscale Imaging, Sensing, and Actuation for Biomedical Applications VIII, International Society for Optics and Photonics: **2011**, 790805.

107 Key, J.; Cooper, C.; Kim, A. Y.; Dhawan, D.; Knapp, D. W.; Kim, K.; Park, J. H.; Choi, K.; Kwon, I. C.; Park, K., In vivo NIRF and MR dual-modality imaging using glycol chitosan nanoparticles. *Journal of controlled release* **2012,** *163* (2), 249-255.

108 Kircher, M. F.; Mahmood, U.; King, R. S.; Weissleder, R.; Josephson, L., A multimodal nanoparticle for preoperative magnetic resonance imaging and intraoperative optical brain tumor delineation. *Cancer research* **2003,** *63* (23), 8122-8125.

109 Cha, E.-J.; Jang, E. S.; Sun, I.-C.; Lee, I. J.; Ko, J. H.; Kim, Y. I.; Kwon, I. C.; Kim, K.; Ahn, C.-H., Development of MRI/NIRF 'activatable'multimodal imaging probe based on iron oxide nanoparticles. *Journal of controlled release* **2011,** *155* (2), 152-158.

110 Shibu, E. S.; Ono, K.; Sugino, S.; Nishioka, A.; Yasuda, A.; Shigeri, Y.; Wakida, S.-i.; Sawada, M.; Biju, V., Photouncaging nanoparticles for MRI and fluorescence imaging in vitro and in vivo. *ACS nano* **2013,** *7* (11), 9851-9859.

111 Tan, Y. F.; Chandrasekharan, P.; Maity, D.; Yong, C. X.; Chuang, K.-H.; Zhao, Y.; Wang, S.; Ding, J.; Feng, S.-S., Multimodal tumor imaging by iron oxides and quantum dots formulated in poly (lactic acid)-d-alpha-tocopheryl polyethylene glycol 1000 succinate nanoparticles. *Biomaterials* **2011,** *32* (11), 2969-2978.

112 Kalimuthu, S.; Jeong, J. H.; Oh, J. M.; Ahn, B.-C., Drug Discovery by Molecular Imaging and Monitoring Therapy Response in Lymphoma. *International journal of molecular sciences* **2017,** *18* (8), 1639.

113 Kelkar, S. S.; Reineke, T. M., Theranostics: combining imaging and therapy. *Bioconjugate chemistry* **2011,** *22* (10), 1879-1903.

114 Agarwal, A.; Ressler, D.; Snyder, G., The current and future state of companion diagnostics. *Pharmacogenomics and personalized medicine* **2015**, *8*, 99.

115 Vats, S.; Singh, M.; Siraj, S.; Singh, H.; Tandon, S., Role of nanotechnology in theranostics and personalized medicines. *Journal of Health Research and Reviews* **2017**, *4* (1), 1.

116 Rosenholm, J. M.; Peuhu, E.; Eriksson, J. E.; Sahlgren, C.; Lindén, M., Targeted intracellular delivery of hydrophobic agents using mesoporous hybrid silica nanoparticles as carrier systems. *Nano letters* **2009,** *9* (9), 3308-3311.

117 von Haartman, E.; Jiang, H.; Khomich, A. A.; Zhang, J.; Burikov, S. A.; Dolenko, T. A.; Ruokolainen, J.; Gu, H.; Shenderova, O. A.; Vlasov, I. I., Core–shell designs of photoluminescent nanodiamonds with porous silica coatings for bioimaging and drug delivery I: fabrication. *Journal of Materials Chemistry B* **2013,** *1* (18), 2358-2366.

118 Prabhakar, N.; Näreoja, T.; von Haartman, E.; Karaman, D. Ş.; Jiang, H.; Koho, S.; Dolenko, T. A.; Hänninen, P. E.; Vlasov, D. I.; Ralchenko, V. G., Core–shell designs of photoluminescent nanodiamonds with porous silica coatings for bioimaging and drug delivery II: application. *Nanoscale* **2013,** *5* (9), 3713-3722.

119 von Haartman, E.; Lindberg, D.; Prabhakar, N.; Rosenholm, J. M., On the intracellular release mechanism of hydrophobic cargo and its relation to the biodegradation behavior of mesoporous silica nanocarriers. *European Journal of Pharmaceutical Sciences* **2016,** *95*, 17-27.

120 Bhowmik, D.; Gopinath, H.; Kumar, B. P.; Duraivel, S.; Kumar, K. S., Controlled release drug delivery systems. *The Pharma Innovation* **2012**, *1* (10, Part A), 24.

121 Mura, S.; Nicolas, J.; Couvreur, P., Stimuli-responsive nanocarriers for drug delivery. *Nature materials* **2013,** *12* (11), 991.

122 Derfus, A. M.; von Maltzahn, G.; Harris, T. J.; Duza, T.; Vecchio, K. S.; Ruoslahti, E.; Bhatia, S. N., Remotely triggered release from magnetic nanoparticles. *Advanced materials* **2007,** *19* (22), 3932-3936.

123 Yuan, Q.; Venkatasubramanian, R.; Hein, S.; Misra, R., A stimulus-responsive magnetic nanoparticle drug carrier: magnetite encapsulated by chitosan-grafted-copolymer. *Acta Biomaterialia* **2008,** *4* (4), 1024-1037.

124 Croissant, J. G.; Fatieiev, Y.; Khashab, N. M., Degradability and clearance of silicon, organosilica, silsesquioxane, silica mixed oxide, and mesoporous silica nanoparticles. *Advanced materials* **2017,** *29* (9), 1604634.

125 Shi, Y.; Hélary, C.; Haye, B.; and Coradin, T., Extracellular versus Intracellular Degradation of Nanostructured Silica Particles. *Langmuir* **2017**, *34* (1), 406-415.

126 Matsumura, Y.; and Maeda, H., A new concept for macromolecular therapeutics in cancer chemotherapy: mechanism of tumoritropic accumulation of proteins and the antitumor agent smancs. *Cancer research* **1986**, *46* (12 Part 1), 6387-6392.

127 Pietersz, G. A.; Wang, X.; Yap, M. L.; Lim, B.; Peter, K., Therapeutic targeting in nanomedicine: the future lies in recombinant antibodies. *Nanomedicine* **2017,** *12* (15), 1873-1889.

128 Peer, D.; Karp, J. M.; Hong, S.; Farokhzad, O. C.; Margalit, R.; Langer, R., Nanocarriers as an emerging platform for cancer therapy. *Nature nanotechnology* **2007,** *2* (12), 751.

129 Eaton, P.; Quaresma, P.; Soares, C.; Neves, C.; de Almeida, M. P.; Pereira, E.; West, P., A direct comparison of experimental methods to measure dimensions of synthetic nanoparticles. *Ultramicroscopy* **2017,** *182*, 179-190.

130 Murdock R.C.; Braydich-Stolle L.; Schrand A.M.; Schlager J.J.; Hussain S.M., Characterization of nanomaterial dispersion in solution prior to in vitro exposure using dynamic light scattering technique. *Toxicol Sci* **2008,***101* (2), 239–253.

131 Malvern Instruments Ltd, Zetasizer Nano Series User Manual 2013. www.malvern.com (accessed 6.11.2018)

132 Haskell, R. J., Physical characterization of nanoparticles. In *Nanoparticle Technology for Drug Delivery*, CRC Press: **2006,** 127-162.

133 Duncan, J. S., Introduction to colloid and surface chemistry. *4thed, Butterworth-Heinemann Ltd* **1992**.

134 Thermo Fisher Scientific Inc., FEI company, An introduction to electron microscopy. www.fei.com (accessed 5.11.2018)

135 PerkinElmer, Inc. Thermogravimetric Analysis (TGA), A Beginner's Guide. www.perkinelmer.com (accessed 5.11.2018)

136 Zhang, S.; Li, L.; Kumar, A., *Materials characterization techniques*. CRC press: **2008**.

137 Bakke, A. C., The principles of flow cytometry. *Laboratory Medicine* **2001,** *32* (4), 207-211.

138 Ormerod, M. G., Flow Cytometry-A Basic Introduction. ISBN. **2008**.

139 Abcam: Introduction to flow cytometry, Abcam plc. www.abcam.com (accessed 6.11.2018)

140 Rahman, M., Introduction to flow cytometry. *Serotec. Ltd* **2010.**

141 Nwaneshiudu, A.; Kuschal, C.; Sakamoto, F. H.; Anderson, R. R.; Schwarzenberger, K.; Young, R. C., Introduction to confocal microscopy. *Journal of Investigative Dermatology* **2012,** *132* (12), 1-5.

142 Semwogerere, D.; Weeks, E. R., Confocal microscopy. *Encyclopedia of Biomaterials and Biomedical Engineering* **2005,** *23*, 1-10.

143 Prasad, V.; Semwogerere, D.; Weeks, E. R., Confocal microscopy of colloids. *Journal of Physics: Condensed Matter* **2007,** *19* (11), 113102.

144 McNamara, K.; Tofail, S. A., Nanoparticles in biomedical applications. *Advances in Physics: X* **2017,** *2* (1), 54-88.

145 Ramos, A. P.; Cruz, M. A.; Tovani, C. B.; Ciancaglini, P., Biomedical applications of nanotechnology. *Biophysical reviews* **2017,** *9* (2), 79-89.

146 Dhawan, A.; Sharma, V., Toxicity assessment of nanomaterials: methods and challenges. *Analytical and bioanalytical chemistry* **2010,** *398* (2), 589-605.

147 Hradil, J.; Pisarev, A.; Babič, M.; Horák, D., Dextran-modified iron oxide nanoparticles. *China Particuology* **2007,** *5* (1-2), 162-168.

148 Bootz, A.; Vogel, V.; Schubert, D.; Kreuter, J., Comparison of scanning electron microscopy, dynamic light scattering and analytical ultracentrifugation for the sizing of poly (butyl cyanoacrylate) nanoparticles. *European journal of pharmaceutics and biopharmaceutics* **2004,** *57* (2), 369-375.

149 Lu, F.; Wu, S. H.; Hung, Y.; Mou, C. Y., Size effect on cell uptake in well-suspended, uniform mesoporous silica nanoparticles. *Small* **2009,** *5* (12), 1408-1413.

150 De Palma, R.; Peeters, S.; Van Bael, M. J.; Van den Rul, H.; Bonroy, K.; Laureyn, W.; Mullens, J.; Borghs, G.; Maes, G., Silane ligand exchange to make hydrophobic superparamagnetic nanoparticles water-dispersible. *Chemistry of Materials* **2007,** *19* (7), 1821-1831.

151 Rosenholm, J. M.; Zhang, J.; Sun, W.; Gu, H., Large-pore mesoporous silica-coated magnetite core-shell nanocomposites and their relevance for biomedical applications. *Microporous and Mesoporous Materials* **2011,** *145* (1-3), 14-20.

152 Desai, D.; Karaman, D. S.; Prabhakar, N.; Tadayon, S.; Duchanoy, A.; Toivola, D. M.; Rajput, S.; Näreoja, T.; Rosenholm, J. M., Design considerations for mesoporous silica nanoparticulate systems in facilitating biomedical applications. *Open Material Sciences* **2014,** *1* (1).

153 Boussif, O.; Lezoualc'h, F.; Zanta, M. A.; Mergny, M. D.; Scherman, D.; Demeneix, B.; Behr, J.-P., A versatile vector for gene and oligonucleotide transfer into cells in culture and in vivo: polyethylenimine. *Proceedings of the National Academy of Sciences* **1995,** *92* (16), 7297-7301.

154 Chen, K.; Zhang, J.; Gu, H., Dissolution from inside: a unique degradation behaviour of core–shell magnetic mesoporous silica nanoparticles and the effect of polyethyleneimine coating. *Journal of Materials Chemistry* **2012,** *22* (41), 22005-22012.

155 Mout, R.; Moyano, D. F.; Rana, S.; Rotello, V. M., Surface functionalization of nanoparticles for nanomedicine. *Chemical Society Reviews* **2012,** *41* (7), 2539-2544.

156 Li, L.; Jiang, W.; Luo, K.; Song, H.; Lan, F.; Wu, Y.; Gu, Z., Superparamagnetic iron oxide nanoparticles as MRI contrast agents for non-invasive stem cell labeling and tracking. *Theranostics* **2013,** *3* (8), 595.

157 Wiehe, J.; Zimmermann, O.; Greiner, J.; Homann, J.; Wiesneth, M.; Hombach, V.; Torzewski, J., Labeling of adult stem cells for in vivo-application in the human heart. *Histology and histopathology* **2005,** *20* (3), 901-906.

158 Zhang, L.; Wang, Y.; Tang, Y.; Jiao, Z.; Xie, C.; Zhang, H.; Gu, P.; Wei, X.; Yang, G.-Y.; Gu, H., High MRI performance fluorescent mesoporous silica-coated magnetic nanoparticles for tracking neural progenitor cells in an ischemic mouse model. *Nanoscale* **2013,** *5* (10), 4506-4516.

159 Zhan, Z.; Zhang, X.; Huang, J.; Huang, Y.; Huang, Z.; Pan, X.; Quan, G.; Liu, H.; Wang, L., Improved gene transfer with functionalized hollow mesoporous silica nanoparticles of reduced cytotoxicity. *Materials* **2017,** *10* (7), 731.

160 Sperling, R. A.; Parak, W. J., Surface modification, functionalization and bioconjugation of colloidal inorganic nanoparticles. *Philosophical Transactions of the Royal Society of London A: Mathematical, Physical and Engineering Sciences* **2010,** *368* (1915), 1333-1383.

161 Xia, T.; Kovochich, M.; Liong, M.; Meng, H.; Kabehie, S.; George, S.; Zink, J. I.; Nel, A. E., Polyethyleneimine coating enhances the cellular uptake of mesoporous silica nanoparticles and allows safe delivery of siRNA and DNA constructs. *ACS nano* **2009,** *3* (10), 3273-3286.

162 Karaman, D. S.; Desai, D.; Senthilkumar, R.; Johansson, E. M.; Råtts, N.; Odén, M.; Eriksson, J. E.; Sahlgren, C.; Toivola, D. M.; Rosenholm, J. M., Shape engineering vs organic modification of inorganic nanoparticles as a tool for enhancing cellular internalization. *Nanoscale research letters* **2012,** *7* (1), 358.

163 Lim, J.; Yeap, S. P.; Che, H. X.; Low, S. C.; Characterization of magnetic nanoparticle by dynamic light scattering. *Nanoscale research letters* **2013,** *8* (1), 381.

164 Min, G. K.; Bevan, M. A.; Prieve, D. C.; Patterson, G. D., Light scattering characterization of polystyrene latex with and without adsorbed polymer. *Colloids and Surfaces A: Physicochemical and Engineering Aspects* **2002,** *202* (1), 9-21.

165 Berne, B. J.; Pecora, R., Dynamic light scattering: with applications to chemistry, biology, and physics. *Mineola, NY: Dover Publications* **2000,** *376*.

166 Campbell, J. L.; Arora, J.; Cowell, S. F.; Garg, A.; Eu, P.; Bhargava, S. K.; Bansal, V., Quasi-cubic magnetite/silica core-shell nanoparticles as enhanced MRI contrast agents for cancer imaging. *PLoS One* **2011,** *6* (7), 21857.

167 Hsiao, J. K.; Tai, M. F.; Lee, Y. C.; Yang, C. Y.; Wang, H. Y.; Liu, H. M.; ...; Chen, S. T., Labelling of cultured macrophages with novel magnetic nanoparticles. *Journal of Magnetism and Magnetic Materials* **2006,** *304* (1), e4-e6.

168 Bhattarai, S. R.; Kc, R. B.; Kim, S. Y.; Sharma, M.; Khil, M. S.; Hwang, P. H.; ...; Kim, H. Y., N-hexanoyl chitosan stabilized magnetic nanoparticles: implication for cellular labeling and magnetic resonance imaging. *Journal of nanobiotechnology* **2008,** *6* (1), 1.

169 Walkey, C. D.; Chan, W. C., Understanding and controlling the interaction of nanomaterials with proteins in a physiological environment. *Chemical Society Reviews* **2012,** *41* (7), 2780-2799.

170 Knop, K.; Hoogenboom, R.; Fischer, D.; Schubert, U. S.; Poly (ethylene glycol) in drug delivery: pros and cons as well as potential alternatives. *Angewandte chemie international edition* **2010,** *49* (36), 6288-6308.

171 Blanco, E.; Shen, H.; Ferrari, M., Principles of nanoparticle design for overcoming biological barriers to drug delivery. *Nature biotechnology* **2015,** *33* (9), 941.

172 He, Q.; Zhang, J.; Shi, J.; Zhu, Z.; Zhang, L.; Bu, W.; ...; Chen, Y., The effect of PEGylation of mesoporous silica nanoparticles on nonspecific binding of serum proteins and cellular responses. *Biomaterials* **2010,** *31* (6), 1085-1092.

173 Elsabahy, M.; Wooley, K. L., Design of polymeric nanoparticles for biomedical delivery applications. *Chemical Society Reviews* **2012,** *41* (7), 2545-2561.

174 Steinmetz, N. F.; Manchester, M., PEGylated viral nanoparticles for biomedicine: the impact of PEG chain length on VNP cell interactions in vitro and ex vivo. *Biomacromolecules* **2009,** *10* (4), 784-792.

175 Papi, M.; Caputo, D.; Palmieri, V.; Coppola, R.; Palchetti, S.; Bugli, F.; ...; Caracciolo, G., Clinically approved PEGylated nanoparticles are covered by a protein corona that boosts the uptake by cancer cells. *Nanoscale* **2017,** *9* (29), 10327-10334.

176 Xia, T.; Kovochich, M.; Liong, M.; Meng, H.; Kabehie, S.; George, S.; ...; Nel, A. E., Polyethyleneimine coating enhances the cellular uptake of mesoporous silica nanoparticles and allows safe delivery of siRNA and DNA constructs. *ACS nano* **2009,** *3* (10), 3273-3286.

177 Zhan, Z.; Zhang, X.; Huang, J.; Huang, Y.; Huang, Z.; Pan, X.; Quan, G.; Liu, H.; Wang, L.; Wu, C., Improved gene transfer with functionalized hollow mesoporous silica nanoparticles of reduced cytotoxicity. *Materials* **2017**, *10* (7), 731.

178 Drummen, G. P., Fluorescent probes and fluorescence (microscopy) techniques—illuminating biological and biomedical research. Multidisciplinary Digital Publishing Institute: **2012**.

179 Progatzky, F.; Dallman, M. J.; Celso, C. L., From seeing to believing: labelling strategies for in vivo cell-tracking experiments. *Interface focus* **2013,** *3* (3), 20130001.

180 Pysz, M. A.; Gambhir, S. S.; Willmann, J. K., Molecular imaging: current status and emerging strategies. *Clinical radiology* **2010,** *65* (7), 500-516.

181 Massoud, T. F.; Gambhir, S. S., Molecular imaging in living subjects: seeing fundamental biological processes in a new light. *Genes & development* **2003,** *17* (5), 545-580.

182 Kircher, M. F.; Hricak, H.; Larson, S. M., Molecular imaging for personalized cancer care. *Molecular oncology* **2012,** *6* (2), 182-195.

183 Seaman, M. E.; Contino, G.; Bardeesy, N.; Kelly, K. A., Molecular imaging agents: impact on diagnosis and therapeutics in oncology. *Expert reviews in molecular medicine* **2010,** *12*.

184 Agdeppa, E. D.; Spilker, M. E., A review of imaging agent development. *The AAPS journal* **2009,** *11* (2), 286-299.

185 Mullin, J. M.; Agostino, N.; Rendon-Huerta, E.; Thornton, J. J., Keynote review: epithelial and endothelial barriers in human disease. *Drug discovery today* **2005,** *10* (6), 395-408.

186 Hawkins, B. T.; Davis, T. P., The blood-brain barrier/neurovascular unit in health and disease. *Pharmacological reviews* **2005,** *57* (2), 173-185.

187 Mueller, S. G.; Weiner, M. W.; Thal, L. J.; Petersen, R. C.; Jack, C. R.; Jagust, W.; Trojanowski, J. Q.; Toga, A. W.; Beckett, L., Ways toward an early diagnosis in Alzheimer's disease: the Alzheimer's Disease Neuroimaging Initiative (ADNI). *Alzheimer's & Dementia* **2005,** *1* (1), 55-66.

188 Brookmeyer, R.; Johnson, E.; Ziegler-Graham, K.; Arrighi, H. M., Forecasting the global burden of Alzheimer's disease. *Alzheimer's & dementia* **2007,** *3* (3), 186-191.

189 Wang, L. Early Diagnosis of Breast Cancer. *Sensors* **2017**, *17*, 1572.

190 Tørring, M. L.; Frydenberg, M.; Hansen, R. P.; Olesen, F.; Vedsted, P., Evidence of increasing mortality with longer diagnostic intervals for five common cancers: a cohort study in primary care. *European journal of cancer* **2013,** *49* (9), 2187-2198.

191 Abbott, N. J.; Patabendige, A. A.; Dolman, D. E.; Yusof, S. R.; Begley, D. J., Structure and function of the blood–brain barrier. *Neurobiology of disease* **2010,** *37* (1), 13-25.

192 Pardridge, W. M., The blood-brain barrier: bottleneck in brain drug development. *NeuroRx* **2005,** *2* (1), 3-14.

193 Alexis, F.; Pridgen, E.; Molnar, L. K.; Farokhzad, O. C., Factors affecting the clearance and biodistribution of polymeric nanoparticles. *Molecular pharmaceutics* **2008,** *5* (4), 505-515.

194 Lee, H.; Fonge, H.; Hoang, B.; Reilly, R. M.; Allen, C., The effects of particle size and molecular targeting on the intratumoral and subcellular distribution of polymeric nanoparticles. *Molecular pharmaceutics* **2010,** *7* (4), 1195-1208.

195 Liu, F.; Zhang, J. Z.; Mei, Y., The origin of the cooperativity in the streptavidin-biotin system: A computational investigation through molecular dynamics simulations. *Scientific reports* **2016,** *6*, 27190.

196 Liu, A.; Wu, L.; He, Z.; Zhou, J., Development of highly fluorescent silica nanoparticles chemically doped with organic dye for sensitive DNA microarray detection. *Analytical and bioanalytical chemistry* **2011,** *401* (6), 2003.

197 Rossi, L. M.; Shi, L.; Rosenzweig, N.; Rosenzweig, Z., Fluorescent silica nanospheres for digital counting bioassay of the breast cancer marker HER2/nue. *Biosensors and Bioelectronics* **2006,** *21* (10), 1900-1906.

198 Choi, A.; Kim, K.; Jung, H.-I.; Lee, S. Y., ZnO nanowire biosensors for detection of biomolecular interactions in enhancement mode. *Sensors and Actuators B: Chemical* **2010,** *148* (2), 577-582.

199 Jain, A.; Cheng, K., The principles and applications of avidin-based nanoparticles in drug delivery and diagnosis. *Journal of controlled release* **2017**, *245*, 27-40.

200 Yumura, K.; Ui, M.; Doi, H.; Hamakubo, T.; Kodama, T.; Tsumoto, K.; Sugiyama, A., Mutations for decreasing the immunogenicity and maintaining the function of core streptavidin. *Protein Science* **2013**, 22 (2), 213-221.

201 Ren, C.-l.; Carvajal, D.; Shull, K. R.; Szleifer, I., Streptavidin– biotin binding in the presence of a polymer spacer. A theoretical description. *Langmuir* **2009,** *25* (20), 12283-12292.

202 Desai, D.; Karaman, D. S.; Prabhakar, N.; Tadayon, S.; Duchanoy, A.; Toivola, D. M.; Rajput, S.; Näreoja, T.; Rosenholm, J. M., Design considerations for mesoporous silica nanoparticulate systems in facilitating biomedical applications. *Open Material Sciences* **2014,** *1* (1).

203 Zhang, J.; Rosenholm, J. M., The viability of mesoporous silica nanoparticles for drug delivery. *Therapeutic delivery* **2015,** *6* (8), 891-893.

204 Maleki, A.; Kettiger, H.; Schoubben, A.; Rosenholm, J. M.; Ambrogi, V.; Hamidi, M., Mesoporous silica materials: From physico-chemical properties to enhanced dissolution of poorly water-soluble drugs. *Journal of Controlled Release* **2017,** *262*, 329-347.

205 Lu, J.; Liong, M.; Zink, J. I.; Tamanoi, F., Mesoporous silica nanoparticles as a delivery system for hydrophobic anticancer drugs. *small* **2007,** *3* (8), 1341-1346.

206 Wang, Y.; Zhao, Q.; Hu, Y.; Sun, L.; Bai, L.; Jiang, T.; Wang, S., Ordered nanoporous silica as carriers for improved delivery of water insoluble drugs: a comparative study between three dimensional and two dimensional macroporous silica. *International journal of nanomedicine* **2013,** *8*, 4015.

207 Scanlon, C.; Inglehart, R.; D'Silva, N., Emerging value: the chick chorioallantoic membrane (Cam) model in oral carcinogenesis research. *J. Carcinog. Mutagen. S* **2013,** *5*.

208 Barnes, P. J.; Adcock, I. M., Glucocorticoid resistance in inflammatory diseases. *The Lancet* **2009**, *373* (9678), 1905-1917.

209 de Lange, D. W.; Meulenbelt, J., Do corticosteroids have a role in preventing or reducing acute toxic lung injury caused by inhalation of chemical agents?. *Clinical Toxicology* **2011**, *49* (2), 61-71.

210 Jonasson, S.; Wigenstam, E.; Koch, B.; Bucht, A., Early treatment of chlorine-induced airway hyperresponsiveness and inflammation with corticosteroids. *Toxicology and applied pharmacology* **2013**, *271* (2), 168-174.

211 Wigenstam, E.; Rocksén, D.; Ekstrand-Hammarström, B.; Bucht, A., Treatment with dexamethasone or liposome-encapsuled vitamin E provides beneficial effects after chemical-induced lung injury. *Inhalation toxicology* **2009,** *21* (11), 958-964.

212 National Center for Biotechnology Information. PubChem Compound Database; CID=5743, https://pubchem.ncbi.nlm.nih.gov/compound/5743 (accessed Nov. 2, 2018).

213 Kumar, D.; Schumacher, K.; von Hohenesche, C. d. F.; Grün, M.; Unger, K., MCM-41, MCM-48 and related mesoporous adsorbents: their synthesis and characterisation. *Colloids and Surfaces A: Physicochemical and Engineering Aspects* **2001,** *187*, 109-116.

214 Muthas, D.; Reznichenko, A.; Balendran, C.A.; Böttcher, G.; Clausen, I.G.; Kärrman Mårdh, C.; Ottosson, T.; Uddin, M.; MacDonald, T.T.; Danese, S.; et al., Neutrophils in ulcerative colitis: A review of selected biomarkers and their potential therapeutic implications. Scand. *J. Gastroenterol.* **2017**, *52*, 125–135.

215 Sun, L.; Guo, R.F.; Newstead, M.W.; Standiford, T.J.; Macariola, D.R.; Shanley, T.P. Effect of IL-10 on neutrophil recruitment and survival after pseudomonas aeruginosa challenge. *Am. J. Respir. Cell Mol. Biol.* **2009**, *41*, 76–84.

216 Sanfins, E.; Correia, A.; Gunnarsson, S. B.; Vilanova, M.; Cedervall, T., Nanoparticle effect on neutrophil produced myeloperoxidase. *PloS one* **2018**, *13* (1), e0191445.

217 Global Health Estimates 2016: Deaths by cause, age, sex, by country and by region, 2000-2016. Geneva, World Health Organization; 2018. http://www.who.int/news-room/fact-sheets/detail/the-top-10-causes-of-death (accessed Nov. 2, 2018).

SAMMANFATTNING

Nanomedicin, känd som den biomedicinska tillämpningen av nanoteknik, har under senare tid fått stor uppmärksamhet för dess potential i utvecklandet av nya och förbättrade metoder för att diagnosticera, behandla och följa upp olika sjukdomstillstånd, med fokus på individbaserad behandling. Målet med en individbaserad behandling är att försäkra att varje enskild person får den mest lämpliga medicineringen och att den är både effektiv och säker. Den breda forskning som pågår inom nanomedicin styr mot detta mål, med nya effektiva bärarmaterial för kommersiellt tillgängliga läkemedel. Dessa bärarmaterial ska vidare skräddarsys för specifika patientgrupper, som väljs ut med hjälp av moderna diagnostiska verktyg. I tillägg ska läkemedelsbärarna vara målstyrda för att nå en specifik förutbestämd plats i kroppen, där också läkemedelsfrisättningen sker. För att nå detta mål är det nödvändigt med en stegvis utvecklingsprocess av nanomedicinerna, där varje beredning- och modifieringssteg noggrant måste övervakas och vidare studeras och evalueras för sina specifika tillämpningar.

Det huvudsakliga målet med denna avhandling var att designa multifunktionella nanopartiklar och evaluera dem för specifika tillämpningar inom diagnostik och terapi. De syntetiserade kiseldioxidpartiklarna karakteriserades grundligt, med fokus på partiklarnas ytfunktionalisering och effekten av denna på partiklarnas dispersionsstabilitet och upptagningsförmåga i celler. Vidare studerades magnetit-kiseldioxid-kompositpartiklar, varvid det intracellulära upptaget kunde ökas med hjälp av ett externt magnetiskt fält. Det magnetiskt inducerade cellulära upptaget av partiklarna tjänade även som grund för att åskådliggöra partiklarnas aggregationsbeteende, och vikten av en optimerad ytfunktionalisering för väldispergerade partiklar. Slutligen validerades nanokompositpartiklarna för användning som kontrastämnen för magnetisk resonanstomografi.

Olika diagnostiska avbildningstekniker har fått stor betydelse för diagnosticering av olika sjukdomstillstånd, såsom cancer, i ett tidigt skede. Speciellt molekylär avbildning (*eng. molecular imaging*) har möjliggjort visualiseringen av molekylära processer i levande organismer på cellulär nivå. För att förbättra kvaliteten på de resulterande bilderna, och för att kunna visualisera och spåra celler (som t.ex. stamceller), behövs nya typer av kontrastämnen, eller så kallade markörer. I denna avhandling undersöktes porösa kiseldioxidnanopartiklar och deras förmåga att fungera som "behållare" för att transportera stora mängder fluorescerande kontrastämnen in i celler och frigöra ämnena där, för att vidare kunna spåra dessa specifika celler under en längre tid. De erhållna resultaten visade en märk-

bart högre detekteringsgrad av dessa celler jämfört med celler märkta med konventionellt använda optiska markörer. En tumör av partikelmärkta bröstcancerceller kunde detekteras under en period på en månad i en musmodell. Samtidigt demonstrerades möjligheten att detektera metastaserande celler, härstammande från den primära tumören, i blodcirkulationen i realtid. På samma sätt som porösa kiseldioxidpartiklar har visat sig vara goda bärare för stora mängder kontrastämnen, kan partiklarnas porstruktur även laddas med läkemedel. I avhandlingen designades därför även partiklar som laddades med en stor mängd antiinflammatoriskt läkemedel. Dessa partiklar administrerades via inhalering för behandling av två olika lunginflammationsmodeller i en musmodell.

Markörer ämnade för medicinsk diagnostik administreras huvudsakligen via intravenös injektion och sprids därefter i kroppen via blodcirkulationen. Dessa kontrastämnen är oftast små molekyler som kan tränga genom blod-vävnadsbarriärer och därefter ackumuleras i vävnader, speciellt om barriären är defekt, vilket kan vara ett symptom på att en sjukdom utvecklas och framskrider. Då ett område där en patologisk förändring skett (såsom vid en tumör eller en inflammation) avbildas kan det vara svårt att skilja mellan signalerna som kommer från kontrastämnena som ännu cirkulerar i blodomloppet och de som ackumulerats i den omgivande vävnaden. Med detta i åtanke presenteras i avhandlingen ett nanopartikel-baserat system ämnat för att fånga upp och därefter avlägsna eller ”släcka” signalen från kontrastämnena i blodomloppet. En sådan metod kan möjliggöra en radikalt förbättrad kontrast mellan vävnader och blod. För att visualisera och demonstrera detta utnyttjades fotoniska interaktioner, med lovande resultat.

Fotoniska interaktioner är ett mycket användbart verktyg för att studera molekylära interaktioner där avståndet är mycket kort. Detta verktyg valdes därför för att även utveckla ett nanopartikel-baserat ”rapporteringssystem” (*eng. reporter system*), för att studera intracellulär redoxinducerad frisättning av aktiva substanser, såsom läkemedel. De aktiva molekylerna konjugerades till nanopartiklarna med hjälp av intracellulärt klyvbara bindningar, och klyvningen av dessa bindningar, dvs. signalförändringen för den fotoniska interaktionen, kunde därför följas med mikroskop. Det är ofta extra utmanande att studera frisättning av ämnen från bärarmaterial inne i celler, eftersom många aktiva substanser inte är toxiska och således inte kan valideras baserat på deras cytotoxiska verkan. Konceptet som presenteras här kan därför komma att fungera som ett användbart verktyg för att övervaka frisättningen av läkemedel intracellulärt i realtid.

Forskningen inom nanomedicin går snabbt framåt och väcker stora förhoppningar om ökad precision i diagnostiken, för att kunna upptäcka och behandla olika sjukdomar tidigare, och vidare för att behandla dessa mer effektivt på

en individbaserad nivå. Det är också en process som det görs stora satsningar på, bl.a. i EU:s åttonde ramprogram Horizon 2020. Resultaten som presenteras i denna avhandling bidrar till denna process och kan möjligen fungera som riktlinjer för att designa skräddarsydda multifunktionella nanopartiklar för liknande diagnostiska och terapeutiska tillämpningar som lyfts fram här.

ACKNOWLEDGEMENTS

The journey towards this PhD started in the Laboratory of Physical Chemistry in Åbo Akademi University. I am sincerely thankful to Professor Jouko Peltonen for providing an excellent lab environment and work atmosphere in FyKe. A lot of thanks go also to all the FyKe members, especially to Christina Luojola and Kenneth Stenlund for all the help on practical issues, as well as to my former roommate Dr. Motolani Sakeye for always brightening up my days.

From the bottom of my heart, I want to thank my supervisor Professor Jessica Rosenholm. Thank you for all the opportunities you have given me during all these years, for sharing your broad knowledge, and most of all; for your guidance and support. I would like to specially thank you for always being available just a few clicks away, no matter of the time of the day (or night). I can really not imagine a better supervisor than you, and I am grateful for the whole PhD journey in your BioNanoMaterials group, starting in FyKe and ending in Biocity in the Pharmaceutical Sciences Laboratory.

Sincere thanks go to all the former and present members in BioNanoMaterials group. It has been a great time working with all of you!! Thank you Diti, Didem, Helene, Eva, Ezgi, Neeraj, and the rest of the group for the positive work atmosphere and collaboration during the years. A special thanks goes to my co-supervisor Assistant Professor Jixi Zhang for all the help and supervision during your time in the group. Thank you for sharing your knowledge and for your invaluable advices.

Intradisciplinary research needs a team of people from different fields with a broad knowledge. I want to express my gratitude to all these persons who made the studies in this thesis possible. Special thanks go to Professor Cecilia Sahlgren and Professor Daniel Abankwa. I have really learned a lot from you and your research teams. I am deeply thankful for all the experiences and knowledge acquired while working in your labs.

The studies would not have been possible without the expertise on the *in vivo* side. I am very thankful to Dr. Evgeny Pryazhnikov and Dr. Leonard Khiroug at Neurotar LtD in Helsinki, and Dr. Sofia Jonasson and Professor Anders Bucht at Swedish Defence Research Agency in Umeå, Sweden, for great collaborations.

The PhD thesis was finalized in the Department of Pharmacy in University of Oslo, Norway, through the NordForsk-funded collaboration NordicPOP. I am very thankful to Professor Ingunn Tho for giving me this opportunity. Thank you Ingunn and all the other members of the group for welcoming me in your department and providing an excellent environment for writing.

Furthermore, I am honored to have Professor Catharina de Lange Davies from Norwegian University of Science and Technology (NTNU) as my opponent and pre-examiner, and Associate Professor Anu Airaksinen from University of Helsinki as pre-examiner for the thesis. I really appreciate your helpful inputs and comments. The graduate school at Åbo Akademi University is gratefully acknowledged for the financial support.

Last, but absolutely not least, I am truly thankful for all the support from family and friends during all these years. Especially to my husband Jawad, who has always been by my side and encouraged me. Huge thanks go also to my parents who have always been ready to step on the bus or flight to come and help with our young girls in the time of need.

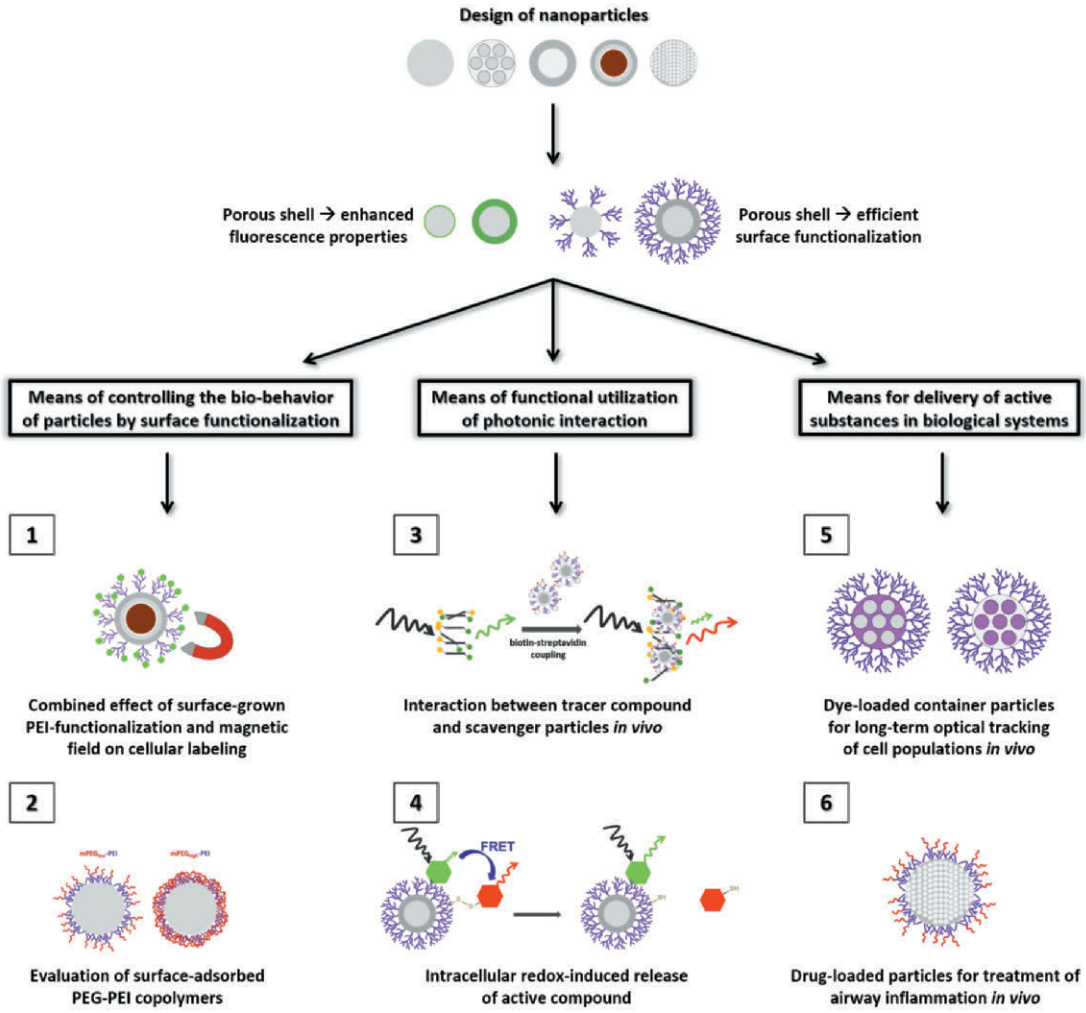

ISBN 978-952-12-3819-2